

**SELF-ASSEMBLED ALKYL-SILANE COATINGS FOR RESORBABLE
BIOMEDICAL DEVICES**

by

Avinash Jagannath Patil

B. E. in Chemical Engineering, Shivaji University, 2002

M. Tech in Biomedical Engineering, Indian Institute of Technology Bombay, 2007

Submitted to the Graduate Faculty of
The Swanson School of Engineering in partial fulfillment
of the requirements for the degree of
Doctor of Philosophy

University of Pittsburgh

2017

UNIVERSITY OF PITTSBURGH
SWANSON SCHOOL OF ENGINEERING

This dissertation was presented

by

Avinash Jagannath Patil

It was defended on

June 19, 2017

and approved by

Prashant Kumta, PhD, Edward R. Weidlein Chair Professor Department of Bioengineering,
Chemical and Petroleum Engineering, MEMS, Department of Oral Biology, University of
Pittsburgh

Tracy Cui, PhD, William Kepler Whiteford Professor Department of Bioengineering,
University of Pittsburgh

Ellen Gawalt, PhD, Hillman Distinguished Professor Department of Chemistry and
Biochemistry, Bayer School of Natural & Environmental Sciences, Duquesne University

Charles Sfeir, DDS, PhD, Associate Department of Oral Biology and Periodontology,
University of Pittsburgh

Dissertation Director: Dr. Elia Beniash, PhD, Professor, Department of Oral, Biology,
University of Pittsburgh

Copyright © by Avinash Jagannath Patil

2017

SELF-ASSEMBLED ALKYL SILANE COATINGS FOR RESORBABLE BIOMEDICAL DEVICES

Avinash J Patil, PhD

University of Pittsburgh, 2017

Magnesium (Mg) and its alloys are excellent candidate materials for resorbable biomedical devices. They are lightweight, biocompatible, osteoinductive and have mechanical properties similar to bone. Most importantly, they can degrade in the body, eliminating the need for device removal surgeries, thus reducing potential complications, patient pain and suffering, and relieving the burden on the healthcare system. The major roadblock for wide implementation of Mg implantable devices is the initial rapid corrosion of the devices, which causes formation of gas pocket around the implant. This can impede healing. One strategy to overcome this problem is use of anticorrosion coatings. We have developed alkylsilane (AS) self-assembled multilayer coatings to control Mg corrosion, increase the biocompatibility of Mg and be further functionalized with bioactive molecules. AS coatings are formed by copolymerization of n-Decyltriethoxysilane and Tetramethoxysilane followed by a dip coating of Mg discs. Some of them were further functionalized with (3-Aminopropyl) triethoxysilane. Structural, chemical and anticorrosive properties of the AS coatings were assessed by numerous characterization techniques. The resulting coatings comprised of highly homogeneous 1 μ m thin layers that significantly reduced corrosion in vitro and in vivo. In vitro and in vivo studies demonstrated the coating's high cytocompatibility and low toxicity. Furthermore, the in vivo studies demonstrated

that AS coatings could slow gas bubble formation around implanted Mg devices. Overall, our study demonstrates that AS coatings can be used to control corrosion of resorbable Mg devices.

TABLE OF CONTENTS

ACKNOWLEDGEMENTS	XVII
1.0 INTRODUCTION.....	1
1.1 MUSCULOSKELETAL DISEASES AND TRAUMA	1
1.2 BONE BIOLOGY AND FRACTURE HEALING	2
1.2.1 Bone Biology.....	2
1.2.2 Bone fracture healing.....	3
1.2.3 Surgical fixation of fracture.....	5
1.3 NON DEGRADABLE IMPLANT MATERIALS	6
1.3.1 Non degradable metals.....	6
1.3.2 Need for non-degradable metallic implant removal.....	6
1.4 DEGRADABLE IMPLANT MATERIALS	7
1.4.1 Biodegradable polymers.....	7
1.4.2 Degradable metals	8
1.5 CORROSION CONTROL OF MG AND ITS ALLOYS	9
1.5.1 Alloying.....	9
1.5.2 Conversion coatings.....	10
1.5.3 Deposition coatings	11
1.5.3.1 Polymer coatings	11

1.5.3.2	Calcium phosphate coating	12
1.5.3.3	Silane coating.....	12
1.6	ALKYLSILANE CHEMISTRY.....	13
1.7	DEGRADATION MECHANISM OF ALKYLSILANE COATINGS	16
2.0	HYPOTHESIS AND SPECIFIC AIMS	18
2.1	HYPOTHESIS	18
2.2	SPECIFIC AIMS	19
2.2.1	Specific Aim 1.....	19
2.2.2	Specific Aim 2.....	20
2.2.3	Specific Aim 3.....	21
3.0	ANTICORROSIVE SELF-ASSEMBLED HYBRID ALKYLSILANE COATINGS FOR RESORBABLE MAGNESIUM METAL DEVICES.	22
3.1	ACKNOWLEDGMENTS.....	22
3.2	ABSTRACT.....	23
3.3	INTRODUCTION	24
3.4	MATERIALS AND METHODS	25
3.4.1	Metal sample preparation.....	26
3.4.2	Synthesis and deposition of self-assembled multilayer AS coating on Mg and Mg alloys.....	26
3.4.3	Functionalization of the coatings.....	27
3.4.4	Scanning Electron Microscope (SEM) characterization.....	27
3.4.5	Atomic Force Microscopy (AFM) characterization.	28

3.4.6	Attenuated total reflectance Fourier transform infrared (ATR-FTIR) spectroscopy characterization.....	29
3.4.7	Contact angle measurement.	29
3.4.8	<i>In vitro</i> corrosion analyses.	29
3.4.9	Cell culture experiments and cytocompatibility tests.	31
3.4.10	Statistical analysis.....	33
3.5	RESULTS	34
3.5.1	SEM characterization.....	34
3.5.2	AFM Analysis.....	35
3.5.3	ATR-FTIR Analysis.	36
3.5.4	Contact angle measurement.	36
3.5.5	Determination of the corrosion rate by H ₂ evolution and weight loss methods.	37
3.5.6	Determination of the corrosion rate by potentiodynamic polarization and Impedance spectroscopy technique.	40
3.5.7	SEM analysis of the sample surfaces after incubation in SBF.	40
3.5.8	Cytocompatibility studies.....	42
3.5.9	Elemental composition of the coated Mg surfaces after 2 weeks in the tissue culture.....	46
3.6	DISCUSSION	47
3.7	CONCLUSIONS	53
4.0	SELECTIVE ALKYL SILANE COATING REMOVAL FOR CORROSION CONTROL OF RESORBABLE MEDICAL DEVICES	55

4.1	ACKNOWLEDGMENTS.....	55
4.2	ABSTRACT.....	55
4.3	INTRODUCTION	56
4.4	MATERIALS AND METHODS	57
4.4.1	Metal sample preparation.....	57
4.4.2	Synthesis and deposition of self-assembled multilayer AS coating on Mg and Mg alloys.....	58
4.4.3	Patterning of AS coated Mg discs.	58
4.4.4	Light microscope characterization.....	59
4.4.5	Hydrogen (H ₂) evolution study on patterned AS coatings on NaOH treated Mg discs.....	59
4.4.6	Scanning electron microscope (SEM) characterization and elemental analysis.....	60
4.5	RESULTS	60
4.5.1	Light microscopy analysis of patterned AS coatings.....	60
4.5.2	H ₂ evolution analysis of AS patterned AS coatings on NaOH-treated Mg discs. 61	
4.5.3	SEM and elemental analysis of patterned AS coatings on NaOH treated Mg discs after corrosion.	62
5.0	CUMULATIVE DRUG RELEASE FROM ALKYL-SILANE COATINGS; THE FEASIBILITY STUDY	65
5.1	ACKNOWLEDGMENTS.....	65
5.2	ABSTRACT.....	65

5.3	INTRODUCTION	66
5.4	MATERIALS AND METHODS	67
5.4.1	Metal sample preparation.....	67
5.4.2	Synthesis and deposition of self-assembled multilayer AS coatings encapsulating TC and Rh on Mg.....	67
5.4.3	<i>In vitro</i> release of TC or Rh in SBF.....	68
5.5	RESULTS	69
5.5.1	Release kinetics of TC or Rh in SBF.....	69
5.5.2	A drug releasing mechanism	70
6.0	IN-VIVO STUDY OF SELF-ASSEMBLED ALKYL-SILANE COATED DEGRADABLE MAGNESIUM DEVICES.....	72
6.1	ACKNOWLEDGMENTS	72
6.2	ABSTRACT.....	73
6.3	INTRODUCTION	74
6.4	MATERIALS AND METHODS	76
6.4.1	Metal disc preparation.	76
6.4.2	Synthesis and deposition of AS coatings on Mg discs.	77
6.4.3	Surgical Procedure.	77
6.4.4	Assessment of the gas pocket formation.	78
6.4.5	Postmortem whole animal μ CT analysis.	79
6.4.6	Optical microscopy analysis of the samples.	79
6.4.7	Histological analysis.	79
6.4.8	The weight loss analysis of corroded discs.	80

6.4.9	High resolution micro-computerized tomography (μ CT) analysis of the samples.....	80
6.4.10	Surface profilometry analysis of the extracted Mg discs.....	81
6.4.11	Statistical analysis.....	82
6.5	RESULTS	82
6.5.1	Light microscopy characterization of Mg discs pre and post implantation. 82	
6.5.2	Gas pocket formation dynamics.....	83
6.5.3	Corrosion analysis by the weight loss method.	85
6.5.4	The μ CT and profilometry analysis of the corroded surfaces.....	86
6.5.5	Postmortem examination and histological analysis of the sites of implantation.....	88
6.6	DISCUSSION	90
6.7	CONCLUSIONS	93
7.0	CONCLUSIONS	94
8.0	FUTURE DIRECTIONS	96
8.1	FUTURE DIRECTIONS FOR AS COATINGS DEVELOPMENT	96
8.1.1	Heat treatment of AS coatings.....	97
8.1.2	Mechanical properties of AS coatings layer.....	97
8.2	FUTURE DIRECTIONS FOR IN VITRO AND IN VIVO STUDIES	98
8.2.1	Study the effect of osteogenic functionalized AS coatings on hBMSC differentiation into osteogenic lineage.....	98
8.2.2	The Antibacterial Activities of Tetracycline encapsulated AS coatings...	99

8.2.3 Evaluating the AS-coated orthopedic fixation implant in higher animal model 99

8.2.4 In vivo anticorrosive properties of laser patterned AS-coated Mg discs100

APPENDIX A 101

BIBLIOGRAPHY 112

LIST OF TABLES

Table 1. Corrosion potential (E_{corr}) and current density (I_{corr}) values for non-coated and coated Mg and AZ31 substrate.....	39
Table 2. Elemental analysis using Energy Dispersive X-ray spectroscopy (EDS) of the surface of Mg-OH-AS discs exposed for 15 days to the tissue culture conditions.	47
Table 3. The elemental composition of the AS-coated (intact) and corroded (exposed) areas of a Mg sample.....	63
Table 4. Surface Ra and Wa values of the Mg discs before and after implantation.....	87

LIST OF FIGURES

- Figure 1. Schematic overview of bone structure and cellular distribution [6] [Figures were produced using Servier Medical Art by authors] 2
- Figure 2. Schematic of the four-phase model for bone fracture healing [15] (Yellow- granulation tissue; dark gray- fibrous tissue, light gray - cartilaginous tissue, dashed - bone). 4
- Figure 3. Schematic of humeral shaft bone fracture with fixation plate and screw [17] 5
- Figure 4. The general structure of an alkylsilane coupling agent [97]. 13
- Figure 5. Schema of the coating process: hydrolysis and polycondensation reaction of alkylsilane and self-assembly upon spin coating [102]..... 15
- Figure 6. SEM micrograph of the amphiphilic alkylsilane coating comprised of self-assembled multilayers [99]. 15
- Figure 7. Alkylsilane cleavage pathways [106]. 17
- Figure 8. SEM micrographs of A) uncoated Mg, B) Mg-OH, inset shows a high magnification micrograph of a Mg-OH surface, C) Mg-OH-AS; D) Mg-OH-AS-APTES; E) low magnification Mg-OH-AS scratched surface; and F) a higher magnification image of a Mg-OH-AS scratched surface with pieces of AS coating peeling off the surface..... 34
- Figure 9. ATR-FTIR spectra of Mg (a), Mg-OH (b), Mg-OH-AS (c), Mg-OH-AS-APTES (d) and B) box graph of static water contact angles measured on Mg sample discs. 37
- Figure 10. Cumulative hydrogen release profiles from Mg discs incubated in SBF over 7 days period (A), 24 hour period (B); C) weight loss of Mg discs incubated in SBF for 7 days; and D) Potentiodynamic polarization curves of Mg sample discs..... 38
- Figure 11. SEM images showing the surface morphologies of A) uncoated Mg, B) Mg-OH, C) Mg-OH-AS, D) Mg-OH-AS-APTES after 1-week incubation in SBF. All micrographs are taken at the same magnification..... 41
- Figure 12. Epifluorescence images of MC3T3 cells grown for 15 days on A) Mg-OH-AS and B) Mg-OH-AS-APTES coated Mg discs. The actin cytoskeleton is visualized using Alexa Fluor® 488 dye (green) and nuclear DNA is stained with Hoechst 33342 dye (blue)..... 42

Figure 13. A) Cell density on AS-coated Mg discs after 15 days in culture. B) Changes in cell density on glass coverslips and glass coverslips coated with AS over a 2-week period. C) Cell viability, determined by alamarBlue assay, on glass coverslips and glass coverslips coated with AS films..... 44

Figure 14. SEM images showing cells morphologies on uncoated and AS-coated glass coverslips. A. and D) Cells on uncoated glass coverslips 24 h and 5 d after seeding. B and E) Cells on AS-coated glass coverslips 24 h and 5 d after seeding. C and F) Cells on AS-coated and aminated glass coverslips 24 h and 5 d after seeding. All micrographs were taken at the same magnification..... 45

Figure 15. Surface of Mg-OH-AS sample exposed for 2 weeks to tissue culture conditions. A) SEM micrograph of the surface; B) SEM micrograph an area of the surface used for the EDS mapping; C) Mg map of the area in B, D) O map of the area in B; E) Si map of the area in B. 48

Figure 16. Optical images of hand patterned 4-Lines (A), 6-Lines (B) AS coatings on NaOH-treated Mg discs 61

Figure 17. Cumulative H₂ release profile from patterned AS-coated on NaOH-treated Mg discs incubated in SBF over a 7 day period (Note- H₂ data on Y axis is not normalized with area of the individual disc)..... 62

Figure 18. SEM images showing the surface morphology of (A) uncoated Mg-OH, (B) AS-coated Mg-OH disc without patterning, (C) Mg-OH-AS-4 Lines patterning, (D) Mg-OH-AS-6 Lines patterning, Scale bar for A and B is 1 mm, for C and D is 500 μ m 64

Figure 19. The cumulative release profile of TC and Rh from AS coatings deposited on NaOH-treated Mg discs in SBF over 21 days. 70

Figure 20. Optical images of Mg-OH and Mg-OH-AS discs as prepared (A and B, respectively), immediately after retrieval at 6 weeks in vivo (C and D) and after cleaning with a CrO₃ solution (E and F). All discs shows muscle side surface topography..... 83

Figure 21. (A) Photographs of a mouse at different time points after implantation of non-coated (left side) and AS-coated (right side) Mg discs. Dotted line indicates the diameter of the implanted Mg disc. (B) Changes in the diameter of the gas pockets around the AS -coated (circle) and non-coated (square) Mg discs and (C) % weight loss of Mg discs implanted in vivo for 6 weeks. For Box plot C, the diamonds (◆) represent individual values. The median values are represented by horizontal lines inside the box; the mean values are represented by the empty rectangle (□); the upper and lower box ranges represent standard deviation (SD). 84

Figure 22. 3D μ CT images of representative samples before (A-D) and 6 weeks after (A'-D') the implantation; (A,A')- muscle side and (B,B')- skin side of an uncoated sample. (C,C') muscle side and (D,D')- skin side of a coated sample..... 87

Figure 23. Box plots of (A) Roughness (Ra) and (B) Waviness (Wa) data of the samples implanted for 6 weeks after the implantation. The diamonds (◆) represent individual values from individual samples. The median values are represented by horizontal lines in the center of the box; the mean values are represented by the empty rectangle (□) on the box plot; the upper and lower box ranges represent standard deviation (SD)...... 88

Figure 24. Photograph of a gas pocket on back of a mouse (A), X-ray images of Mg-OH (B) and Mg-OH-AS (C) disc in mice subcutaneous region, H & E stained images of muscle tissue collected around (D) no implanted disc (control mice) (E) Mg-OH disc (non-coated) and (F) Mg-OH-AS discs (coated)...... 89

Figure 25. Schematic illustration of the laser-patterned AS coated Mg discs and screw..... 100

ACKNOWLEDGEMENTS

This dissertation is dedicated to my father (Dr. Jagannath B. Patil), mother (Mrs. Sunita J. Patil), Pillu, my family members (Abhijit, Ajit, Arati, Suchita, Amruta, Veena and Sharanya) and friends, whose endless love and encouragement have been my constant sources of support, happiness, and inspiration.

This work would not have been possible without the support of countless individuals. Special thanks to Dr. Charles Sfeir, Dr. Prashant N. Kumta, Dr. Tracy Cui and Dr. Ellen Gawalt for their ongoing guidance throughout my research. Thank you to the entire Center for Craniofacial Regeneration past and present lab members, who have not only provided research support, but immeasurable happiness. Thank you to the Department of Bioengineering, for your support over the many years. Finally, I would like to thank Dr. Elia Beniash for being a truly wonderful mentor and supporting me throughout my research endeavor.

1.0 INTRODUCTION

1.1 MUSCULOSKELETAL DISEASES AND TRAUMA

Musculoskeletal diseases and injuries are very common conditions [1]. According to the 2015 Global Burden of Disease Study, musculoskeletal disorders (including rheumatoid arthritis and others) accounted for 90.1 million deaths world-wide in 2015, an increase of 18.2 percent since 2005 [2]. Musculoskeletal disorders resulted in 21.3 percent of total years lived with disability (YLDs) globally [3]. According to the United States Bone and Joint Initiative (USBJI), more than 65.8 million treatments of musculoskeletal injuries were reported in hospital settings between 2010-2011 [4].

Due to an aging population, osteoporotic fractures and trauma to bones are the primary factors driving the United States (U.S.) market for fracture fixation products. In 2010, U.S. sales of fracture fixation products totaled approximately \$2,997.6 million and sales are expected to grow at a compound annual rate of 7.4 percent, reaching an estimated \$4,276.8 million in the year 2015 [5]. Hence, development of novel advanced bone fixation devices is required to meet the growing needs of the population.

1.2 BONE BIOLOGY AND FRACTURE HEALING

1.2.1 Bone Biology

A deep understanding of bone biology and fracture healing is required for successful treatment of bone fractures. The musculoskeletal system is composed of bone, cartilage, and other connective tissues. The musculoskeletal system supports and protects organs, facilitates movement and maintains mineral homeostasis on the systemic level. In general, bones consist of a central marrow space surrounded by cancellous bone covered by cortical bone and periosteum [6] (Fig. 1). Bone is living tissue with blood supply which plays an important role in bone growth and bone healing [7].

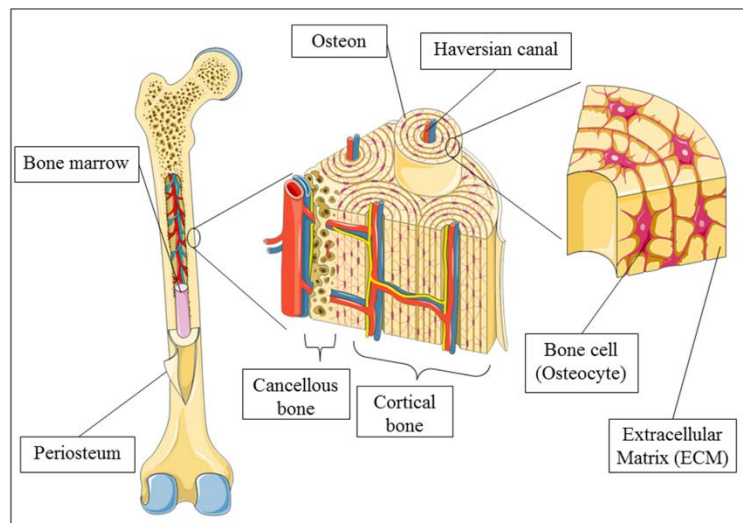


Figure 1. Schematic overview of bone structure and cellular distribution [6] [Figures were produced using Servier Medical Art by authors]

The outer surface of the cortical bone is covered with periosteum which is highly innervated and contains a population of osteoprogenitor cells [8, 9]. Bone is a highly vascularized tissue and this extensive blood supply plays an important role in bone growth and healing [7]. Bone marrow and periosteum contain mesenchymal stem cells, which serve as a source for the bone healing and bone remodeling processes.

Bone tissue is comprised of cells and the extracellular matrix. There are three major cell types found in bone. Two of them, osteoblasts and osteocytes, originate from the osteoprogenitor mesenchymal cell lineage while the third, osteoclasts, are of hematopoietic origin [10]. The bone consists of proteinaceous matrix, primarily comprised of collagen type I, calcium phosphate mineral, in the form of carbonated apatite, and water [10]. Bone is a hierarchical nanocomposite with a unique combination of fracture toughness and strength [11]. Bone forms either via endochondral or intramembranous ossification. Endochondral ossification occurs via cartilaginous intermediate whereas intramembranous ossification takes place via concentration of mesenchymal without a cartilaginous intermediate [10]. Bone remodeling is a highly coordinated physiological process of bone renewal. It involves resorption of old and mechanically weak bone by osteoclasts and deposition of new bone osteoblasts [12, 13]. Bone remodeling is essential for bone health since it replaces old and damaged bone, and maintains mineral homeostasis.

1.2.2 Bone fracture healing.

Musculoskeletal injuries, including fractures and dislocations, are very common. Typically, injury involves multiple tissues including bone, periosteum, bone marrow, blood vessels and surrounding soft tissue [14]. The healing of fractured bone is a complex process encompassing

biological and mechanical aspects as shown in figure 2. The healing process involves the following four stages: inflammation, soft callus formation, hard callus formation and bone remodeling [15]. During the inflammation stage, a hematoma forms and activated platelets release cytokines. Later, the hematoma is gradually replaced with granulation tissue.

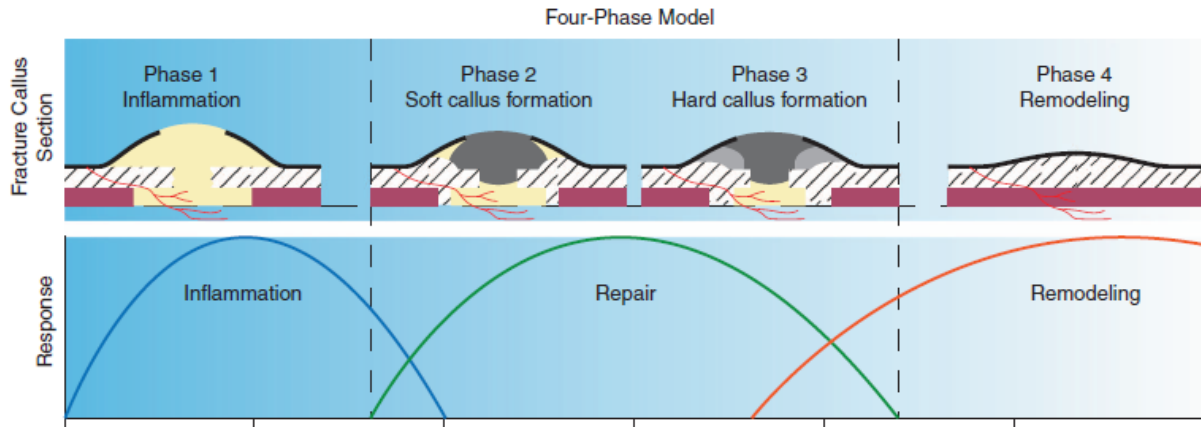


Figure 2. Schematic of the four-phase model for bone fracture healing [15] (Yellow- granulation tissue; dark gray- fibrous tissue, light gray - cartilaginous tissue, dashed - bone).

In the soft callus formation stage, progenitor cells migrate to the site of injury and deposit fibrocartilage. At the hard callus stage, the soft callus is replaced by woven bone. Finally, through the remodeling process, woven bone is replaced by mechanically strong and highly organized cortical bone. The natural bone healing process can repair relatively small defects. However for larger and more complex fractures, clinical intervention is necessary.

1.2.3 Surgical fixation of fracture

Fractural treatment involves the use of non-operative techniques, i.e. splints and casts, or stable internal fixation implants. The internal fracture implants help to achieve the reduction of bone without formation of malunion or nonunion [16].

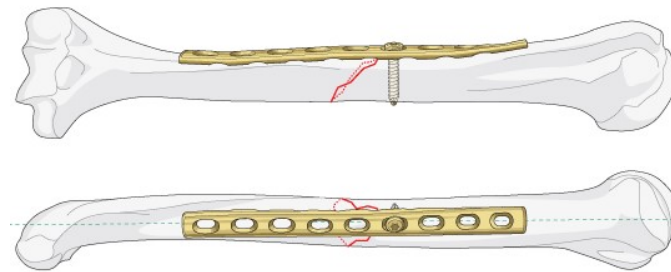


Figure 3. Schematic of humeral shaft bone fracture with fixation plate and screw [17]

The internal fracture implants provide relative stability and allows interfragmentary movement that can stimulate callus formation [18] One such example of humeral shaft fracture fixation with plates and screw is shown in figure 3. Generally, these fracture fixation implants are made up of biocompatible but non-degradable metals such as stainless steels or Ti alloys [19, 20]. Once placed in the body, these devices can be left there even after the defect is fully healed or removed. Both scenarios can be problematic. Leaving the device in situ can lead to fracture, bacterial infections and in the case of children the devices have to be removed to allow for continuing growth. On the other hand removal of the device can cause additional pain and suffering to the patient, causing complications such as bacterial infection and scar tissue formation placing additional pressure on the healthcare system.

1.3 NON DEGRADABLE IMPLANT MATERIALS

1.3.1 Non degradable metals

Metallic internal fixation implants are generally made from stainless steel, titanium and more. Recently, titanium alloys, cobalt-chromium alloys and zirconium alloys have been used. These materials have sufficient mechanical strength and excellent biocompatibility. There are several differences between titanium and stainless steel. The modulus of elasticity of Ti and its alloys is low compared to stainless steel [21]. As opposed to stainless steel, a thick oxide layer forms on Ti surfaces in contrast to stainless steel. This layer helps to better integrate the Ti devices into bone when compared to stainless steel [22]. In certain instances, fibrous tissue has been observed around the stainless steel implants [23]. Some of the impurities in stainless steel (cobalt, chromium, nickel and iron) have toxic effects on human health [24] Hence titanium is considered safer and more biocompatible than stainless steel [25]. Apart from implant material, other factors such as surface topography, surface modifications (coatings) and mechanical properties are also considered in the implant design in order to achieve better clinical outcomes.

1.3.2 Need for non-degradable metallic implant removal

Permanent metallic fixation devices are widely used as outlined above. They are typically left in the body after the healing process is complete. However, when left *in situ*, they can cause a number of problems, such as stress shielding, which can lead to implant failure and injury [26], corrosion [27] and metal sensitivity [28] and can cause infection, discomfort and limit mobility. Because of the above complications, a second surgery is often needed to remove the metallic

implant once the bone has healed [29]. The internal fracture fixation implant removal procedure accounts for 5% of all orthopedic procedures done in the United States [30]. Decision to remove an internal fracture fixation devices is controversial [31] and there are no standard clinical guidelines to remove implants. The decision to remove an implant is taken by an orthopedic surgeon based on patients' preference, implant cost and second surgery expenses. Those who are against implant removal argue that implant removal involves several complications such as re-fracture, wound infections and nerve damage [30]. It is difficult to compare the different implant removal studies because of the different anatomical sites (upper or lower extremity or ankle joint) and different geometry of implants (plates, screws and nails). To overcome the limitations of metallic implants degradable Mg implants were tested in human in 1930 [32, 33] and biodegradable polymeric implants were introduced in 1984 [34].

1.4 DEGRADABLE IMPLANT MATERIALS

1.4.1 Biodegradable polymers

In the late 1984s, biodegradable polymeric implants were designed to overcome the disadvantages of metal-based internal fixation devices [34]. Biodegradable fixations devices made of Polyglycolic acid (PGA) and Poly-L-Lactic acid (PLLA) or their blends offer some advantages over metallic devices such as gradual load transfer to the healing tissue, eliminating the need for the hardware removal surgery, and radiolucency [35]. However, polymeric internal fixation devices lack strength [35], induce inflammatory response in certain cases [36], and have a higher failure rate than metallic devices [37]. Because of these complications use of

biodegradable polymer implant is limited. To overcome above limitations, degradable metals are currently explored as an alternative material for biomedical devices such as stent, orthopedic plate and screws and interference screw [38].

1.4.2 Degradable metals

Degradable metallic implants were first proposed for use more than 100 years ago in orthopedic and cardiovascular application to overcome the drawbacks of permanent metallic devices. In recent years, degradable metallic implants have become a very active area of research [39-41]. Mg has a number of advantages that make it an attractive choice as a material for resorbable implants. It is lightweight and its density and mechanical properties match those of bone tissue [42]. Mg can readily corrode in the body and these implants can be completely absorbed by the body in a matter of months. The first reports of Mg use in medical devices appeared in the nineteenth century [40]. However, these early attempts to use Mg metal in orthopedic fixation devices were unsuccessful due to the gas pocket formation. Hydrogen (H₂) gas is a product of Mg corrosion and accumulates around corroding Mg devices leading to the formation of gas pockets. H₂ is produced at a high rate, especially during the initial corrosion phase. This high rate of production happens before solid corrosion products, which play a passivating role, are formed on the metal's surface. In the 1930s, McBride evaluated Mg devices in humans [32]. He did not notice any toxicity of Mg. However, he reported formation of large gas pockets around the devices. More recently, Witte et al. confirmed that Mg metal is non-toxic. They also found it to have osteoinductive properties [42, 43]. Still to this day gas pocket formation around devices remains the major limitation for use of Mg and its alloys [44]. Hence, in order to use Mg metal in orthopedic implantable devices, it is necessary to control its corrosion rate. Various methods

including metal processing, new Mg alloy development and new coating technologies are currently being investigated as potential means to control corrosion rate [45-48].

1.5 CORROSION CONTROL OF MG AND ITS ALLOYS

A number of different strategies were used over the years to control the *in vitro* and *in vivo* corrosion rate of Mg. These strategies can be broadly divided into three categories such as metallurgical (increasing purity of Mg and adding alloying elements), surface modification and surface coating.

1.5.1 Alloying

The addition of a rare earth elements (RE) to alloys is the primary method to improve the mechanical strength and corrosion resistance of Mg [49]. Several Mg alloys have been developed with improved corrosion resistance and mechanical properties matching to bone [50]. Many alloys such as LAE442 [42, 51], ZEK100 [52, 53], ZX50 [54, 55] were developed specifically to overcome the limitations of fast corroding pure Mg. However, some alloys degrade inhomogeneously [56] and gas pockets are still formed around the implant. The rare earth elements can leach out and produce detrimental effects on surrounding tissue [52]. Many alloying elements such as nickel and beryllium are toxic [57] which limits their use. The long term toxic effects of REs on human body are well documented[58], and they should be used cautiously in the development of new Mg alloys for medical applications [59, 60]. Development of new Mg alloys is also challenging because of poor solubility of alloying elements in Mg [61].

Due to the challenges and limitations of alloying approaches, surface modifications of Mg are often used as alternative approaches to Mg corrosion control. These surface modification techniques include passivation of Mg and its alloys by metallurgical techniques, such as heat treatment, hot rolling conducted under controlled reactive atmospheres, plasma treatment and others [62, 63].

Another group of techniques commonly used to control Mg corrosion is surface coating. Surface coating methods can be broadly divided into two classes: conversion coating and deposition coating [61].

1.5.2 Conversion coatings.

Conversion coating involves formation of an insoluble layer on Mg substrate either by chemical or electrochemical reaction that converts Mg metal on the surface into Mg salts or oxides. The insoluble layer acts as a barrier to solution diffusion towards Mg substrate and can slow the corrosion rate. Mg oxide (MgO) [64, 65], Mg hydroxide (Mg(OH)₂) [64, 65] and Mg fluoride (MgF₂) [66, 67] are examples of conversion coatings. Witte et al. reported a decrease in the corrosion rate of LAE442 alloy coated with MgF₂ in a rabbit model [68]. Ye et al. also showed that MgF₂ treatment improved corrosion resistance and *in vitro* biocompatibility of Mg-Zn-Zr alloy [67]. However, Thomann et al. reported that MgF₂ coating did not decrease the corrosion rate or improve mechanical strength during a three-month study in a rabbit tibia model [69]. Many factors influence the quality of a conversion coating such as surface composition of the substrate, pretreatment processes, composition of conversion coating solution and operational parameters (pH, temperature and immersion time) [70]. It is important to control most of the

above factors while forming conversion coating. One of the disadvantages of oxide coatings is that they are unstable at a higher pH and dissolved as corrosion proceeds [71].

1.5.3 Deposition coatings

Deposition coating involves formation of a physical coating layer on Mg substrate. Often this layer is formed using organic materials such as synthetic [72] or natural polymers [73], silanes [74, 75] and ceramic materials such as calcium phosphate [76].

1.5.3.1 Polymer coatings

Biodegradable polymers have long been used in biomedical applications such as regenerative medicine, medical device manufacturing and drug delivery [77]. Biodegradable polymers are widely used in clinical applications. They possess numerous advantages including biocompatibility and processability. Synthetic biodegradable polymers [78] such as polylactic acid (PLA), polycaprolactone (PCL) and polylactic-co-glycolic acid (PLGA); and natural polymers [79] such as a polysaccharide (Chitosan and Alginate) and proteins (Collagen and Gelatin) were used to control corrosion of Mg and its alloys. Coating with degradable polymers can slow down Mg corrosion but poor adhesion of polymers to Mg substrate hinders its long-term effect of corrosion control [79, 80]. It was suggested that polymer coating alone is not an effective anticorrosion strategy and a polymer hybrid coating system can lead to a better corrosion control [78]. Recently, Johnson et al. [81] used a hybrid composite system formed by mixing hydroxyapatite (nHA) with PLA, PLGA or PCL. They found that nHA/PCL provides effective corrosion protection.

1.5.3.2 Calcium phosphate coating

Deposition of calcium phosphate has been extensively studied in the orthopedic biomaterial field because calcium phosphate coated materials have shown excellent osteointegration [82]. However, deposition of calcium phosphate coatings on Mg substrates is a technologically challenging process and only limited success was achieved in development of these coatings[83]. Experiments with calcium phosphate deposition from SBF produced a highly porous coating with poor anticorrosive properties [84].

In another study, the sol-gel approach was followed by heat treatment to densify the coating layer [61]. There are numerous challenges in producing anticorrosive calcium phosphate coatings. One of the important parameters of the phosphate coatings is thickness, which depends on multiple difficult-to-control parameters. Batch to batch variations in the coating thickness were observed [85]. Adhesion of calcium phosphate to Mg substrate is based on a physical anchorage rather than chemical interactions and depends on the surface roughness of a substrate making it susceptible to delamination during clinical use [83]. The majority of the studies of calcium phosphate coatings were performed *in vitro*. There are only a few studies looking into the *in vivo* performance of calcium phosphate-coated Mg [86]. Overall, although calcium phosphate coatings offer some advantages, the challenges outlined above hinder their use in biomedical applications.

1.5.3.3 Silane coating

Silane coupling agents initially were used as adhesion promoters of polymeric resins to substrates such as glass and silica [87, 88]. Various silane coupling agents have been used for corrosion control of metals since early 1990 [89]. Chou et al. used organic-inorganic hybrid coatings prepared by mixing tetraethylorthosilicate (TEOS) and 3-

Methacryloxypropyltrimethoxysilane (MPS) on steel and showed that the derived hybrid coating significantly enhances the corrosion protection of stainless steel [90]. Numerous studies demonstrated good anticorrosive properties of silane coatings on Mg, although all of these studies were performed *in vitro* [91-96].

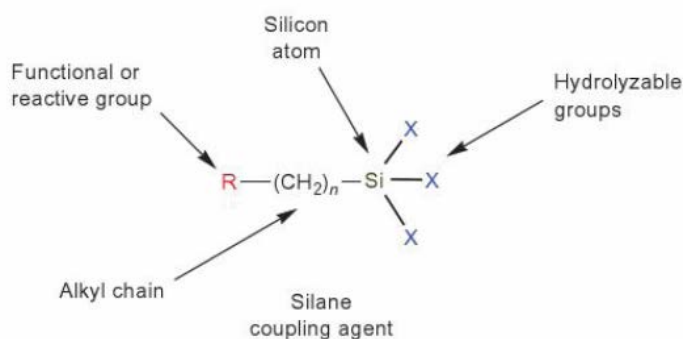


Figure 4. The general structure of an alkylsilane coupling agent [97].

1.6 ALKYL SILANE CHEMISTRY

Alkylsilanes (AS) are a class of organosilane molecules widely used in materials synthesis. AS is a monomeric silicon based molecule attached to the hydrolysable group on one end and a nonhydrolyzable organic moiety on the another end as shown in figure 4 [97].

The hydrolysable groups are alkoxy moieties such as methoxy or ethoxy which can react with a hydroxyl group to form methanol or ethanol. After hydrolysis AS molecules become amphiphils, comprising an aliphatic tail and a hydrophilic silane head (Figure 5). The hydrolyzed form of AS can covalently bind to a substrate containing surface hydroxyl groups. These

compounds self-assemble into a multilayered structure comprising 3-4 nm thick layers. These structures are eventually cross-linked, forming polysiloxane planar networks (Figure 6) [98]. They can be spin coated or dip coated onto a substrate where they form thin self-assembled multilayered films [99]. There are several advantages to this technology: **1)** The system is highly tunable. The thickness of the coating and its mechanical properties can be controlled. For example, by using AS with UV cross linkable groups one can increase their stiffness by simple exposure to UV [99] which might be beneficial for coatings of orthopedic screws. On the other hand, copolymerization of AS with tetramethoxysilane (TMOS) will produce more flexible liquid like coatings [100, 101], which might be useful for cardiovascular applications. Furthermore, the surface of the coating can be functionalized by crosslinking with silanes with different active groups such as amines, carboxyls, thiols or hydroxyls; **2)** It is a very simple method utilizing inexpensive commercially available chemicals. **3)** The chemicals used are biologically inert, which should make it easier to get through the FDA approval process.

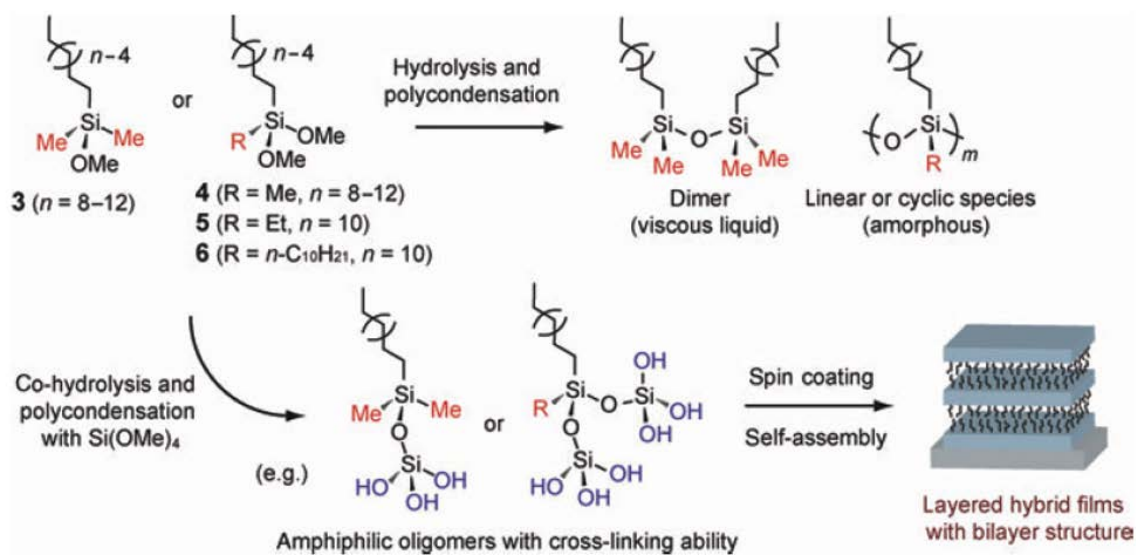


Figure 5. Schema of the coating process: hydrolysis and polycondensation reaction of alkyldimethylsilyl methoxides and self-assembly upon spin coating [102].

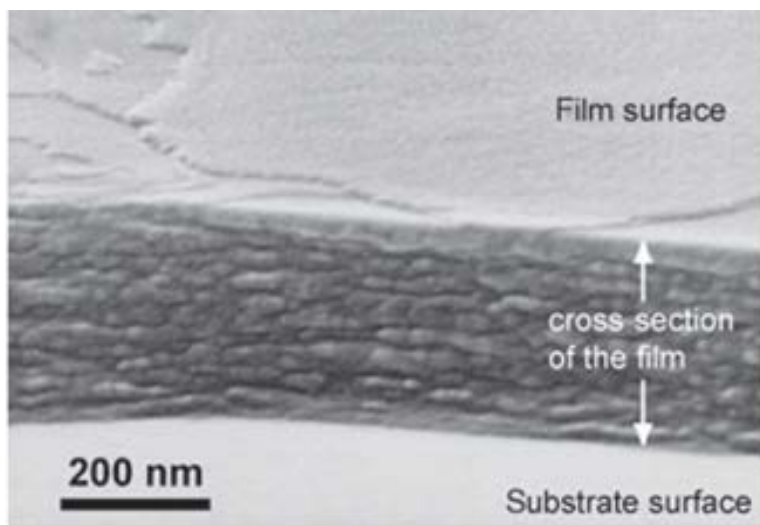


Figure 6. SEM micrograph of the amphiphilic alkyldimethylsilyl methoxide coating comprised of self-assembled multilayers [99].

In this work, we will investigate the application of AS coatings to regulate Mg corrosion. We anticipate that this approach will overcome the challenges facing other approaches described above. AS-based anti-corrosive coatings for Mg devices have a number of advantages including tunable coating chemistry and the ability to use silane chemistry for biological molecule attachment, as well as cytocompatibility and biocompatibility.

1.7 DEGRADATION MECHANISM OF ALKYL-SILANE COATINGS

Understanding of the mechanisms of AS coatings degradation *in vivo*, and how the degradation products are metabolized and cleared from the body is extremely important. This question, however, is beyond the scope of this study. There are several literature reports which shed light on the potential degradation. Garrido et al. investigated the degradation products of polysiloxane (silicones) emulsion injected in subcutaneous pocket of a rat by ^{29}Si NMR study [103]. They found polysiloxane, hydrolyzed silicone, silica gel and high coordinated silicone complexes in the rat tissue. One possible reason for the formation of various silicone functional groups is the substitution of methyl groups with hydroxyl groups. This study confirmed that polysiloxanes are not inert and degrade when implanted *in vivo*. Xu et al. detected linear molecule such as dimethylsilanediol ($\text{Me}_2\text{Si}(\text{OH})_2$) in plasma samples of workers exposed to methyl siloxanes but not in a control group or indoor air and dust samples [104]. This observation indicates that $\text{Me}_2\text{Si}(\text{OH})_2$ is formed in the human body by breaking down large polysiloxanes molecule. Similar results have been observed in a rat study where octamethylcyclotetrasiloxane showed high pulmonary and hepatic clearance along with higher metabolizing enzyme activity at high

levels of siloxane [105] . The above studies indicate that polysiloxane can be cleaved into oligomers and finally into monomers and secreted outside the living system [106].

Human and animal studies suggest that Si-alkyl cleavage is achieved via reactions shown in Figure 7 [106]. Initial enzymatic oxidation occurs at the methyl or alkyl group, followed by the migration of a silyl group from carbon to oxygen, referred to as Brook rearrangements, and hydrolysis of the alkoxy silane formed.

There is a possibility that some of the AS degradation products will linger in the body for extended periods of time. However, since AS coatings are micron thin, the total amount of AS around a resorbable device is negligible and we do not anticipate any adverse effects associated with the coatings. The results of our *in vivo* studies, outlined in Section 6, did not reveal any adverse effects of the coating on the surrounding tissue, which supports this notion. Future studies using analytical techniques such as nuclear magnetic resonance (NMR) spectroscopy can help us understand degradation byproducts of AS coatings on Mg devices.

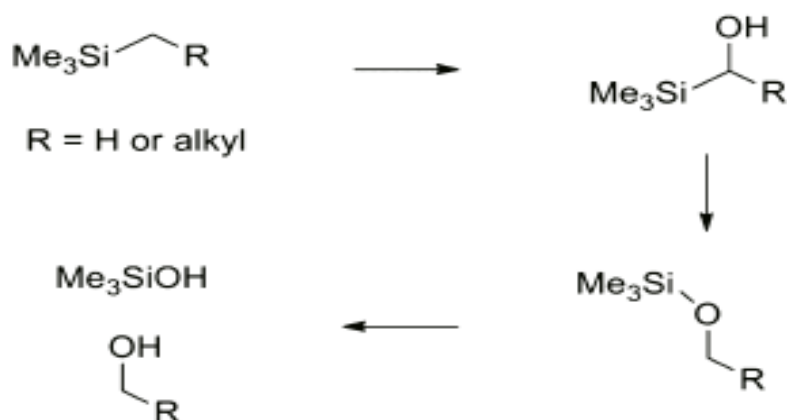


Figure 7. Alkylsilane cleavage pathways [106].

2.0 HYPOTHESIS AND SPECIFIC AIMS

The overall goal of this dissertation was to use hybrid self-assembled AS nanostructured coatings to control the corrosion rate of Mg and its alloys. The AS coating should satisfy some or all of the following design parameters: 1) Regulate the rate of metal resorption by forming a passivating layer on the metal surface; 2) Facilitate better integration of implants into the target hard tissue; 3) Promote new bone formation at the implant interface. **We anticipate that this work will lead to the development of better coating strategies for resorbable orthopedic implant devices.**

2.1 HYPOTHESIS

The central hypothesis of the dissertation is that self-assembled multilayer AS coatings will control the corrosion rate of Mg and its alloys and AS coatings will be cytocompatible and nontoxic. To test this hypothesis, we propose three experimental aims. In the first aim, we will develop a method of AS layer deposition on the Mg surface and explore the feasibility of surface functionalization of this layer. Several characterization techniques will be used to characterize the coating. The ability of the coatings to regulate Mg corrosion will be thoroughly tested. In the second aim, we will study the cytocompatibility of AS layer coating in an *in vitro* tissue culture

model. In the third aim, we will evaluate the anticorrosive properties and toxicity of AS coatings *in vivo* in a mouse subcutaneous model.

2.2 SPECIFIC AIMS

2.2.1 Specific Aim 1

It is important to precisely regulate degradation rates of resorbable devices in order to ensure their safety and efficiency. Alkylsilane and organic coatings have been used for number of biomedical applications [107-110]. The overarching goal of this study is to use self-assembled multilayer AS coatings to control the corrosion rate of degradable Mg and its alloys. It is challenging to design such a coating under a dynamic corroding environment.

Specific Aim 1 is to develop self-assembled multilayer AS coatings on Mg and its alloys.

We hypothesize that AS coatings will reduce the corrosion rate and will be amenable to further surface modifications.

Specific Aim 1 is to develop self-assembled multilayer AS coatings on Mg and its alloys.

We hypothesize that AS coatings will reduce the corrosion rate and will be amenable to further surface modifications.

Aim 1A: In this sub aim, self-assembled multilayer AS coating will be formed on Mg and its alloys. The quality of the coating will be confirmed by various physio-chemical characterization techniques such as scanning electron microscopy (SEM), Attenuated Total Reflectance Fourier Transform Infrared spectroscopy (ATR-FTIR), contact angle measurement and others.

Aim 1B: In this sub aim, we will functionalize the surface of AS coatings with (3-Aminopropyl) triethoxysilane (APTES) or silane-maleimide molecules. This surface functionalization can be used to change the surface properties of AS coatings, such as wettability, or to further functionalize it with a bioactive molecule.

Aim 1C: In this sub aim, the ability of of the self-assembled multilayer AS coating to regulate the rate of Mg corrosion will be studied using H₂ release and potentiodynamic polarization assays.

Aim 1D: In this sub aim, we will test the hypothesis that Mg device corrosion can be further regulated by selective removal of a portion of the AS coatings. This can potentially allow for the fine tuning of the corrosion rate of Mg devices.

Aim 1E: In this sub aim, we will assess the feasibility of use in the self-assembled multilayer AS coatings as a drug release system.

2.2.2 Specific Aim 2

Several *in vitro* direct cell culture studies on Mg and its alloys showed adverse effect of rapid corrosion on cell [111-114]. The reason for this adverse effect is a rapid increase in pH and osmolality of cell culture medium around the corroding device [113]. **We hypothesize that AS coatings will eliminate such adverse effects by regulating the corrosion rate of Mg and its alloys.** At the same time, it is important to assess toxicity and cytocompatibility of AS coatings. We will study cytocompatibility of AS coating in an *in vitro* tissue culture model. **We hypothesize that AS coating will be cytocompatible and further functionalization of AS coatings with APTES molecule will enhance cell attachment to the AS coatings.**

Aim 2A: In this sub aim, we will assess cell adhesion to AS-coated Mg discs on cell adhesion and cytoskeletal arrangement of MC3T3 cells. We will further study the effects of APTES functionalization of AS coatings on the cells.

Aim 2B: In this sub aim, we will assess the cytocompatibility of coatings using cell proliferation and cell viability assays.

2.2.3 Specific Aim 3

The third aim is to evaluate anticorrosive properties and toxicity of the self-assembled multilayer AS-coated Mg discs in a mouse subcutaneous model. **We hypothesize that AS coatings will control the corrosion rate of Mg and it will not be toxic to the tissues surrounding the implants in a mouse subcutaneous model.**

Aim 3A: In this sub aim, the *in-vivo* corrosion rate of AS-coated Mg discs will be measured by visual observations of the diameter of gas pocket formation around the implantation site over six weeks. As another measure of corrosion rate, percentage weight loss of non-coated and AS-coated Mg discs will be measured at the end of the experiment.

Aim 3B: In this sub aim, surface topography of the Mg discs after six weeks of implantation will be studied by micro-computed tomography (μ CT) and surface profilometry.

Aim 3C: In this sub aim, we will study the toxic effect of AS coatings on muscle tissues surrounding implants in a mouse subcutaneous model over a six-week period using histological methods.

3.0 ANTICORROSIVE SELF-ASSEMBLED HYBRID ALKYL-SILANE COATINGS FOR RESORBABLE MAGNESIUM METAL DEVICES.

3.1 ACKNOWLEDGMENTS

The authors gratefully acknowledge the financial support of NSF-ERC, Grant # EEC-0812348 (E.B., P.N.K.) and the Swanson School of Engineering Undergraduate Summer Research Program (O.J.). P.N.K would like to acknowledge the Edward R. Weidle in Chair Professorship Funds and the support of the Center for Complex Engineered Multifunctional Materials (CCEMM) in the Department of Bioengineering, Swanson School of Engineering, University of Pittsburgh for providing funds towards the acquisition of equipment to support the research. The work presented in this chapter has been published in ACS Biomaterials Science & Engineering [115]. We thank John Holmes and Thorin Tobiassen from the Swanson Center for Product Innovation of the Swanson School of Engineering for aiding in the preparation of the samples, Jonathan Franks from the Center for Biological Imaging of at the University of Pittsburgh, Mr. Cole M. Van Ormer from the Department of Mechanical Engineering and Materials Science of the Swanson School of Engineering for providing their expertise in Scanning Electron Microscopy and Mr. Akhil Patel from the Department of Pharmaceutical Sciences, School of Pharmacy, University of Pittsburgh for his help in confocal microscopy.

3.2 ABSTRACT

Magnesium (Mg) and its alloys are promising candidates for use as resorbable materials for biomedical devices which can degrade in situ following healing of the defect, eliminating the need for second surgery to remove the device. Hydrogen gas is the main product of magnesium corrosion and one of the limitations for use of Mg devices in the clinic is the formation of gas pockets around them. One potential solution to this problem is reducing the rate of corrosion to the levels at which H₂ can diffuse through the body fluids. The study's aim was to evaluate the potential of hybrid self-assembled multilayer AS coatings to reduce Mg corrosion and to modify physicochemical properties of the coatings using surface functionalization. The coating was made by co-polymerization of n-Decyltriethoxysilane and Tetramethoxysilane followed by dip coating of metal discs. This resulted in a formation of homogeneous, micron thick, and defect free coating. The coated surface was more hydrophobic than bare Mg, however, functionalization of the coating with 3-Aminopropyltriethoxysilane reduced the hydrophobicity of the coating. The coatings reduced several folds the rate of Mg corrosion based on the H₂ evolution and other assessment methods and effectively prevented the initial corrosion burst over the first 24 hours. *In vitro* tissue culture studies demonstrated cytocompatibility of the coatings. These results reveal excellent anticorrosive properties and good cytocompatibility of the hybrid AS coatings and suggest great potential for use of these coatings on resorbable Mg devices.

3.3 INTRODUCTION

Magnesium is a great candidate for use in resorbable devices because of its light weight, mechanical properties closely matching natural bone, low toxicity and high corrosion characteristics [45, 116]. Moreover, Mg^{2+} can activate osteogenic differentiation and promote bone formation[117-120]. Attempts to use Mg as a biomaterial trace back to the 19th century when several physicians and surgeons were experimenting with Mg for orthopedic, cardiovascular and other applications[40]. However, these initial attempts faced limitations since the corrosion reaction of Mg produces H_2 leading to the formation of gas pockets around the device and increases the pH thus significantly limiting the applicability of Mg in the biomedical field[40]. Furthermore, fast, uncontrolled degradation can also lead to premature resorption of the devices. In the last couple of decades, a renewed interest in the biomedical use of Mg has developed, with researchers around the world trying to overcome these obstacles. There are two major approaches for control of Mg degradation rate, namely developing new alloys with desirable corrosion properties[121, 122] and use of anticorrosive coatings[61]. In addition to corrosion regulation, coatings can be used as controlled release systems [123, 124] and surface modifications of the coatings with bioactive molecules can improve tissue regeneration around coated devices[125, 126]. A number of different chemistries are used for anticorrosive coatings, including organic polymers[127, 128], inorganic minerals [68, 129], peptides[130] and polysiloxanes [74, 93, 131, 132] .

Use of aliphatic alkylsilanes (AS) provides means to introduce structural organization into the coating through self-assembly, allowing for greater control of the coating properties and increased functionality of the coatings [98, 99, 133, 134]. ASs, and specifically alkyltriethoxysilanes (C_n TES) with general formula $C_nH_{2n+1}(SiOEt)_3$ can form self-assembled

multilayered films on solid surfaces. CnTES molecules become amphiphilic upon hydrolysis and self-assemble into multilayered films comprising 3-4 nm thick lamellae, with alkyl tails of these amphiphilic molecules forming hydrophobic cores and silane heads undergo polycondensation, leading to formation of crosslinked polysiloxane planes sandwiching the hydrophobic cores [98, 99, 133]. It is important to note here that the self-assembly of the AS films is primarily driven by the properties of the precursor molecules, the solute composition, and other properties of the precursor solution and not by the properties of the substrate [134]. The properties of the film can be modified by changing the length of the alkyl tails, by adding UV cross-linkable moieties [99] or by co-polymerizing with other siloxanes, such as tetraethoxysilane (TEOS) or tetramethoxysilane (TMOS) [98]. Furthermore, surface functionalization of these films can be achieved using well developed chemistries [135, 136]. Another advantage of these coatings is that they comprise biocompatible and biodegradable compounds such as hydrocarbons (fat) and polysiloxanes, which are widely used as biomaterials [137-140].

The aim of this study was to design anticorrosive hybrid self-assembled AS coatings for implantable Mg devices. We assessed compositional, structural and anticorrosive properties of the coatings, conducted surface functionalization of the coatings and tested cytocompatibility of the coatings *in vitro* in tissue culture.

3.4 MATERIALS AND METHODS

All the reagents were purchased from Sigma Aldrich (St. Louis, MO, USA) and used as received unless otherwise stated.

3.4.1 Metal sample preparation.

Six mm diameter discs were stamped from 1 mm thick Mg (99.9 % purity) and AZ31 alloy (96% Mg, 3% Al, and 1% Zn) sheets (Alfa Aesar, Ward Hill, MA, USA) and polished with 1200 grit (5 μ m) MicroCut® SiC abrasive discs (Buehler Inc., Lake Bluff, IL, USA). We used Dr. Witte's protocol [141] to Etch Mg samples, in brief, the polished discs were then etched in etching solution comprising 20 ml 85% Glycerol, 5 ml 65% HNO₃ and 5 ml glacial acetic acid for 60 seconds, . Chemical etching was done to remove debris, impurities and the oxide layer from the surface of the metal and to smooth the scratches introduced during polishing. Etched discs were sonicated in acetone for 30 minutes and stored under vacuum until further use. Prior to the AS coatings, a thin uniform hydroxide layer was formed on the discs by immersion in 3.0 M sodium hydroxide (NaOH) solution for 2 h. In addition to the passivating properties, MgOH₂ provides a surface for covalent binding of the silanes to the metal surface as described elsewhere [132, 142, 143].

3.4.2 Synthesis and deposition of self-assembled multilayer AS coating on Mg and Mg alloys

Self-assembled hybrid AS films on Mg and AZ31 alloys were prepared by a dip-coating technique as described elsewhere [98, 99, 133]. The precursor solution was prepared by mixing 0.25 ml (0.73 mM) n-Decyltriethoxysilane (DTEOS) (Alfa Aesar, Ward Hill, MA, USA), 0.43 ml (2.92 mM) Tetramethoxysilane (TMOS) (Alfa Aesar, Ward Hill, MA, USA), 2 ml (0.032 mM) of Ethanol and 0.25 ml 0.010 mM HCl (aq.). The precursor solution was stirred for 24 h at room temperature to induce hydrolysis of DTEOS and TMOS. Mg or AZ31 alloy discs

passivated with NaOH were dip coated in the solution for 1 minute and dried in air for 10 minutes at room temperature. The discs were then subsequently dried in an incubator at 37°C for 24 h for removal of any trace amount of organic solvents.

3.4.3 Functionalization of the coatings.

For functionalization with 99% pure 3-Aminopropyltriethoxysilane (APTES), a following solution was prepared: 0.25 mL of 0.01 M HCl was added to a mixture of 2.0 ml ethanol (EtOH) and 0.43 ml APTES solution. This precursor solution was stirred for 24 h at room temperature prior to functionalization. The AS coated samples were then dipped in the APTES solution at room temperature for 1 minute and dried in air for 10 minutes at room temperature. The disc was subsequently dried in an incubator at 37°C for 24 h for removal of any trace amount of organic solvents.

Four groups of samples were used in this study as follows:

- Polished and etched Mg and AZ31 discs (Mg, AZ31)
- NaOH treated Mg and AZ31 discs (Mg-OH; AZ31-OH),
- AS coated NaOH treated Mg and AZ31 discs (Mg-OH-AS; AZ31-OH-AS)
- APTES functionalized AS coated Mg and AZ31 discs (Mg-OH-AS-APTES; AZ31-OH-AS-APTES).

3.4.4 Scanning Electron Microscope (SEM) characterization.

The surface morphology of the uncoated and AS coated Mg and AZ31 discs were studied using JSM-6330F (JEOL, Peabody, MA, USA) SEM at 3.0-20.0 kV operating voltage and the working

distance of 10 mm. All samples were sputter-coated with gold prior to SEM using Cressington sputter coater 108 auto model (Cressington Scientific Instruments Ltd, Watford, United Kingdom). The elemental composition of the non-coated and coated samples were analyzed using energy dispersive X-ray spectroscopy (EDS) in SEM. EDS INCA analysis system (Oxford Instruments, Oxfordshire, UK) equipped with a beryllium-window protected Si (Li) detector was used for the elemental analysis at the operating voltage of 15 kV.

To assess the thickness of the coating a several micron deep trough was created in some samples using the focused ion beam milling (FIB). The ion milling and imaging was done on a FEI SCIOS Focused Ion Beam/Scanning Electron Microscope dual beam system with gallium ion source (Thermo Fisher Scientific, Waltham, MA, USA). Au/Pt depositions were carried out before the ion milling to protect the coating from the gallium ion beam.

3.4.5 Atomic Force Microscopy (AFM) characterization.

High resolution AFM was used to assess the thickness of individual lamellae by scanning the surface of AS coatings deposited on AS coated Mg films deposited on glass substrates (generous gift from Dr. Sergey Yarmolenko, NCAT, Greensboro, NC). Use of Mg films instead of polished discs significantly reduced the roughness of the samples, allowing high resolution AFM imaging of the samples. The AFM analysis was carried out using a Veeco Dimension V scanning probe microscope (SPM) controlled by a Nanoscope V controller (Bruker Corporation, Billerica, MA, USA). Tapping mode was employed with an AFM probe of 58 – 80 kHz nominal resonance frequency and ~3 N/m spring constant. The acquired images were flattened using the Nanoscope V software. Measurements were carried out on the flattened images.

3.4.6 Attenuated total reflectance Fourier transform infrared (ATR-FTIR) spectroscopy characterization.

The AS coatings on the Mg and AZ31 substrates were analyzed by Vertex-70 ATR-FTIR (Bruker Optik GmbH, Ettlingen, Germany) using a diamond Miracle ATR accessory (Pike Technology, WI, USA). Spectra were obtained at 4 cm^{-1} resolution averaging 120 scan in the $400\text{-}4000\text{ cm}^{-1}$ frequency range.

3.4.7 Contact angle measurement.

The wettability of the AS coated Mg and AZ31 discs were assessed by the sessile drop (5 μl , Milli-Q water) contact angle measurement using VCA 2000 Goniometer (AST Products, Billerica, MA, USA).

3.4.8 *In vitro* corrosion analyses.

The corrosion resistance of AS coated Mg and AZ31 discs was measured using hydrogen evolution method, weight loss assessment and electrochemical corrosion tests.

Hydrogen evolution test The H_2 evolution was measured in a simulated body fluid (SBF) pH 7.2, prepared according to a published formulation by Kokubo[144] (Supplementary Table 1), at room temperature over 24 hrs and 7-day period. Each sample group was prepared in triplicate and the samples were immersed in SBF. A glass graduated measuring cylinder was placed over the samples in a glass beaker to collect the released gases (Supplementary Figure 1). The experiments were carried out for 1 week and the solution was changed on day 2, 4 and 6.

The ratio of solution volume to the total surface area of the tested samples was kept above 6.7 to mimic in-vivo degradation behavior of Mg [130, 145, 146]. The SBF level in each beaker was maintained constant throughout the study to avoid evaporation effects affecting the validity of the measurements.

Weight loss analysis. The mass loss analysis after 7 days of degradation in SBF at room temperature was performed according to ASTM G1 standards and works by Lorking [147] and Bobe et al. [148]. Prior to corrosion experiments all the samples were weighted using a microbalance Mettler Toledo XPE26 (Mettler Toledo, Columbus, OH, USA). After experiments the corroded sample discs were removed from SBF and placed in a beaker containing an aqueous solution of CrO_3 at a concentration of ~ 180.0 g/L. The beaker was sonicated for 10 min to remove the corroded products in the chromic acid solution. The chromic acid solution was changed between samples to ensure complete removal of the corroded products. After chromic acid cleaning, the sample discs were rinsed with deionized water followed by absolute ethanol. The sample discs were completely dried in a vacuum desiccator overnight and weighed. The percentage weight change was calculated for all the samples.

Electrochemical corrosion test. Electrochemical measurements of the non-coated Mg and AS coated Mg and AZ31 alloy samples were performed using a CH604A electrochemical workstation (CH Instruments Inc, Austin, TX, USA). All the samples were prepared as described above (sections 2.1. and 2.2.); one side of each sample disc was connected to an electric wire with conductive silver-containing epoxy and then electrically insulated with an epoxy resin, such that a working area of 0.283cm^2 was exposed to the electrolyte for electrochemical testing. A platinum wire was used as the counter electrode and an Ag/AgCl electrode (4.0 M KCl, Accumet, Fisher Scientific, MA, USA) as the reference electrode. Electrochemical

measurements were carried out in a three neck water circulated jacket flask (Ace Glassware, NJ, USA) filled with 120 ml of SBF and maintained at room temperature. Each sample was immersed in the SBF and then the stable open circuit potential (OCP) was monitored for 10 min., before starting the potentiostatic polarization test at a scan rate of 1.0mV s^{-1} . The CHI 604A software program was used to perform the analysis and plot the data. The corrosion current density (I_{corr}) and corrosion potential (E_{corr}) were determined by the Tafel extrapolation method [149, 150].

3.4.9 Cell culture experiments and cytocompatibility tests.

Tissue culture experiments on AS coated Mg discs. MC3T3 cells were seeded on Mg-OH-AS and Mg-OH-AS-APTES discs (n=3 per group) with the seeding density of $10,000\text{ cells cm}^{-2}$ and cultured for 15 days in phenol red free α -MEM medium (Catalog number: 41061-029, Thermo Fisher Scientific, MA, USA) supplemented with 10% FBS and 1% penicillin/streptomycin at 37°C and 5% CO_2 . The medium was changed every 3 days. After 15 days, cells were stained with Hoechst 33342 NucBlue Live Ready Probes nuclear stain (Thermo-Fisher Scientific, Waltham, MA, USA) and ActinGreen™ 488 ReadyProbes® f-actin stain (Life Technologies, Carlsbad, CA, USA) following the manufacturer's protocols. After three washes in PBS, samples were studied using a Nikon TE2000 microscope (Nikon Instruments Inc., Melville, NY, USA) in epifluorescence mode using a DAPI filter for nuclear DNA staining and FITC filter for F-actin staining. Micrographs were captured and processed using Nikon NIS Elements software.

Cell density on Mg-OH-AS, Mg-OH-AS-APTES discs after 15 days in tissue culture was calculated from integrated DAPI fluorescence intensity in 3 epifluorescence micrographs per group. Each micrograph contained $53.49 \times 10^4\ \mu\text{m}^2$ ($731.42\ \mu\text{m} \times 731.42\ \mu\text{m}$) field of view. A

blue channel was isolated from RGB images using ImageJ image processing package (ImageJ, Bethesda, MD). The grayscale of each image was adjusted to minimize the background intensity. In each micrograph 10 nuclei were randomly selected and their integrated intensity values were measured. The average signal intensity per nucleus was calculated for each image, and the integrated intensities of the images were divided by corresponding average nucleus intensities, providing us with the total cell number per image. Cell density on the discs was presented as a number of nuclei per $1 \times 10^4 \mu\text{m}^2$.

Tissue culture experiments on AS coated glass coverslips. In a separate set of experiments MC3T3 cells were seeded on bare glass coverslips (CS), AS coated coverslips (CS-AS) and AS coated coverslips functionalized with APTES (CS-AS-APTES). The cells were seeded at a density of $10,000 \text{ cells cm}^{-2}$ and allowed to grow for 2 weeks in phenol red free α -MEM supplemented with 10% FBS and 1% penicillin/streptomycin at 37°C and 5% CO_2 .

The cells were counted using the method described in the previous section. In addition, the number of cells was calculated using a spectrophotometric method. The amount of DNA per coverslip was assessed on the 7th and 14th day in culture by spectrophotometric assay using NanoDrop 1000 (Thermo-Fisher Scientific, Waltham, MA, USA) in each experimental group in triplicates. The number of cells per coverslip was calculated using a conversion factor of 7.6 pg of DNA per cell [151]. Cell density was calculated as a number of nuclei per $1 \times 10^4 \mu\text{m}^2$.

AlamarBlue fluorescence assay (Thermo-Fisher Scientific, Waltham, MA, USA) was used to monitor cell viability[152]. AlamarBlue assays were conducted at first, third, seventh and 14th day in triplicates according to the manufacturer's protocol. In brief, the culture medium was replaced with 1 ml 10 % v/v almarBlue reagent in complete growth medium and the samples were incubated for 4 hrs at 37°C . After the incubation, the alamarBlue solution was collected and

replaced with regular medium and the tissue culture samples were allowed to grow till the next time point. This design allowed us to monitor the metabolic activity in individual samples over a 2-week period. Fluorescence intensity of each sample was calculated as an average of 3 separate readings measured at excitation/emission wavelengths of 530/590 nm using a Synergy H1 microplate reader (BioTek instruments, Winooski, VT, USA). The wells containing only alamarBlue solution in medium were used as controls for background fluorescence correction.

The cells grown for 1, 3, 5 and 7 days on all three experimental substrates were studied using SEM. The samples were washed twice with phosphate buffered saline (PBS), fixed in 2.5% glutaraldehyde in 0.1 M PBS (pH 7.4) for 10 minutes and washed thoroughly with 0.1 M PBS for 3x15 min. The samples were further fixed in 1% OsO₄ in 0.1 M PBS for 60 minutes and washed thoroughly with 0.1 M PBS for 3x15 min. Each sample was dehydrated in a graded ethanol series (concentrations 30%, 70% and 100%) for 3x15 min. After dehydration, samples were immersed in Hexamethyldisilazane (HMDS) solution for 15 min and subsequently air-dried overnight and sputter coated with gold prior to SEM using Cressington sputter coater 108 Auto (Cressington Scientific Instruments Ltd, Watford, UK). The SEM analysis was conducted using JSM-6330F (JEOL, Peabody, MA, USA) at 3.0-20.0 kV operating voltage and the working distance of 10 mm.

3.4.10 Statistical analysis

All the experiments were performed in triplicate for each experimental group and time point. The data were compared between groups using analysis of variance (ANOVA) followed by Tukey's multiple comparison test with 95% confidence level in Origin Pro 2015 software (OriginLabs, Northhampton, MA, USA). The data were presented as mean \pm standard deviation (S. D.).

3.5 RESULTS

3.5.1 SEM characterization.

SEM characterization of the coatings was conducted to assess the structural integrity of the AS films (Figure 8). Analysis of the polished and etched Mg surface revealed individual grains, grain boundary contours and the shallow scratch marks produced by polishing (Figure 8A).

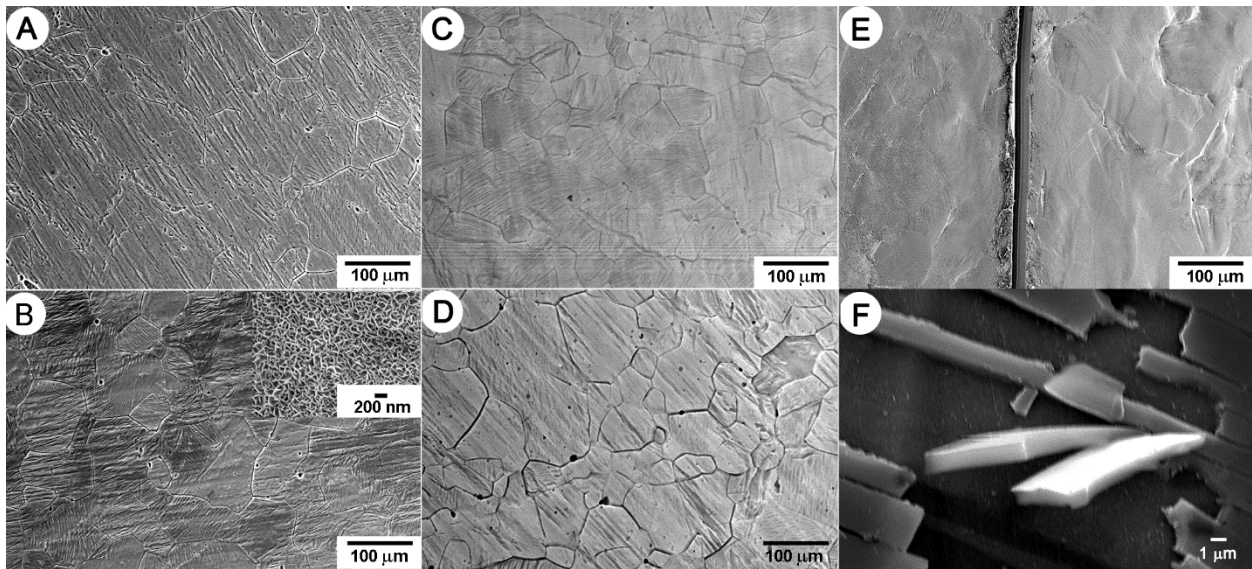


Figure 8. SEM micrographs of A) uncoated Mg, B) Mg-OH, inset shows a high magnification micrograph of a Mg-OH surface, C) Mg-OH-AS; D) Mg-OH-AS-APTES; E) low magnification Mg-OH-AS scratched surface; and F) a higher magnification image of a Mg-OH-AS scratched surface with pieces of AS coating peeling off the surface.

At the intermediate magnification, the alkali treated surface appeared very similar to the bare Mg surface (Figure 8B). However, a nano-structured hydroxide layer on the Mg surface was clearly recognizable at a higher magnification (Figure 8B'). Dip-coating procedure produces a micron

thick uniform AS film on the Mg-OH disc (Figure 8C). Interestingly, because the AS films are extremely thin, the grain boundaries of the underlying metal were clearly visible. APTES functionalized AS coated discs had similar appearance to AS coated discs (Figure 8D). The grain boundaries and scratch marks were still visible on this sample although they were less pronounced, suggesting that the coating followed the surface topography. Scratching of the AS coated samples with a scalpel did not lead to major defects of the coating away from the scratched mark (Figure 8E). Analysis of the broken coating in the scratched area allowed us to determine the thickness of the AS coating by measuring the pieces of the coating detached from the metal surface (Figure 8F). Based on this analysis the thickness was approximately 1 μm . To further assess the coating thickness a several μm deep trough was created in the coated samples using FIB. The analysis of the sample cross-sections showed that the coating is ~ 1 μm thick (Supplementary Figure 2).

3.5.2 AFM Analysis.

To assess the thickness of individual AS lamellae comprising the coating we have conducted an AFM study of the AS coated Mg films. Edges of multiple lamellae are exposed on the surface creating step like patterns (Supplementary Figure 3). By measuring the height of these steps an average thickness of the lamellae was determined to be 2.8 nm (SD=0.6; n=9) which is in a good agreement with the lamellae thickness data reported elsewhere [98, 133]

3.5.3 ATR-FTIR Analysis.

ATR-FTIR spectroscopy was used to analyze the chemical composition of the coatings on the Mg surface. Figure 9A shows the spectra of non-coated and AS coated Mg discs. Polished and etched Mg disc did not show any major absorbance peaks as expected (Figure 9A), while alkali treated discs presented a sharp peak around 3600 cm^{-1} consistent with the -O-H stretching band. The spectra of Mg-OH-AS coating reveal peaks in the $1045\text{--}1127\text{ cm}^{-1}$ that correspond to Si-O asymmetric stretching in -Si-O-Si- bond (Figure 9A). The C-H stretching in alkyl chain of DTEOS is evident around $3000\text{--}2850\text{ cm}^{-1}$. After amination with APTES, -NH₂ absorption band appeared in the $1500\text{--}1700\text{ cm}^{-1}$ region indicating the presence of amines on the surface of the coating. Results of the experiments with AZ31 samples were similar (Supplementary figure 4A).

3.5.4 Contact angle measurement.

The surface wettability of non-coated Mg, alkali treated Mg and AS coated Mg were examined by measuring the static contact angle using deionized water droplet. The contact angle of polished and etched Mg discs was approximately $58.98 \pm 11.78^\circ$ (Figure 9B). Alkali treatment of Mg surface made it more hydrophilic and significantly reduced the contact angle down to $21.62 \pm 1.87^\circ$ ($p \leq 0.05$). The static contact angle of AS coated samples was $110.60 \pm 1.05^\circ$, indicating the hydrophobic nature of these samples. The contact angle of these samples was significantly higher than both Mg ($p \leq 0.01$) and Mg-OH samples ($p \leq 0.0001$). Amination of the AS layer with APTES significantly reduced the contact angle of the surface to $67.44 \pm 22.43^\circ$ ($p \leq 0.01$), and made it similar to the bare Mg discs ($P > 0.05$). The results of contact angle analysis on AZ31 samples showed similar trends (Supplementary Figure 4B.).

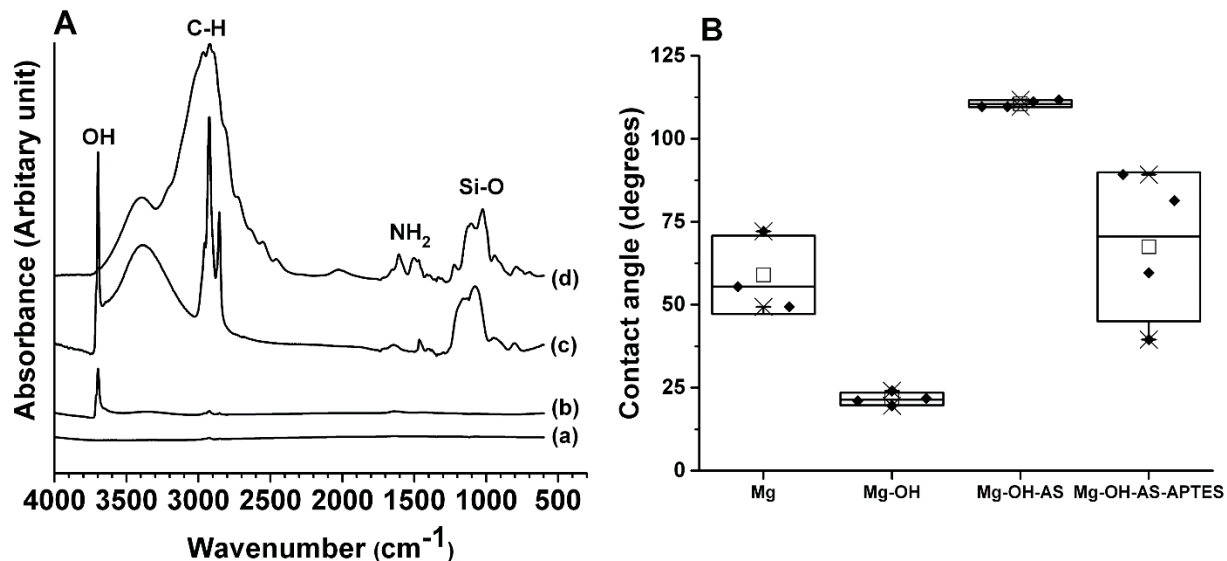


Figure 9. ATR-FTIR spectra of Mg (a), Mg-OH (b), Mg-OH-AS (c), Mg-OH-AS-APTES (d) and B) box graph of static water contact angles measured on Mg sample discs.

3.5.5 Determination of the corrosion rate by H₂ evolution and weight loss methods.

Cumulative H₂ released from the uncoated Mg discs over 7 days was ~7 fold higher than that of AS coated Mg discs; this difference was highly significant ($p < 0.0001$) (Figure 10A). The alkali treatment did not have any significant effect on the extent of corrosion over the 7 days period. The hydrogen release profiles of the Mg-OH-AS and Mg-OH-AS-APTES groups were not significantly different ($p > 0.9974$) (Figure 10A, Supplementary Table 2). Experiments with AZ31 samples yielded similar results (Supplementary Figure 5A, Supplementary Table 2). To assess the ability of the AS coating to slow down the initial burst of corrosion we have followed H₂ evolution over the initial 24 hours after immersion of the discs in SBF. The results of these experiments indicate that the AS coating reduced the initial Mg corrosion rate 5 fold from 0.16

ml/h to 0.03 ml/h effectively preventing the initial burst of corrosion (Figure 10B, Supplementary Table 2).

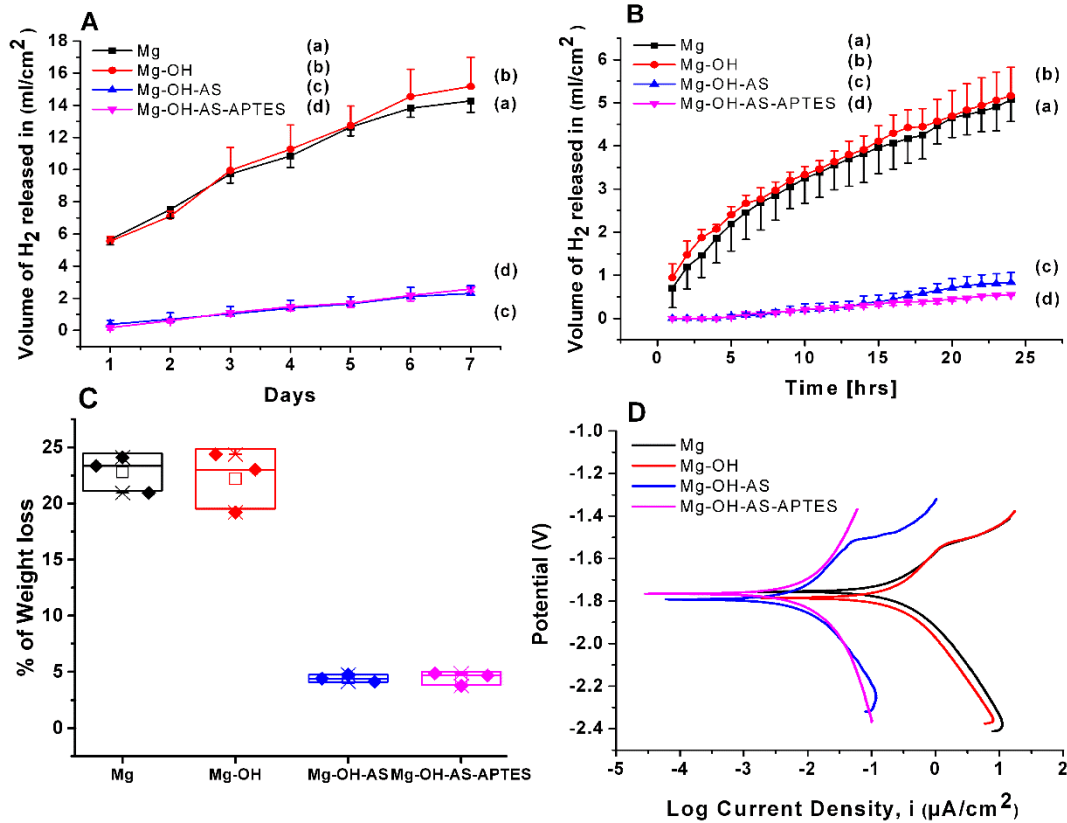


Figure 10. Cumulative hydrogen release profiles from Mg discs incubated in SBF over 7 days period (A), 24 hour period (B); C) weight loss of Mg discs incubated in SBF for 7 days; and D) Potentiodynamic polarization curves of Mg sample discs.

After the initial 24 hours, the corrosion rate of non-coated samples significantly decreased and achieved steady state (Figure 10B, Supplementary Table 2). This decrease in the corrosion rate can be potentially attributed to deposition of corrosion products, which can have a passivating effect. Nevertheless, the corrosion rate of the AS coated Mg over the following 6-

days period was 4.5 times lower than that of the bare Mg, 0.013 ml/h vs. 0.06 ml/h, (Figure 10A, Supplementary Table 2). The results of the experiments with AZ31 were very similar to those obtained with Mg (Supplementary Figure 5B, and Supplementary Table 2).

The results of the weight loss measurements were in excellent agreement with the hydrogen release experiments. Both Mg and Mg-OH samples showed significantly higher % weight loss compared to Mg-OH-AS and Mg-OH-AS-APTES samples (Figure 10C). The weight loss of the Mg-OH was similar to Mg group. Weight loss measurements of AZ31 samples also yielded similar results (Supplementary Figure 5C).

Table 1. Corrosion potential (E_{corr}) and current density (I_{corr}) values for non-coated and coated Mg and AZ31 substrate.

Treatment	E_{corr}(V)(SD)	I_{corr} ($\mu\text{A}/\text{cm}^2$) (SD)
Mg bare	-1.77 (0.014)	171.97 (26.40)
Mg-OH	-1.75 (0.027)	151.84 (31.78)
Mg-OH-AS	-1.78 (0.020)	10.85 (3.93)
Mg-OH-AS-APTES	-1.80 (0.038)	3.66 (2.56)
AZ31 bare	-1.49 (0.009)	96.43 (65.90)
AZ31-OH	-1.54 (0.032)	100.84 (50.26)
AZ31-OH-AS	-1.62 (0.014)	6.06 (1.13)
AZ31-OH-AS-APTES	-1.59 (0.006)	4.07 (3.04)

3.5.6 Determination of the corrosion rate by potentiodynamic polarization and Impedance spectroscopy technique.

The average corrosion potential (E_{corr}) measured for the untreated Mg discs was -1.77 V and it was not significantly different from Mg-OH ($p=0.81$), Mg-OH-AS ($p=0.93$) and Mg-OH-AS-APTES ($p=0.55$) samples (Figure 10D, Table 1). A slightly more negative value of E_{corr} was observed for both Mg and AZ31 coated samples suggesting a weak dependence of the thermodynamic corrosion potential on the coating system and the nature of the coated films. However, the potentiodynamic polarization curves for the coated Mg samples were shifted to lower I_{corr} values compared to pure Mg indicative of the changes in corrosion kinetics. Passivation of the Mg discs with alkali did not seem to show a significant change ($p<0.75$) in the I_{corr} value compared to the non-coated Mg discs, likely due to the porous nature of the hydroxide layer. The AS coated Mg discs however, showed a significant reduction in the I_{corr} value compared to non-coated Mg discs ($p<0.0002$) (Figure 10D, Table 1). Moreover, APTES functionalized AS coated Mg discs showed an almost 50 times reduction in I_{corr} values compared to the non-coated Mg discs ($p<0.0001$). We observed similar trends in the electrochemical corrosion parameters for the AZ31 samples (Supplementary Figure 5D, Table 1).

3.5.7 SEM analysis of the sample surfaces after incubation in SBF.

SEM and light microscopy observations of the discs incubated in SBF for 7 days reveal that the AS coatings lead to a significant decrease in formation of corrosion products, in agreement with our hydrogen evolution and weight loss assessments (Figure 11). The SEM micrographs of the

uncoated samples show the presence of surface cracks and corrosion products on the untreated and alkali treated Mg discs (Figure. 11A, B). The SEM analysis of the coated Mg discs revealed a much better surface preservation. The surface of both Mg-OH-AS and Mg-OH-AS-APTES samples were for the most part intact with a few areas, 200 μm or less across, in which the surface of the coating was pushed out by the expanding corrosion products, leading to cracking of the coating (Figure 11C, D). This observation suggests that initial stages of pitting corrosion are occurring under the coating.

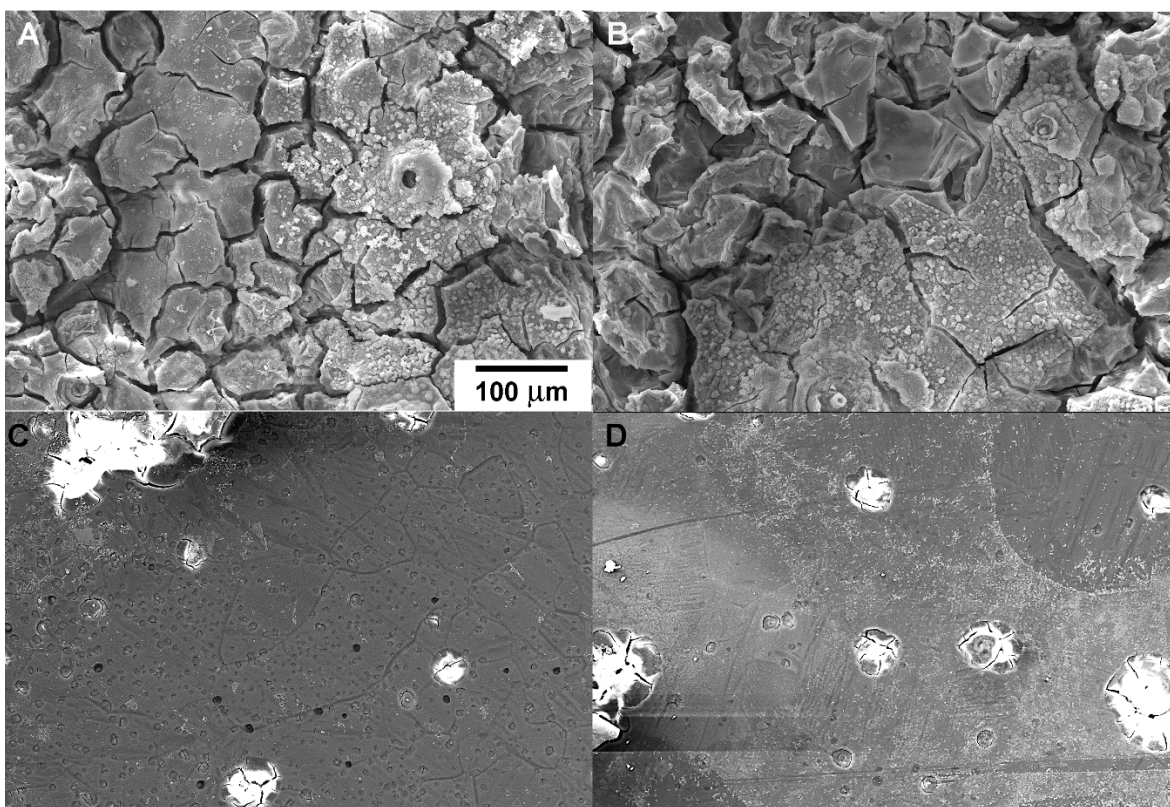


Figure 11. SEM images showing the surface morphologies of A) uncoated Mg, B) Mg-OH, C) Mg-OH-AS, D) Mg-OH-AS-APTES after 1-week incubation in SBF. All micrographs are taken at the same magnification.

3.5.8 Cytocompatibility studies.

Tissue culture experiments on AS coated Mg discs. Tissue culture experiments were conducted to assess the cytocompatibility of the AS coated Mg discs. MC3T3 cells were seeded on Mg discs coated with AS (Mg-OH-AS) and aminated AS (Mg-OH-AS-APTES) and the tissue culture experiments were carried out for 2 weeks in α -MEM medium. After 15 days in culture, the cells were present on both non-aminated and aminated AS coated discs. Light microscopy revealed that the cells formed a dense confluent layer with a well-developed actin cytoskeleton (Figure 12), suggesting that the coated discs are cytocompatible and sustain cell adhesion and proliferation. The cell density was not significantly different on AS coated vs AS coated aminated discs (13 cells/100 μm^2 vs 15 cells/100 μm^2 , $p=0.38$, Figure 13A), which indicates that hydrophobicity of the coating does not have a long lasting effect on cell proliferation.

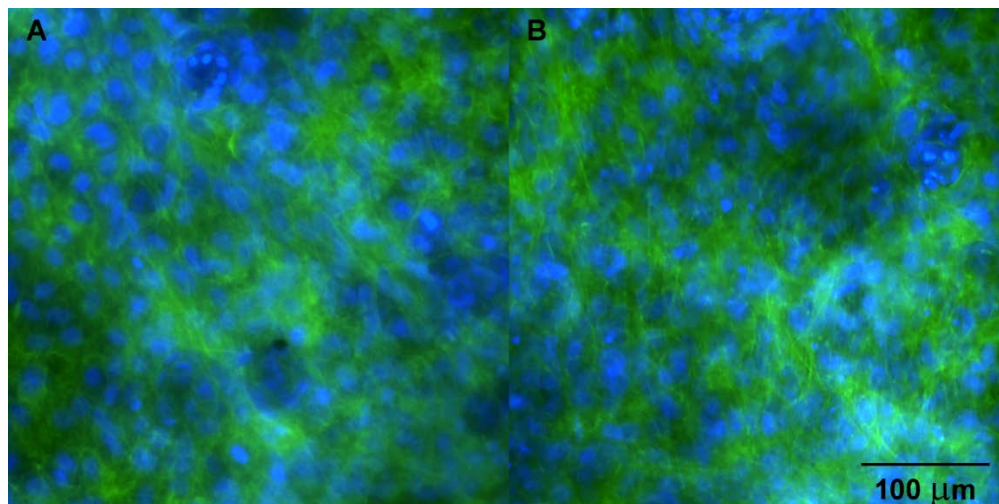


Figure 12. Epifluorescence images of MC3T3 cells grown for 15 days on A) Mg-OH-AS and B) Mg-OH-AS-APTES coated Mg discs. The actin cytoskeleton is visualized using Alexa Fluor® 488 dye (green) and nuclear DNA is stained with Hoechst 33342 dye (blue).

Tissue culture experiments on AS coated glass coverslip. Tissue culture studies on the Mg discs pose some limitations, such as the lack of transparency, which restricts light microscopy observations, as well as the porosity and chemical composition of the corrosion products which interfere with many biological assays⁴⁵. In order to further assess the cytocompatibility of the AS films themselves we conducted a series of experiments using MC3T3 cells plated on bare glass coverslips, AS coated glass coverslips and AS coated and aminated glass coverslips. During the experiments cell morphology was monitored by light microscopy and SEM. Cell density was calculated from fluorescent images as described in the preceding section and using spectrophotometric DNA assay. Cell vitality was assessed using alamarBlue metabolic assay.

We conducted cell density analysis in a manner used for the quantification of cells on the coated Mg discs from the fluorescence images of tissue cultures on the samples from all 3 experimental groups at day 7 and 14 (Figure 13B). No significant differences were observed between the experimental groups at each time point while significant differences in cell densities were observed in each experimental group between day 7 and day 14. We also compared the cell density on the AS coated and AS coated and aminated glass coverslips with similarly treated Mg discs two weeks in the cell culture. The statistical analysis revealed that the cell density on the AS coated and aminated Mg samples was significantly higher than the cell density on the coated glass coverslips ($p=0.03$ for Mg-OH-AS-APTES vs. CS-AS and $p=0.001$ for Mg-OH-AS-APTES vs. CS-AS-APTES). No significant difference was observed between the Mg-OH-AS group and both coated glass coverslip groups. Overall, our results demonstrate that the AS coatings can sustain cell proliferation over a 2-week period in the tissue culture conditions at a rate similar to or higher than on the glass coverslips. We also conducted spectrophotometric

assays of the cells grown on non-coated, AS coated and AS coated and aminated glass coverslips.

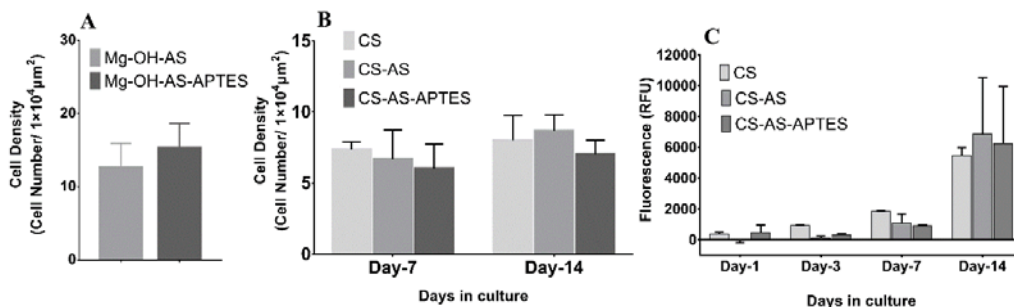


Figure 13. A) Cell density on AS-coated Mg discs after 15 days in culture. B) Changes in cell density on glass coverslips and glass coverslips coated with AS over a 2-week period. C) Cell viability, determined by alamarBlue assay, on glass coverslips and glass coverslips coated with AS films.

These studies did not reveal any statistically significant differences in the cell density at each time point. (Supplementary Figure 6). At the same time the cell density on day 14 was significantly higher than on day 7 in all 3 experimental groups ($p=0.002$). These results indicate that AS coatings support cell proliferation in the tissue culture conditions. AlamarBlue incubations were conducted at day 1, 3, 7 and 14. At each time point the fluorescence intensity values were not statistically different among the groups, suggesting that there were no differences in cell viability on different substrates. At the same time, for all 3 groups the changes in the fluorescence intensity over time were highly significant ($p<0.0001$), potentially reflecting increases in cell density. Overall, the results of these studies demonstrate that the viability and

the metabolic activity of the cells grown on the AS films is similar to the cells grown on glass coverslips, indicating that the AS coatings are cytocompatible.

Light microscopy and SEM studies revealed that one day after plating the cells on the bare glass coverslips and on the AS coated and aminated glass coverslips were well attached and spread on the surface of the substrate (Figure 14A,C; Supplementary Figure 7). In contrast, cells on the AS coated substrates formed aggregates, potentially in an attempt to minimize their interactions with a hydrophobic substrate (Figure 14B, Supplementary Figure 7). By day 3 this clustering has significantly diminished and by day 5 the cell layer was indistinguishable from the cell layers formed on the bare coverslips (Figure 14D-F, Supplementary Figure 7). We also conducted studies of the actin cytoskeleton on the AS coated and bare glass coverslips which showed no observable differences between the groups (Supplementary Figure 8).

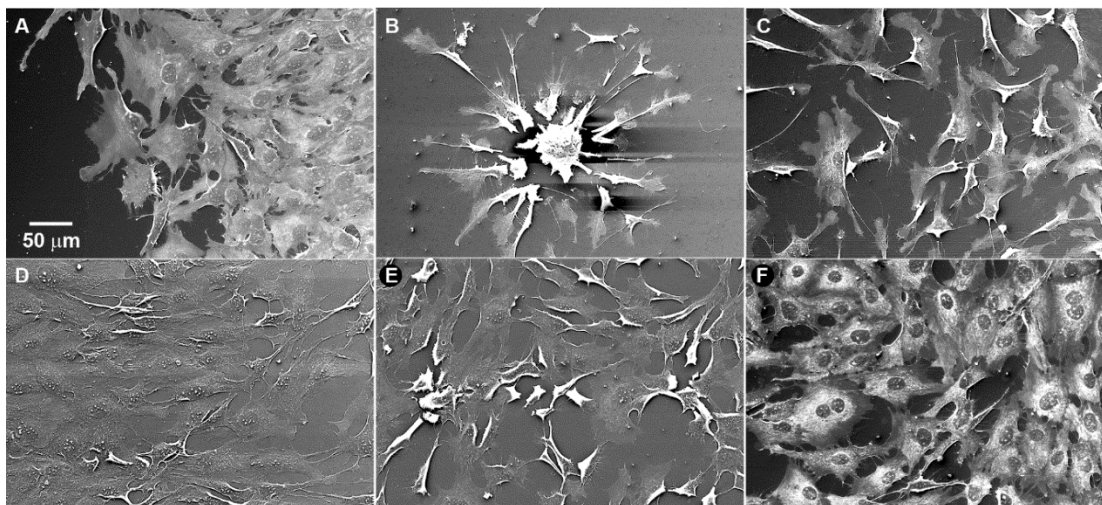


Figure 14. SEM images showing cells morphologies on uncoated and AS-coated glass coverslips. A. and D) Cells on uncoated glass coverslips 24 h and 5 d after seeding. B and E) Cells on AS-coated glass coverslips 24 h and 5 d after seeding. C and F) Cells on AS-coated and

aminated glass coverslips 24 h and 5 d after seeding. All micrographs were taken at the same magnification.

3.5.9 Elemental composition of the coated Mg surfaces after 2 weeks in the tissue culture.

The coated Mg samples were studied with SEM after exposure for 15 days to the cell culture conditions. The coatings were present on the surfaces although multiple cracks have formed leading to the typical mud crack appearance of the surface (Figure 15A). Minimal amounts of the corrosion products and debris were present on the disc surfaces, however most of the surface area was clear. EDS analysis of the surfaces has revealed strong O and Si K edge signals from the surface of the coating consistent with the presence of siloxanes in the coatings, while Mg signal was consistently confined to the crevices of the cracked regions (Figure 15B-E). Interestingly, only traces of Ca and no P were detected by EDS (Table 2), potentially due to the restricted access of Ca^{2+} and PO_4^{3-} to the metal surface and lower surface pH of the coating. This is remarkable since calcium phosphate is typically present on the corroding Mg surfaces exposed to body fluids [153-155] (Supplementary Figure 9. Supplementary Table 3).

Table 2. Elemental analysis using Energy Dispersive X-ray spectroscopy (EDS) of the surface of Mg-OH-AS discs exposed for 15 days to the tissue culture conditions.

Element K edge	Weight%	Atomic%
O K	36.46	48.39
Mg K	33.58	29.32
Si K	28.15	21.28
Cl K	0.77	0.46
Ca K	1.05	0.55

3.6 DISCUSSION

The results of our study show that AS coating produces micron-thick smooth and homogeneous films with excellent anticorrosion properties. Importantly, these coatings can not only slow down the corrosion rate but effectively prevent the initial burst of corrosion over the first 24 hours of the exposure. Hence, these coatings can potentially reduce formation of gas pockets around Mg implantable devices, which is one of the limitations for use of Mg in medical applications [40]. Our data also indicate that AS coatings can reduce spontaneous precipitation of calcium phosphates on the device surfaces. Our *in vitro* tissue culture data demonstrate good cytocompatibility of the AS coatings. Overall, the results of our studies demonstrate a high potential of AS films for use in coating applications for degradable Mg devices. Smooth surface morphology and homogeneity of AS coatings are important factors in reduction of corrosion

[156-158]. Furthermore, the lamellar nanostructure of the AS films with alternating hydrophobic alkyl and covalently bound polysiloxane layers can provide an effective barrier for the solution access to the implant surface. We have assessed anticorrosive properties of the AS coatings by three independent methods commonly used in the corrosion research, namely, hydrogen evolution [145, 159, 160], weight loss [147, 161, 162] and potentiodynamic polarization [163-165].

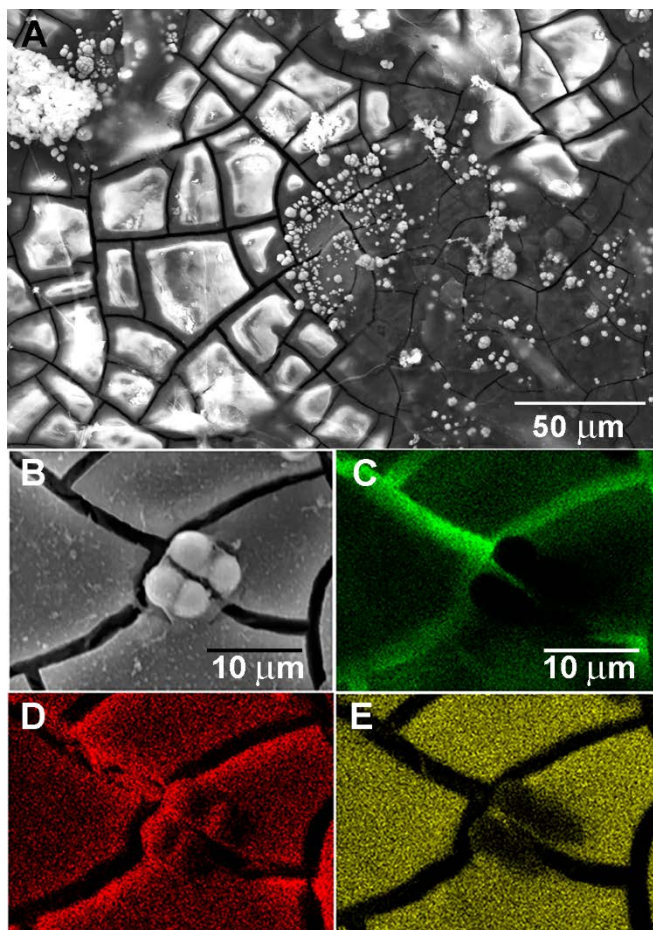


Figure 15. Surface of Mg-OH-AS sample exposed for 2 weeks to tissue culture conditions. A) SEM micrograph of the surface; B) SEM micrograph an area of the surface used for the EDS mapping; C) Mg map of the area in B, D) O map of the area in B; E) Si map of the area in B.

The results obtained by the three independent methods agreed extremely well and demonstrated a dramatic decrease in the corrosion rate. In agreement with the corrosion studies our SEM observations of the coated samples revealed that AS layer remained relatively intact after 7 days in SBF and 14 days in cell culture medium. Importantly, the results of H₂ release analysis over first 24 hours clearly demonstrate that AS coating effectively prevents the initial hydrogen release burst, which is critical for preventing or minimizing gas pocket formation at the most critical time- immediately after surgery. A number of earlier studies showed that the corrosion rate is fastest during the first day after immersion of Mg in aqueous solution, leading to a corrosion burst and fast formation of gas pockets around the device [116, 120, 122, 166, 167]. After the initial burst the rate of corrosion typically slows down and enters a steady state phase. The slowdown of the corrosion can be mainly attributed to a combination of two factors, namely an increase in the pH and formation of Mg hydroxide and Mg/Ca phosphate layer on the metal surface [167]. We have noticed in our experiments an increase in pH from 7.2 to 8.2 over 7 days period. Therefore, it is possible that pH increase can affect the corrosion rate. At the same time, the fact that the SBF changes did not lead to any significant changes in the corrosion rate indicates that the accumulation of the corrosion products on the metal surface is the primary factor affecting the rate of corrosion.

A number of coating strategies were used over the years to control corrosion of Mg and its alloys including Ca phosphate [168, 169], Mg fluoride [68], polymer [128, 170] and others coatings [61]. Gray-Munro et al [169] used calcium phosphate coating on AZ31 alloy discs. They demonstrated that calcium phosphate coating did not have a significant effect on the overall corrosion rate of AZ31 alloy. Synthetic and natural polymers were also used to control the corrosion rate of Mg and its alloys. Park et al [171] used dip coating technique to form

polycaprolactone (PCL) coating on Mg samples. Our results suggest that AS coating has better anticorrosive properties compared to PCL. Specifically, 3.8 ml/cm² H₂ released from Mg discs coated with PCL by single dipping in 1 day. Even after 10 iterations of dip-coating by PCL, only a small decrease in corrosion was observed. In contrast, a single step dip-coating with AS substantially reduces the corrosion rate (2.3 ml/cm² H₂ released over 7-days period). Gray-Munro et al. [169] used poly(L-lactic acid) (PLA) coating on AZ31 discs and observed that PLA coating led to a significant reduction of corrosion vs. bare AZ31 sample. Our results demonstrated that AS coating of AZ31 samples led to a significantly greater reduction of the corrosion rate compared to PLA coating, with the corrosion rate of AS coated samples at 0.2815 mg/day vs. 5.6 mg/day of the PLA coatings. Cui et al [130] used a biomimetic peptide comprising three Asp-Ser-Ser (DSS) amino acid repeats based on the highly acidic dentin matrix protein, phosphophoryn. The average daily H₂ evolution rate of the peptide-coated AZ31 was 0.96 ml/cm² compared to 0.35 ml/cm² with the AS coated AZ31. The higher corrosion rate in the case of DSS₃ peptide-coated AZ31 is likely due to the poor coverage of the peptide coating and its high hydrophilicity. In contrast, the AS coating minimizes the solution access to the metal surface due to its homogeneity and its lamellar structure comprising alternating hydrophobic alkyl and poly-siloxane layers[99]. Although it is often difficult to compare results of studies using different experimental design, overall, our analysis of the literature indicates that the micron thick AS coatings provide corrosion control which is better or compatible to other deposited coating systems.

It has been reported that a hydroxide conversion layer on Mg surface can slow down initial corrosion [61, 147, 172, 173]. We saw a small but significant decrease in corrosion in Mg-OH samples by weight loss and H₂ evolution methods. Interestingly, potentiodynamic

polarization experiments did not show any significant differences between Mg and Mg-OH in both E_{corr} and I_{corr} . Potentially, this can be due to the high variability of the bare Mg and Mg-OH data. Also, the hydroxide layers formed by the alkali treatment typically result in porous coatings which do not have a strong bearing in differentiating the surface from the pristine metal. Hence, despite the presence of hydroxyl species, the porous surface does not alter the E_{corr} as well as the I_{corr} values. In addition to passivation of the Mg surface, alkali treatment might further improve adhesion of the coating layer to Mg surface due to its higher surface area and the presence of hydroxyls which provide a substrate for covalent bonding of silanes[136].

Because of the hydrophobic nature of the AS coated layers, there is a reduction in SBF diffusion and electron transport towards the Mg surface resulting in decrease in the total cathodic current density [132]. The hydrophobic AS layer acts as a physical barrier preventing access of the aqueous medium to the metal surface. Further modification of the coating with APTES did not reduce the I_{corr} value significantly which is expected since the surface functionalization did not change the structural and chemical properties of the bulk of the AS layer. The mud cracked appearance of the coating after prolonged exposure to the cell culture medium potentially suggests that after initial breach of the coating layer in blister-like point defects, the corrosion propagates along the grain boundaries and the forming corrosion products push against the coating layer leading to the crack generation. The fact that, unlike many polymer coatings the AS layer does not delaminate from the surface, supports the notion that it is tethered to the surface via covalent bonds with the hydroxide layer, as shown elsewhere [132, 142, 143]. These strong bonds might potentially present a barrier to propagation of electrolyte, confining it to the cracked regions.

One critical requirement for the biomedical coatings is low toxicity and good biocompatibility. Results of our *in vitro* tissue culture studies demonstrate that AS coatings support cell proliferation and active cell metabolism at the same rate as the uncoated glass coverslips in 2-week long experiments. Furthermore, the results of our tissue culture experiments demonstrate that MC3T3 cells can survive, spread, proliferate and maintain high cell density on the surface of AS coated Mg samples for 2 weeks.

Good adsorption of biomolecules and cell attachment are beneficial for the integration of orthopedic implantable devices [174], while reducing cell and protein attachment might be important for cardiovascular applications [175]. It is therefore essential that the coating exhibits surface chemistry characteristics optimal for a specific application. Among the various surface characteristics surface wettability profoundly affects the protein adsorption and cell attachment to the surface [176, 177]. In the case of polymers, optimal wettability for cell attachment was observed on the moderately hydrophilic surfaces [176]. In our experiments we did not see any differences in cell attachment between hydrophobic and hydrophilic coatings few days after seeding, however in the first day after seeding cells form aggregates in an attempt to minimize their interactions with hydrophobic AS coatings. It is possible that a layer of biomolecules is formed on the hydrophobic surface with time, allowing for cell spreading.

In the earlier *in vitro* studies cells directly seeded on the coated Mg samples were followed only for several days [128, 175, 178, 179]. Typically cells cannot survive on the corroding Mg surfaces more than 48 hours and other coatings reported in the literature would degrade much faster than the AS hybrid self-assembled coatings. The fact that the cells could survive and proliferate on the AS coated Mg samples is quite remarkable. The only long term study we were able to identify was the study by Kunjukunju et al [170] in which the cells were

cultured on AZ31 coated with MgF₂ and poly-L-lysine/chitin multilayer over 2 weeks. In this study the cell density after 14 days was similar to the one on Ti. At the same time it is hard to compare these results with ours, since the alloy corrosion was extremely low in these experiments and the seeding density was much higher. There were several tissue culture *in vitro* studies of the cytocompatibility of the silanated substrates. The study by Curran et al. [180] has shown that the number of cells on the aminated surfaces after 7 days was significantly higher than on methylated or bare glass surfaces. In another study (3-Glycidoxypropyl)trimethoxysilane coated Ti samples were tested *in vitro* for 14 days in the primary gingival fibroblast tissue culture [181]. The cell density on the coated surfaces was 1.4×10^5 , close to the cell density in our experiments and 40% higher than in the Ti group [181]. Overall, the AS coatings demonstrate cytocompatibility which is similar or better than other siloxane based coatings.

3.7 CONCLUSIONS

In this study we used a dip coating technique to self-assemble multilayer AS films on degradable Mg and AZ31 alloy to control their corrosion rate. We further functionalized the AS layer with APTES to reduce its hydrophobicity and improve cell adhesion. We finally tested cytocompatibility of the coated Mg samples *in vitro* under tissue culture conditions. Our results clearly demonstrate that AS coatings can effectively reduce the corrosion rate and prevent the initial burst of corrosion which *in situ* can lead to the formation of gas pockets around an implantable device. We further demonstrate that the AS coatings can be functionalized to modify physicochemical properties, i.e. wettability, or bioactivity of the device. In our *in vitro* tissue culture experiments cells survived and proliferated on the AS coated Mg discs for more than 2

weeks which indicates that the coatings are not cytotoxic and support cell attachment, spreading and proliferation. Importantly, no calcium or phosphate was detected on the sample surface after 2 weeks under tissue culture conditions, suggesting that the coating can prevent calcium phosphate formation. Overall our study clearly demonstrates a great potential for the use of hybrid AS coatings for the corrosion control and biocompatibility of the resorbable Mg devices.

In this chapter, we successfully completed the Aim 1 and sub aims 1A (AS coating development), 1B (AS coatings functionalization with APTES) and 1C (anticorrosive properties of AS coatings). In this chapter, we also addressed aim 2A (cell attachment study) and 2B (cell viability study). Overall, AS coating is cytocompatible and APTES functionalization improves the cells attachment.

4.0 SELECTIVE ALKYL SILANE COATING REMOVAL FOR CORROSION CONTROL OF RESORBABLE MEDICAL DEVICES

4.1 ACKNOWLEDGMENTS

The authors gratefully acknowledge the financial support of NSF-ERC, Grant # EEC-0812348 (E.B.). The work presented in this chapter has been filed for a patent disclosure. We thank John Holmes and Thorin Tobiassen from the Swanson Center for Product Innovation of the Swanson School of Engineering for aiding in the preparation of the samples, Jonathan Franks from the Center for Biological Imaging of at the University of Pittsburgh, Mr. Cole M. Van Ormer from the Department of Mechanical Engineering and Materials Science of the Swanson School of Engineering for providing their expertise in Scanning Electron Microscopy

4.2 ABSTRACT

In this study, we prepared the AS coated Mg-OH discs by dip coating as described in section 3. The deposited AS coating was partially removed to control the corrosion rate of Mg substrate. We selectively removed ~0.52 mm wide lines of AS coated layer to expose the uncoated substrate on both surfaces by hand with a sharp blade. Four experimental groups including fully coated Mg discs, noncoated Mg discs, Mg discs with 4 exposed lines (two on each side) and Mg

discs with 6 exposed lines (three on each side) were used in the study. The H₂ evolution experiments were conducted in simulated body fluid (SBF) over 1 week period to study the differences in the *in vitro* corrosion rate among the groups. Light and scanning electron microscopy were used to study the morphology of AS patterned discs before and after the 1 week exposure to SBF. The optical microscopy revealed that the selective removal of the coating from the Mg surface did not cause any damage to the surrounding coating. Two way ANOVA analysis of the H₂ evolution results revealed that the differences among four groups were highly significant ($p < 0.0001$). The initial corrosion burst was observed only in the noncoated Mg samples. The SEM analysis revealed the formation of dense corrosion product layers in the areas where the coating was selectively removed. Furthermore, EDS analysis detected Ca and P signals in the exposed areas but not in the coated areas, indicating that the coating has effectively prevented calcium phosphate deposition. These results support the notion that the corrosion rate of a medical implant device made of Mg, can be fine-tuned by partial removal of the coating.

4.3 INTRODUCTION

There is a desire to develop a mechanism for controlling the rates of corrosion of Mg and Mg alloys in order to reduce or minimize the production and accumulation of hydrogen around the devices and to construct medical implant devices from materials that possess sufficient mechanical strength when needed and can degrade over time when no longer needed. Furthermore, there is a desire to develop a coating that can effectively control rates of corrosion of Mg and Mg alloys and to reduce or minimize the production and accumulation of gas around the resorbable devices and demonstrates good adhesion to the devices. Moreover, it would be

advantageous to be able to customize or modify to the coatings to allow a fine tuning of the corrosion. The AS coatings on Mg substrate can be selectively removed, e.g., patterned, to expose portions of uncoated Mg substrate, which can be used achieve spatial and temporal control over the device corrosion.

4.4 MATERIALS AND METHODS

All the reagents were purchased from Sigma Aldrich (St. Louis, MO, USA) and used as received unless otherwise stated.

4.4.1 Metal sample preparation.

Six mm diameter discs were stamped from 1 mm thick Mg (99.9 % purity) and AZ31alloy (96% Mg, 3% Al, and 1% Zn) sheets (Alfa Aesar, Ward Hill, MA, USA) and polished with 1200 grit (5 μ m) MicroCut® SiC abrasive discs (Buehler Inc., Lake Bluff, IL, USA). The polished discs were then etched in an etching solution comprising 20 ml 85% Glycerol, 5 ml 65% HNO₃ and 5 ml glacial acetic acid for 60 seconds. Chemical etching was done to remove debris, impurities and the oxide layer from the surface of the metal and to smooth the scratches introduced during polishing. Etched discs were sonicated in acetone for 30 minutes and stored under vacuum until further use. Prior to the AS coatings, a thin uniform hydroxide layer was formed on the discs by immersion in 3.0 M Sodium Hydroxide (NaOH) solution for 2 h. In addition to the passivating properties, MgOH₂ provides means for covalent binding of the silanes to the metal surface as described elsewhere.

4.4.2 Synthesis and deposition of self-assembled multilayer AS coating on Mg and Mg alloys

Self-assembled hybrid AS films on Mg and AZ31 alloys were prepared by a dip-coating technique as described elsewhere [98, 99, 133]. The precursor solution was prepared by mixing 0.25 ml (0.73 mM) n-Decyltriethoxysilane (DTEOS) (Alfa Aesar, Ward Hill, MA, USA), 0.43 ml (2.92 mM) Tetramethoxysilane (TMOS) (Alfa Aesar, Ward Hill, MA, USA), 2 ml (0.032 mM) of Ethanol and 0.25 ml 0.010 mM HCl (aq.). The precursor solution was stirred for 24 h at room temperature to induce hydrolysis of DTEOS and TMOS. Mg or AZ31 alloy discs passivated with NaOH were dip-coated in the solution for 1 minute and dried in air for 10 minutes at room temperature. The discs were subsequently dried in an incubator at 37°C for 24 h for removal of any trace amount of organic solvents.

4.4.3 Patterning of AS coated Mg discs.

The AS coated on NaOH treated Mg discs were patterned with the use of sharp blade. In the control group, no patterning was done on AS coated Mg discs. In the second group, two 0.52 mm-wide lines were etched on each of the top and bottom sides of AS coated on NaOH treated Mg discs by sharp blade making total four lines on a disc and in the third group, three 0.52 mm-wide lines were etched on each of the top and bottom sides of AS coated on NaOH treated Mg discs by sharp blade, making total six lines on a disc (see Figure 16). The patterning was made carefully without damaging the AS coatings such that the treatment removed only the AS coating and the underlying magnesium substrate was intact.

Four groups of samples were used in this study as follows:

- NaOH treated Mg discs (Mg-OH),
- No patterning on AS coatings deposited on NaOH treated Mg discs (Mg-OH-AS)
- Four lines patterned on AS coatings on NaOH treated Mg discs (Mg-OH-AS-4 Lines)
- Six lines patterned on AS coatings on NaOH treated Mg discs (Mg-OH-AS-6 Lines)

4.4.4 Light microscope characterization.

The surface microstructures of patterned AS coated on NaOH treated Mg discs were observed using the Greenough stereo microscope Leica S8 APO equipped with Leica DFC295 digital microscope color camera with a resolution of 2048x1536 pixels (3 Megapixels) (Leica Microsystems Inc., Buffalo Grove, IL, USA). The light intensity and exposure settings were the same for all images.

4.4.5 Hydrogen (H₂) evolution study on patterned AS coatings on NaOH treated Mg discs.

The H₂ evolution experiments were conducted on four sample groups mentioned above. The H₂ evolution was measured in a simulated body fluid (SBF) pH 7.2, prepared according to a published formulation by Kokubo [144] (Supplementary Table 1), at room temperature over a 7 day period. Each sample group was prepared in triplicate and the samples were immersed in SBF. A glass graduated measuring cylinder was placed over the samples in a glass beaker to collect the released gases (Supplementary Figure 1). The experiments were carried out over a 7 day period the solution was changed on day 2, 4 and 6. The ratio of solution volume to the total surface area of the tested samples was kept above 6.7 to mimic in-vivo degradation behavior of

Mg [130, 145, 146]. The SBF level in each beaker was maintained constant throughout the study to avoid evaporation effects affecting the validity of the measurements.

4.4.6 Scanning electron microscope (SEM) characterization and elemental analysis.

The surface morphology of the non-patterned and patterned AS coatings on NaOH treated Mg discs after the 1 week of corrosion in SBF were studied using JSM-6330F (JEOL, Peabody, MA, USA) SEM at 3.0-20.0 kV operating voltage and the working distance of 10 mm. All samples were sputter-coated with gold prior to SEM using Cressington Sputter coater 108 auto model (Cressington Scientific Instruments Ltd, Watford, United Kingdom). The elemental composition of the non-patterned and AS coatings on NaOH treated Mg discs were analyzed using energy dispersive X-ray spectroscopy (EDS) in SEM. EDS INCA analysis system (Oxford Instruments, Oxfordshire, UK) equipped with a beryllium-window protected Si (Li) detector was used for the elemental analysis at the operating voltage of 15 kV.

4.5 RESULTS

4.5.1 Light microscopy analysis of patterned AS coatings.

The light microscope inspection of patterned AS coatings on NaOH-treated Mg discs demonstrated that the discs do not have major defects and patterned shapes are well defined (Figure. 16, A, B).

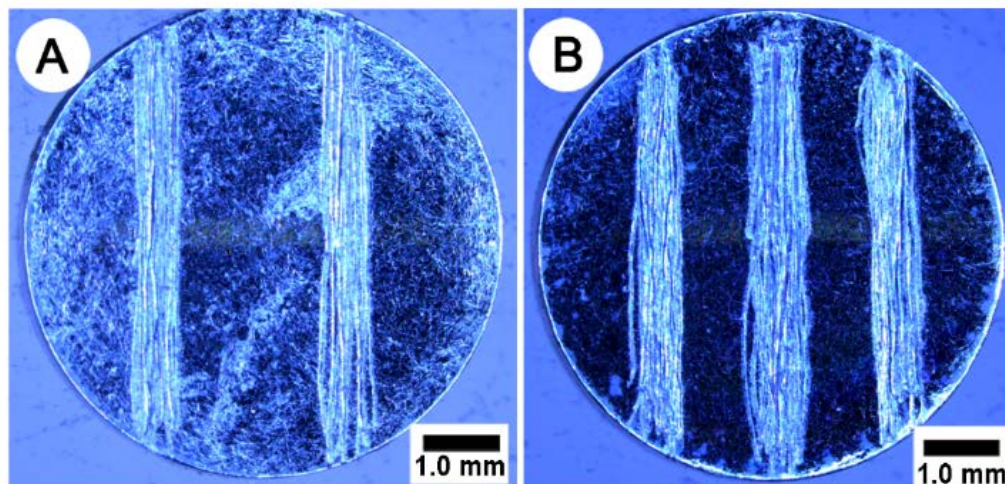


Figure 16. Optical images of hand patterned 4-Lines (A), 6-Lines (B) AS coatings on NaOH-treated Mg discs

4.5.2 H₂ evolution analysis of AS patterned AS coatings on NaOH-treated Mg discs.

The results of H₂ evolution experiment demonstrated that patterning increased the corrosion rate of Mg-OH-AS samples, while their rate of corrosion was significantly lower than the bare Mg samples, as shown in Figure 17. The differences among all the groups were highly statistically significant ($p < 0.0001$). Importantly, the initial corrosion burst was prevented in the patterned Mg-OH-AS samples (Figure 17). These results demonstrated that the corrosion rate can be fine-tuned by partial removal of the AS coatings.

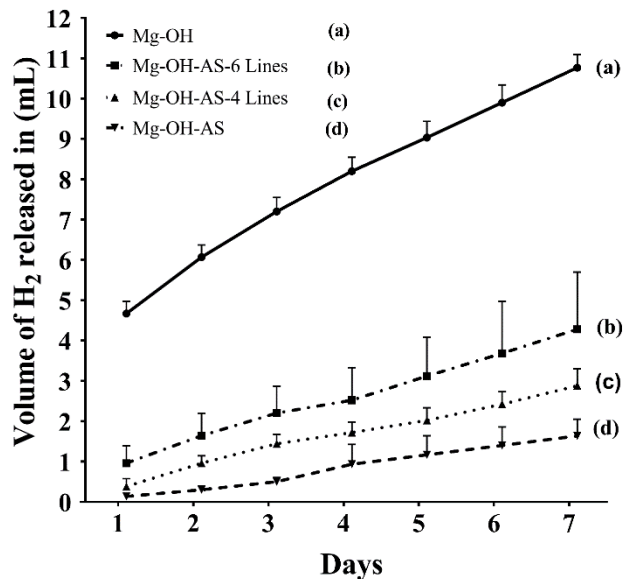


Figure 17. Cumulative H₂ release profile from patterned AS-coated on NaOH-treated Mg discs incubated in SBF over a 7 day period (Note- H₂ data on Y axis is not normalized with area of the individual disc)

4.5.3 SEM and elemental analysis of patterned AS coatings on NaOH treated Mg discs after corrosion.

The SEM characterization of the patterned AS coatings on NaOH treated Mg discs was conducted to assess the surface morphology of patterned discs after 1-week corrosion in SBF. Inspection of the discs immediately after their retrieval 1 week post corrosion revealed that the discs were covered with more corrosion products on patterned area compared to the intact AS coating (Figure. 18, C, D).

Elemental analysis of the AS coatings intact (intact) and patterned AS coatings on NaOH treated Mg disc (exposed area) revealed the presence of calcium and phosphate on the

patterned areas while these elements were not detected on the coated areas (Supplementary Figure 9). The results of the elemental composition are shown in Table 3 below.

It was found that a local pH increase in an area around the corroding Mg discs led to spontaneous calcium phosphate precipitation. The SEM images and EDS analysis indicated that the AS coatings effectively prevented calcium phosphate precipitation on the AS coatings wherein the AS coating is intact compared to corroded areas which indicated that the AS coatings were removed.

Table 3. The elemental composition of the AS-coated (intact) and corroded (exposed) areas of a Mg sample

Element K edge	Corroded (Exposed) Area		Coated (Intact) Area	
	Weight%	Atomic%	Weight%	Atomic%
O	48.79	62.24	25.81	35.57
Mg	29.69	24.93	50.88	46.14
P	<u>8.76</u>	<u>5.77</u>	-	-
Cl	8.57	4.93	-	-
Ca	<u>4.19</u>	<u>2.13</u>	-	-
Si	-	-	23.31	18.30

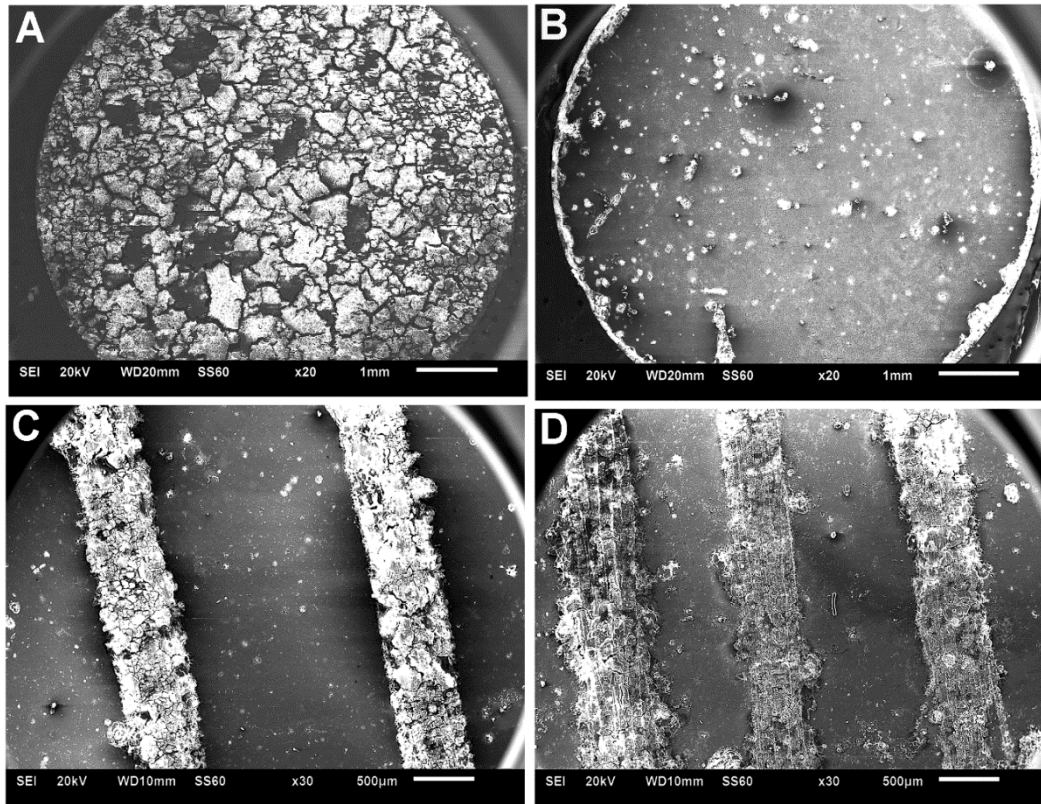


Figure 18. SEM images showing the surface morphology of (A) uncoated Mg-OH, (B) AS-coated Mg-OH disc without patterning, (C) Mg-OH-AS-4 Lines patterning, (D) Mg-OH-AS-6 Lines patterning, Scale bar for A and B is 1 mm, for C and D is 500µm

In this chapter, we addressed the sub aim 1D (patterning of AS coatings to control the corrosion rate of Mg substrate). Successful completion of aim 1D proves the feasibility of fine-tuning the corrosion control of Mg substrate. This method of corrosion control by selective patterning can be directly applicable to control the corrosion rate of degradable medical devices based on their intended *in vivo* implantation time.

5.0 CUMULATIVE DRUG RELEASE FROM ALKYL-SILANE COATINGS; THE FEASIBILITY STUDY

5.1 ACKNOWLEDGMENTS

The authors gratefully acknowledge the financial support of NSF-ERC, Grant # EEC-0812348 (E.B.). The work presented in this chapter has been filed for patent disclosure. We thank John Holmes from the Swanson Center for Product Innovation of the Swanson School of Engineering for aiding in the preparation of the samples. Mr. Cole M. Van Ormer from the Department of Mechanical Engineering and Materials Science of the Swanson School of Engineering for providing their expertise in Scanning Electron Microscopy and Dr. Taboas, Juan M, Assistance Professor from Department of Oral Biology, School of Dental Medicine, University of Pittsburgh for his help in training microplate reader.

5.2 ABSTRACT

In this study, we encapsulated Tetracycline (TC) and Rhodamine 6G (Rh) in AS coatings deposited on Mg discs. We dissolved Tc and Rh powders in AS solution and used dip coating method to form self-assembled AS coatings on Mg disc. We used optical and scanning electron microscopies to study the surface morphology of Tc and Rh encapsulated AS coated Mg discs.

The release kinetics of TC and Rh were measured in simulated body fluid (SBF) over 21 days. The microscope study confirmed that TC and Rh encapsulation into the AS coatings did not lead to any major changes in the coating structure. Kinetic release studies of demonstrated a cumulative increase of TC and Rh concentrations in the medium over 21 days. Overall, our results demonstrate the feasibility of use of AS coatings as a drug release system.

5.3 INTRODUCTION

Orthopedic trauma implant-related infection is a major challenge and can lead to amputation or death [182]. Current efforts to reduce the implant infections focus on the increased surgical rooms sterility, antibiotic prophylaxis and irrigating wounds with a variety of antimicrobial agents [183]. However, improved strategies are needed to fight the infections. Once such strategy is a local antibiotic delivery from an implant coatings [184]. The main advantage of local antibiotic delivery is its greater efficacy and improved safety [185]. There are no previous reports to the best of our knowledge on the incorporation of TC in AS coatings. Sustained TC release from AS coatings may be an attractive treatment approach for local trauma implant related infections. The aim of the present study was to evaluate Tc and Rh release kinetics from AS coatings in SBF over 21 days.

5.4 MATERIALS AND METHODS

All the reagents were purchased from Sigma Aldrich (St. Louis, MO, USA) and used as received unless otherwise stated.

5.4.1 Metal sample preparation

Six mm diameter discs were stamped from 1 mm thick Mg (99.9 % purity) and AZ31alloy (96% Mg, 3% Al, and 1% Zn) sheets (Alfa Aesar, Ward Hill, MA, USA) and polished with 1200 grit (5 μ m) MicroCut® SiC abrasive discs (Buehler Inc., Lake Bluff, IL, USA). The polished discs were then etched in an etching solution comprising 20 ml 85% Glycerol, 5 ml 65% HNO₃ and 5 ml glacial acetic acid for 60 seconds. Chemical etching was done to remove debris, impurities and the oxide layer from the surface of the metal and to smooth the scratches introduced during polishing. Etched discs were sonicated in acetone for 30 minutes and stored under vacuum until further use. Prior to the AS coatings, a thin uniform hydroxide layer was formed on the discs by immersion in 3.0 M sodium hydroxide (NaOH) solution for 2 h. In addition to the passivating properties, MgOH₂ also provides the surface for covalent binding of the silanes to the metal surface as described elsewhere.

5.4.2 Synthesis and deposition of self-assembled multilayer AS coatings encapsulating TC and Rh on Mg

Self-assembled hybrid AS films on Mg was prepared by a dip-coating technique as described elsewhere [99, 133]. The precursor solution was prepared by mixing 0.25 ml (0.73 mM) n-

Decyltriethoxysilane (DTEOS) (Alfa Aesar, Ward Hill, MA, USA), 0.43 ml (2.92 mM) Tetramethoxysilane (TMOS) (Alfa Aesar, Ward Hill, MA, USA), 2 ml (0.032 mM) of Ethanol and 0.25 ml 0.010 mM HCl (aq.). The precursor solution was stirred for 24 h at room temperature to induce hydrolysis of DTEOS and TMOS. After 24 h, TC or Rh was added into the hydrolyzed precursor solution at a concentration of 5 mg/ml and further stirred for 24 h at room temperature to mix TC or Rh well in the hydrolyzed solution. Both the solutions were kept in dark to avoid light contact. Mg discs passivated with NaOH were dip coated in the TC or Rh containing the solution for 1 minute and dried in air for 10 minutes at room temperature. All the coating procedure was also done in dark. The discs were subsequently dried in an incubator at 37°C for 24 h for removal of any trace amount of organic solvents. The TC or Rh encapsulated AS coated Mg discs were stored in dark until further use.

Two groups of samples were used in this study as follows:

- AS coatings encapsulating TC deposited on NaOH treated Mg discs (Mg-OH-AS-TC)
- AS coatings encapsulating Rh deposited on NaOH treated Mg discs (Mg-OH-AS-Rh)

5.4.3 *In vitro* release of TC or Rh in SBF.

Prior to release study, TC or Rh encapsulated AS coated Mg discs were placed in DI water and shaken for 1 h to remove any non-specific bound TC or Rh to coated discs. *In vitro* release of TC or Rh was carried out in SBF at room temperature. A disc of TC or Rh was placed in 5 ml of SBF containing plastic tube and every two days 150 µl of SBF was pipetted out and used for analyzing the released amount of TC or Rh in 5 ml of SBF by measuring absorbance or fluorescence of SBF solution. The 150 µl of SBF used was poured back into respective 5 ml SBF tubes to avoid the cumulative concentration discrepancies. The 5 ml SBF tube caps were closed to

avoid SBF evaporation. We maintained a constant volume of SBF solution (5 ml) throughout the experiment by adding fresh SBF solution to compensate for the loss due to pipetting and evaporation. The concentration of TC or Rh in SBF at each time point was determined by measuring the absorbance at 280 nm for TC and by fluorescence at excitation/emission wavelengths of 525/555 nm for Rh using a Synergy H1 microplate reader (BioTek Instruments, Winooski, VT, USA). Absorbance and fluorescence intensity of each sample was calculated as an average of 3 separate readings. Standard calibration curves were obtained by measuring samples with known concentrations of TC or Rh in SBF curves were obtained and concentrations of TC or Rh in the experimental solutions at each time point were calculated using a standard calibration curve. Cumulative release of TC or Rh in ng/ μ l of SBF over every two other days was measured over the 21 day period. Since ASs are not autofluorescent, they did not affect the fluorescence reading.

5.5 RESULTS

5.5.1 Release kinetics of TC or Rh in SBF.

Our experiments demonstrated the feasibility of using hybrid multilayered self-assembled AS coatings for drug release. An incremental increase in the concentration of TC and Rh in SBF media in which the AS coated Mg discs were incubated was apparent (Figure 19). One way ANOVA analysis demonstrated that the increases in the dye concentrations for both groups were highly significant ($p= 2.71 \times 10^{-4}$ for Rh and $p= 3.42 \times 10^{-5}$ for TC).

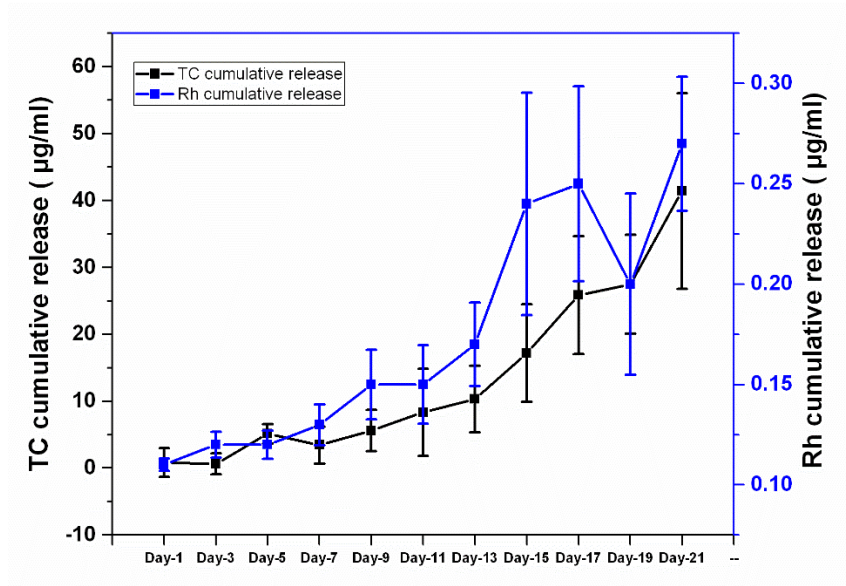


Figure 19. The cumulative release profile of TC and Rh from AS coatings deposited on NaOH-treated Mg discs in SBF over 21 days.

5.5.2 A drug releasing mechanism

A number of drug release mechanisms are identified such as diffusion, swelling, dissolution, convection, erosion and degradation [186]. The SEM analysis of AS coatings containing TC and Rh on Mg discs exposed to SBF for 7 days revealed the signs of erosion and degradation of the coating. The SEM study also showed signs of pitting corrosion underneath the AS coatings. The expanding corrosion products beneath the AS coatings push it outward leading to cracking of the AS coatings as shown in 11C. This AS coatings cracking and gradual erosion of AS coatings releases the encapsulated drug from the coating. This finding indicates that film erosion and degradation plays a major role in the release of TC or Rh from AS coatings. Brinker et al suggested that thin sol-gel film formed from acid-catalyzed and fresh solution may have low

porosity or non-porous [187]. There is low possibility of diffusion of TC or Rh from AS coatings and the release is most likely occurs through the cracks in the degrading coating. The fact that there is no burst or rapid release of encapsulated drug during initial period supports this notion.

In this chapter, we addressed sub aim 1E (drug release from AS coatings). Use of AS coatings as drug releasing system has considerable potential in designing drug releasing orthopedic fixation devices that will be used for local delivery of antibiotics at the infection site.

6.0 IN-VIVO STUDY OF SELF-ASSEMBLED ALKYL SILANE COATED DEGRADABLE MAGNESIUM DEVICES

6.1 ACKNOWLEDGMENTS

The authors gratefully acknowledge the financial support of NSF-ERC, Grant # EEC-0812348 (E.B.). We thank Mr. John Holmes from the Swanson Center for Product Innovation of the Swanson School of Engineering for aiding in the preparation of the samples. We thank Dr. Shilpa Sant, Dr. Manjulata Singh and Mr. Akhil Patel from the Department of Pharmaceutical Sciences, School of Pharmacy, University of Pittsburgh, Pittsburgh, PA, USA for their help in histological studies. We thank Miss. Dandan Hong from the Department of Bioengineering, University of Pittsburgh and Mr. Xu Yang, DDS from the Department of Oral Biology, School of Dental Medicine, University of Pittsburgh, Pittsburgh, PA, USA for their help in sample preparation and embedding for histological studies. We thank Jonathan W. Yu from the Department of Statistics, University of Pittsburgh, Pittsburgh, PA, USA for his expert help in performing the statistical analysis. We thank Kelly Hoffmann CVT, RLATG and Alyssa-Diana Falcione from the Division of Laboratory Animal Resources (DLAR), University of Pittsburgh, Pittsburgh, PA, USA for their assistance during surgery on the animals. We also thank Dr. Esta Abelev and Mr. Matthew France from the Nanoscale Fabrication and Characterization Facility,

Swanson School of Engineering, University of Pittsburgh, Pittsburgh, PA, USA for providing their expertise in surface profilometry.

6.2 ABSTRACT

Magnesium and its alloys are extensively investigated as potential materials for resorbable implantable devices, such as orthopedic plates and screws or cardiovascular stents. Magnesium has a number of important advantages, including its mechanical properties, light weight, its osteogenic effects and the fact that its degradation products are nontoxic and can be naturally cleared out of the body. However, production of H₂ gas during the corrosion reaction can cause formation of gas pockets at the implantation site leading to a number of complications. It is therefore desirable to develop methods to control Magnesium corrosion rate and the formation of gas pockets around the implanted Magnesium devices. Here we evaluate the potential of hybrid self-assembled multilayer alkylsilane coatings to control Mg corrosion and formation of gas pockets *in-vivo* and to assess potential negative effects of the alkylsilane coatings on the tissues surrounding the implanted device in a subcutaneous mouse model over a 6 weeks period. The coating has effectively prevented gas pocket formation during the first 3 weeks. Micro-computerized tomography analysis revealed more even corrosion pattern on the alkylsilane coated samples than on the uncoated controls. Furthermore, the roughness of alkylsilane coated samples was significantly lower than the non-coated controls, suggesting that the coating leads to a more homogeneous corrosion. Histological assessment of the muscle tissues under the implant revealed no inflammation or foreign body reaction. Overall, our results demonstrate the

feasibility of use of alkylsilane coatings for reduction of gas pocket formation around the resorbable Mg devices.

Keywords: Magnesium, corrosion, coating, roughness, degradable implant, alkylsilane, self-assembly, toxicity

6.3 INTRODUCTION

Magnesium (Mg) and its alloys has emerged as promising materials for resorbable orthopedic devices due to their degradability in the body which eliminates the need for an implant removal surgery [41, 45, 54, 188, 189]. Mg is light-weight and its mechanical properties closely match those of bone. Divalent Mg^{2+} ion is one of the essential ions and its corrosion products- MgO and $Mg(OH)_2$ are safe and can be cleared from the body. Mg is highly biocompatible and several studies showed that Mg^{2+} ions can induce new bone formation [119, 190]. However, one of the obstacles for use of Mg in clinical application is its initial rapid corrosion reaction leading to the formation of hydrogen (H_2) which creates gas pockets around the implanted Mg devices. Pure Mg readily corrodes when in contact with an aqueous solution and as shown in equation (1) H_2 gas is one of the reaction products:



In addition to H_2 , a complex mixture of insoluble Mg corrosion products forms in biological electrolytes *in vivo* and *in vitro* which consist of a complex mixture of mineral salts, oxides and hydroxides which form a passivating layer around the corroding metal [191, 192], leading to the decrease of the corrosion rate in the first 24 hours *in vitro* [115]. A portion of H_2

gas is absorbed in the surrounding tissues and blood, while the remaining H₂ forms pockets surrounding the implant [44]. Although, H₂ escapes the body quickly it is exchanged with other gases *in vivo* [44]. Attempts to use Mg as a material for resorbable devices can be traced to the 19th century, however the issues with the gas pocket formation and other drawbacks created obstacles for a widespread use of these devices in clinical practice [40]. In 1938 McBride performed fracture fixation surgeries of long bones using Mg plates and screws and observed the gas pocket formation around the implantation site [33, 120]. Patient discomfort and gas embolism are two main clinical consequences of H₂ accumulation in body [192]. The gas pocket formed in tissue can slow down the tissue healing process and the rapid degradation of implants may initiate an inflammatory response in surrounding tissues [52, 193]. It is therefore important to control the Mg device degradation rate to improve clinical outcomes [193]. Ideally, the degradation rate should be such that formed H₂ is absorbed by surrounding tissues and degradation products do not cause inflammatory response [44, 192, 194]. With time the corrosion products forming around the device lower its degradation rate, however, it is highly desirable to prevent the initial corrosion burst [44, 195]. More rapid degradation of Mg implant can occur during the initial period of implantation because of accumulation of body fluids around the implant due to trauma or surgery so it is important to control the H₂ gas evolution in the early period of implantation. To overcome the issue of the initial rapid corrosion and the H₂ burst leading to the formation of the gas pockets, three different strategies were used, namely, alloying, surface treatment and surface coating [46, 47]. A variety of surface coating materials is used to control degradation of Mg including polymers [196, 197], calcium phosphate [76] and polysiloxanes [92, 93, 198]. Polysiloxanes have a number of advantages over other coating

technologies, such as their well established chemistry [87], biocompatibility [199] and the potential for the surface functionalization of the coatings [200].

We recently applied a micron thick self-assembled multilayer alkylsilane (AS) coatings on Mg devices and demonstrated *in vitro* that it significantly reduces the rate of corrosion and H₂ production and is cytocompatible [115]. The aim of the present study was to evaluate anticorrosive properties and toxicity of the self-assembled AS coatings on tissues surrounding the implants in a mouse subcutaneous model over a 6 weeks period.

6.4 MATERIALS AND METHODS

All the reagents were purchased from Sigma Aldrich (St. Louis, MO, USA) and used as received unless otherwise stated. The Mg disc preparation, synthesis and deposition of the self-assembled multilayer AS coatings was conducted as described previously and is briefly outlined below [115].

6.4.1 Metal disc preparation.

Six mm diameter discs were stamped from 1 mm thick Mg (99.9 % purity) sheet (Alfa Aesar, Ward Hill, MA, USA) and polished with 1200 grit (5µm) MicroCut® SiC abrasive discs (Buehler Inc., Lake Bluff, IL, USA), followed by etching in a solution comprising 20 ml 85% Glycerol, 5 ml 65% HNO₃ and 5 ml glacial acetic acid for 60 seconds. The discs were sonicated in acetone for 30 minutes and stored under vacuum until further use. Prior to the AS coating, a thin uniform hydroxide layer was formed on the discs by immersion in 3.0 M sodium hydroxide

(NaOH) solution for 2 h. In addition to the passivating properties, MgOH₂ provides the substrate for covalent binding of the silanes to a surface [94, 142, 143].

6.4.2 Synthesis and deposition of AS coatings on Mg discs.

Self-assembled multilayer alkylsilane (AS) films on Mg was prepared by a dip-coating technique as described elsewhere [98, 99, 133]. The precursor solution was prepared by mixing 0.25 ml (0.73 mM) n-Decyltriethoxysilane (DTEOS) (Alfa Aesar, Ward Hill, MA, USA), 0.43 ml (2.92 mM) Tetramethoxysilane (TMOS) (Alfa Aesar, Ward Hill, MA, USA), 2 ml (0.032 mM) of Ethanol and 0.25 ml 0.010 mM HCl (aq.). The precursor solution was stirred for 24 h at room temperature to induce hydrolysis of DTEOS and TMOS. Mg discs passivated with NaOH were dip coated in the solution for 1 minute and dried in air for 10 minutes at room temperature. The discs were subsequently dried in an incubator at 37°C for 24 h for removal of any trace amount of organic solvents.

Two groups of samples were used in this study as follows:

- Polished, etched and NaOH treated Mg disc (Mg-OH)
- AS coated NaOH treated Mg disc (Mg-OH-AS)

6.4.3 Surgical Procedure.

The University of Pittsburgh's Institutional Animal Care and Use Committee approved all animal studies. Eight weeks old, five male SKH1-Elite hairless mice of albino background (strain Code- 477) from Charles River Laboratories International Inc. (Wilmington, MA, USA) were used for this study. Prior to surgery the mice were placed on a pre-warmed heating pad to reduce

hypothermia and decrease metabolic rate. Surgery took place under isoflurane inhalation anesthesia. The skin of the mouse was cleaned with alcohol swab and a 6 mm incision was made on its back. The non-coated and AS coated Mg discs were weighed prior to implantation and implanted subcutaneously on the left and right dorsal side of the mouse in the midsection of the body. The discs were inserted through the incision in the mid-sagittal plane of the animals and placed ~5 mm away from the spine. The incision was closed using coated VICRYL™ plus antibacterial (polyglactin 910) suture (Ethicon Inc., Johnson & Johnson, New Brunswick, NJ, USA). After surgery, the animals were given water containing Silapap liquid containing 160 mg/ml Acetaminophen (National Drug Code- 54838-0144-40; Silarx Pharmaceuticals Inc., Carmel, NY, USA) as an analgesic for two days and then all mice were placed on normal diet and water until the end of study. All animals were observed every day and received day-to-day managed care through the Division of Laboratory Animal Resources (DLAR) facility of the University of Pittsburgh. The *in vivo* experiment was carried out for 6 weeks after which mice were euthanized.

6.4.4 Assessment of the gas pocket formation.

The formation of a gas pockets around the implanted discs was monitored by visual observation and images were taken every week with a digital camera every week throughout the experiment. The diameter of the gas pockets was measured from the images using ImageJ image processing package (ImageJ, Bethesda, MD, USA).

6.4.5 Postmortem whole animal μ CT analysis.

Immediately after euthanasia, the μ CT scans of the implantation sites containing the discs were performed using Viva-CT40 μ CT scanner (Scanco Medical, Brütisellen, Switzerland) with 30 μ m voxel size and a 70 kVp beam energy (200 ms exposure, 1 frame per view)

6.4.6 Optical microscopy analysis of the samples.

The discs surface microstructures were observed using the Greenough stereo microscope Leica S8 APO equipped with Leica DFC295 digital microscope color camera (Leica Microsystems Inc., Buffalo Grove, IL, USA) prior to implantation, immediately after retrieving the discs from the subcutaneous site at 6 weeks post-implantation and after removal of the corrosion products (section 2.8.). The light intensity and exposure settings were maintained the same for all images.

6.4.7 Histological analysis.

After the Mg discs were retrieved, soft tissues beneath the Mg discs were carefully collected and immersed in 10% ethylenediaminetetraacetic acid (EDTA) (in 0.1 M phosphate buffer, pH 7-8 for approximately 72 h, solution changed every 24 h and fixed in 10 % neutral buffered formalin for 24 h prior to embedding. Fixed samples were placed in Tissue-Tek® MESH Biopsy Cassette (Sakura Finetek U.S.A., Inc., Torrance, CA, U.S.A.) and processed in a fully automated Leica ASP300 S tissue processor (Leica Biosystems Inc., Buffalo Grove, IL, USA). After paraffin infiltration, samples were placed in a mold and embedded in paraffin using Leica EG1160 paraffin embedding station (Leica Biosystems Inc. Buffalo Grove, IL, USA). The embedded

specimens were cut into 5 μm thick sections using a Leica RM2255 fully automated rotary Microtome (Leica Biosystems Inc., Buffalo Grove, IL, USA) and mounted on a glass slide. The sections were H&E stained and observed using Nikon TE2000 microscope (Nikon Instruments Inc, Melville, NY, USA) in a bright field mode. The images were captured and analyzed using Nikon NIS Elements software.

6.4.8 The weight loss analysis of corroded discs.

Prior to the experiments each disc was weighed using microbalance Mettler Toledo XPE26 (Mettler Toledo, Columbus, OH, USA). After retrieving the discs from subcutaneous pouch the soft tissues attached to discs were removed carefully and the discs were cleaned in a 180 gm/l CrO_3 solution to remove the corroded products. The discs were weighed and the % weight loss was calculated for each disc.

6.4.9 High resolution micro-computerized tomography (μCT) analysis of the samples.

The discs were scanned before and after surgery. The extracted discs were cleaned with CrO_3 as described in section 2.8. Prior to scanning the discs were packed in a plastic tube and separated by Parafilm spacers to avoid overlap. The discs were scanned on a Skyscan 1172 (Bruker-Skyscan, Contich, Belgium) μCT system prior to implantation and post retrieval after 6 weeks *in vivo*. The scans were conducted with an eight-micron voxel size (180 degree-angular range) and a 60 KVp beam energy with the use of a 0.5 mm Al filter, 400 ms exposure time and 12 frames per view. The ReCon (Bruker-Skyscan) software system was used for reconstruction of the 3D

volumes, that are provided as stacks of bmp images for every scan. The images were digitally truncated to limit the volume to the areas surrounding discs and saved as a separate file and all scanned volumes were similarly reoriented along the sagittal plane in a 3-plane-view mode using the DataViewer (Bruker-Skyscan) software. CTAn 3D morphometry and densitometry analysis software (version 1.13.5.1; Skyscan-Bruker) was used to calculate the total surface area and volume of each disc, after a regions of interest (ROI) was user-defined around it. The disc regions within the ROIs was segmented from the background and eroded areas using a global threshold that represented the interface between the Mg alloy and the background.

6.4.10 Surface profilometry analysis of the extracted Mg discs.

The arithmetic average surface roughness (Ra) and waviness (Wa) of CrO₃ cleaned Mg discs (section 2.8.) were measured using the Alpha-Step IQ stylus-based surface profiler (KLA-Tencor Corporation, Milpitas, CA, USA). The Ra is the arithmetic average of the absolute values of the profile heights over the scan length[201]. The Wa is the average of the peak heights of the surface after applying low pass and high pass filtering to the primary profile[202, 203]. The measurement control parameters used were as follows, a scan length of 2500 μm with scan speed of 100 $\mu\text{m}/\text{sec}$ and sampling rate of 50 Hz was used. A standard 5 μm radius stylus tip was used with a 60° cone angle at contact speed of 3. The sensor range was chosen at 400 $\mu\text{m}/23.8$ μm with required stylus force of 34.4 mg and selected adjustment as center bias (optimized to measure a randomly distributed surface (e.g. roughness measurement)). The data acquisition and processing was done by Alpha-Step IQ software. The collected profile was leveled using two zones method. The roughness/waviness filter cut-off (λ_c) was set at value of 25 μm and microroughness (noise) filter was turned off.

6.4.11 Statistical analysis.

The data were compared between groups using paired t-tests and the analysis of variance (ANOVA) followed by Tukey's multiple comparison test with 95% confidence level based on the assumption of normal distribution and unequal variance. All statistical analysis was performed using Origin Pro 2015 (OriginLabs, Northhampton, MA, USA) software package. The data were presented as mean \pm standard deviation (S.D.).

6.5 RESULTS

6.5.1 Light microscopy characterization of Mg discs pre and post implantation.

The light microscope inspection of bare and AS coated Mg discs prior to implantation demonstrated that the discs did not have major defects and were free of debris (Figure 20 A, B). The inspection of the discs immediately after their retrieval 6 weeks post-implantation revealed that the discs were covered with organic debris and corrosion products (Figure 20 C, D). The inspection of the samples after CrO₃ treatment confirmed the complete removal of the corrosion products and organic debris from the corroded discs' surfaces (Figure 20 E, F).

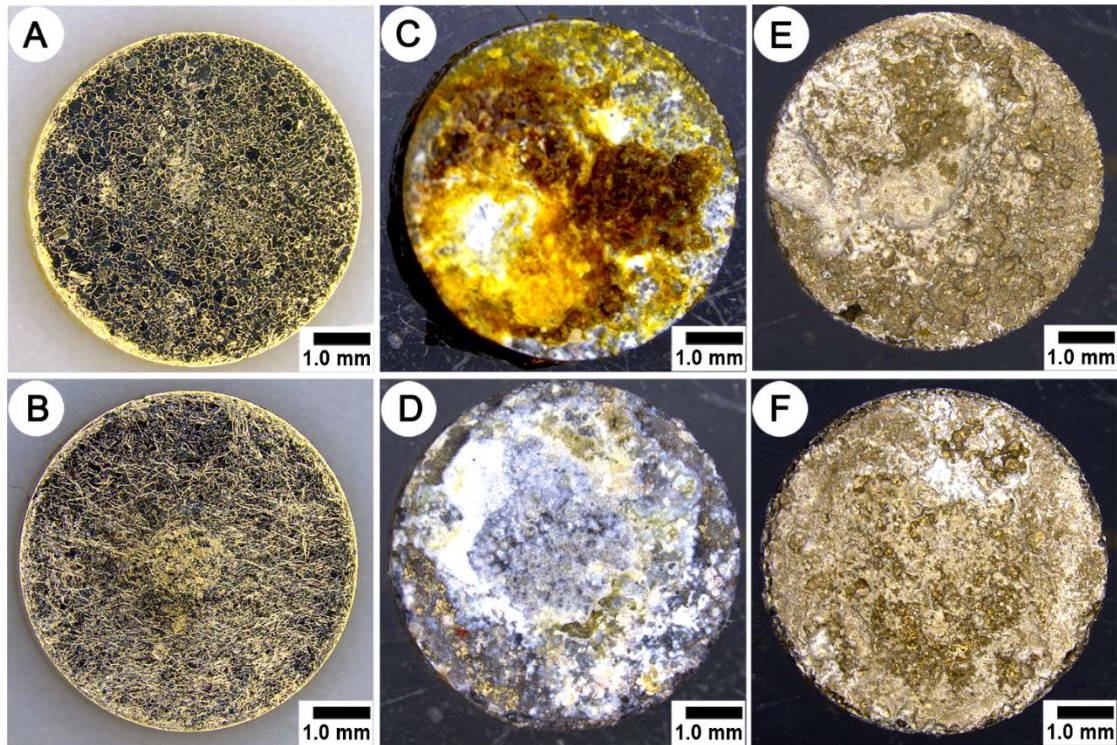


Figure 20. Optical images of Mg-OH and Mg-OH-AS discs as prepared (A and B, respectively), immediately after retrieval at 6 weeks in vivo (C and D) and after cleaning with a CrO₃ solution (E and F). All discs shows muscle side surface topography.

6.5.2 Gas pocket formation dynamics.

The gas pocket analysis showed that the AS coating effectively inhibited the gas pocket formation for the 3 weeks after the surgeries, while gas pockets formed around the bare discs in the first week post operation and their diameters increased linearly over the course of the experiment (Figure 21 A). Paired t-test analyses of the data from weeks 2 and 3 showed that the diameters of the gas pockets around the AS coated samples were significantly smaller than around bare Mg discs ($p=0.01$ and $p=0.005$ respectively) (Figure 21 B). At the 3rd week post-

surgery the diameters of gas pockets around the AS coated discs started to increase (Figure 21 B), yet the differences between coated and uncoated samples were highly significant.

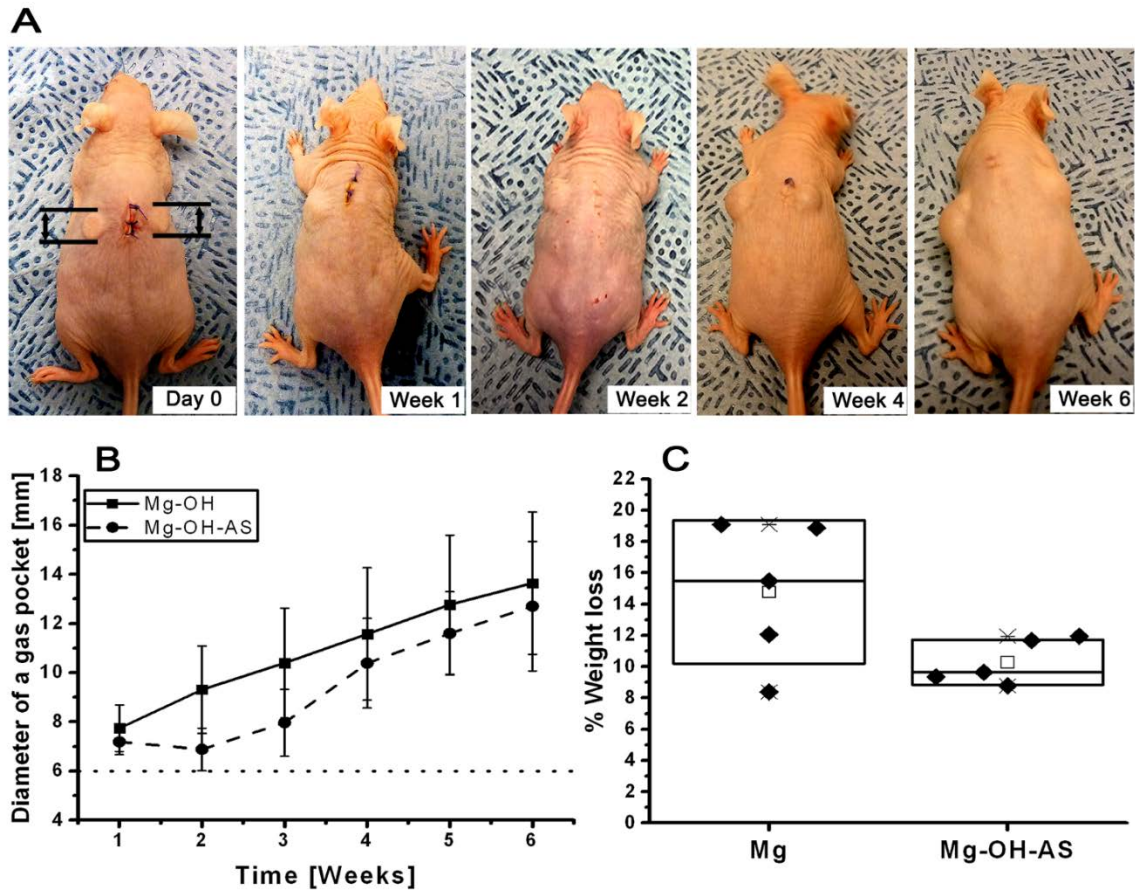


Figure 21. (A) Photographs of a mouse at different time points after implantation of non-coated (left side) and AS-coated (right side) Mg discs. Dotted line indicates the diameter of the implanted Mg disc. (B) Changes in the diameter of the gas pockets around the AS-coated (circle) and non-coated (square) Mg discs and (C) % weight loss of Mg discs implanted in vivo for 6 weeks. For Box plot C, the diamonds (♦) represent individual values. The median values are represented by horizontal lines inside the box; the mean values are represented by the empty rectangle (□); the upper and lower box ranges represent standard deviation (SD).

Paired t-tests at weeks 4-6 did not show any significant differences between coated and uncoated samples, although the mean pocket diameters around the coated discs were consistently smaller (Figure 21 B). Nevertheless, a two-way ANOVA analysis of the data revealed that the differences between the experimental groups over 6 weeks were highly significant ($p=0.01$). These results indicate that the AS coating effectively prevented the gas pocket formation around the Mg implant, especially in the initial post-implantation period in a subcutaneous model.

AS coatings effectively controls the initial burst of H_2 for up to 3 weeks. The volume of a gas pocket formed in the AS coated groups was less than non-coated group at any time point after 3 weeks but the rate of gas pocket formation was the same. This observation suggests that around week 3 the coating has sufficiently degraded and the corroding Mg surface was exposed to the environment. The longevity of the coating can be potentially improved by use of crosslinkable AS molecules.

6.5.3 Corrosion analysis by the weight loss method.

The mean percentage weight loss for uncoated samples was 15 ± 4.60 vs. 10 ± 1.43 (mean \pm SD) for the AS coated samples (Figure 21 C). The paired t-test showed that these differences are only marginally significant ($p=0.07$), which is attributed to the large standard deviation in the percentage of the weight loss of the uncoated samples (Figure 21 C). At the same time, the 3-fold smaller SD in the AS coated vs uncoated group suggests that the coating dramatically improves the corrosion rate reproducibility.

6.5.4 The μ CT and profilometry analysis of the corroded surfaces.

The analysis of the μ CT surface renderings of the corroded discs prior to the implantation revealed smooth and homogeneous surfaces for both coated and uncoated samples (Figure 22 A-D) The discs retrieved from the implantation sites after 6 weeks revealed significant degree of corrosion for both experimental groups (Figure 22 A'-D'). The degree of corrosion on the surfaces facing muscles was greater (Figure 22 A', C') than on the opposite surfaces in both experimental groups (Figure 22 B', D'). The corrosion patterns on the AS coated vs non-coated samples demonstrated noticeable differences. The topography of the non-coated discs was very uneven with a several deep pits, indicating the presence of pitting corrosion, while the corrosion profile of the AS coated samples was much more homogeneous, with multiple small and shallow pits evenly distributed throughout the surface. To assess the differences in surface corrosion observed by μ CT in a quantitative manner we conducted profilometry studies. Two parameters were used in the surface topography analysis of the samples. The Ra is a parameter describing surface texture at the submicron scale, while waviness Wa describes the texture at the microscopic scale. The intergroup comparison showed that Ra values were significantly higher for both surfaces in Mg-OH vs. Mg-OH-AS samples ($p=0.0069$ for the surface facing the muscle side and $p=0.042$ for the surface facing the skin side) (Table 4, Figure 23 A). Importantly, the Ra parameters in both groups were not significantly different between the two disc surfaces, suggesting that Ra is determined by the treatment type rather than the environment. Wa mean values were up to two times lower in the coated samples, although these differences were not statistically significant due to the very large variance of the non-coated samples (Table 4, Figure 23 B).

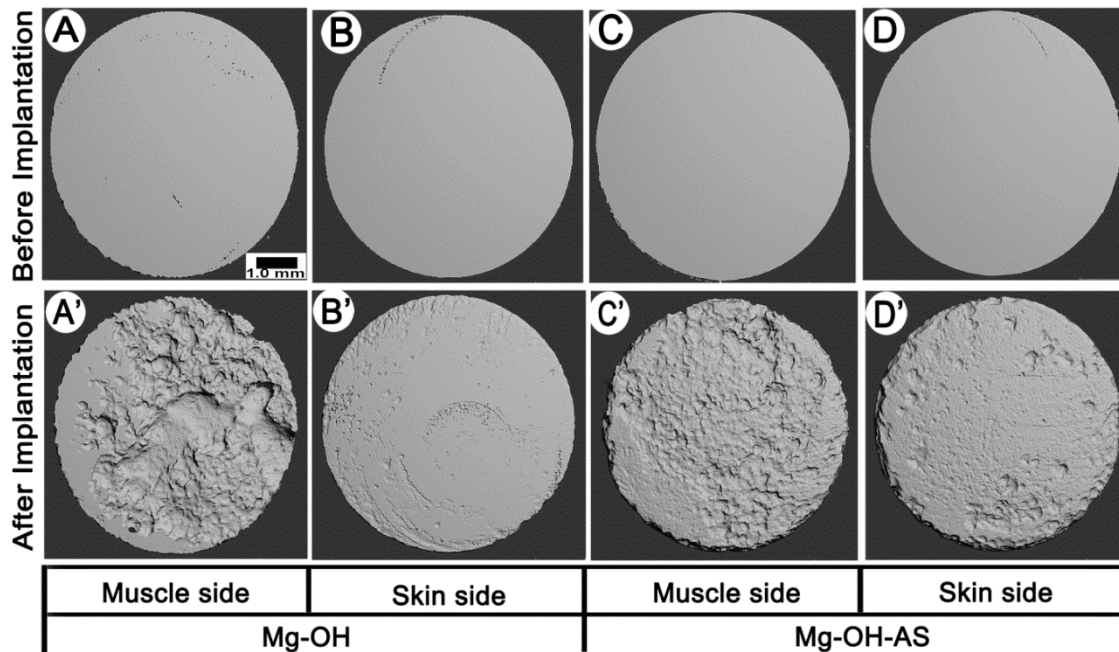


Figure 22. 3D μ CT images of representative samples before (A-D) and 6 weeks after (A'-D') the implantation; (A,A')- muscle side and (B,B')- skin side of an uncoated sample. (C,C') muscle side and (D,D')- skin side of a coated sample.

Table 4. Surface Ra and Wa values of the Mg discs before and after implantation.

Sr No	Sample	Ra (nm)	Wa (μ m)
1)	Mg-OH before implantation	10.86 ± 1.10	0.47 ± 0.12
2)	Mg-OH-AS before implantation	13.98 ± 2.52	0.41 ± 0.09
3)	Mg-OH Muscle side	273.43 ± 24.17	22.01 ± 18.27
4)	Mg-OH Skin side	256.40 ± 37.76	15.24 ± 14.76
5)	Mg-OH-AS Muscle side	206.27 ± 27.98	10.24 ± 3.73
6)	Mg-OH-AS Skin side	202.10 ± 11.31	6.70 ± 2.41

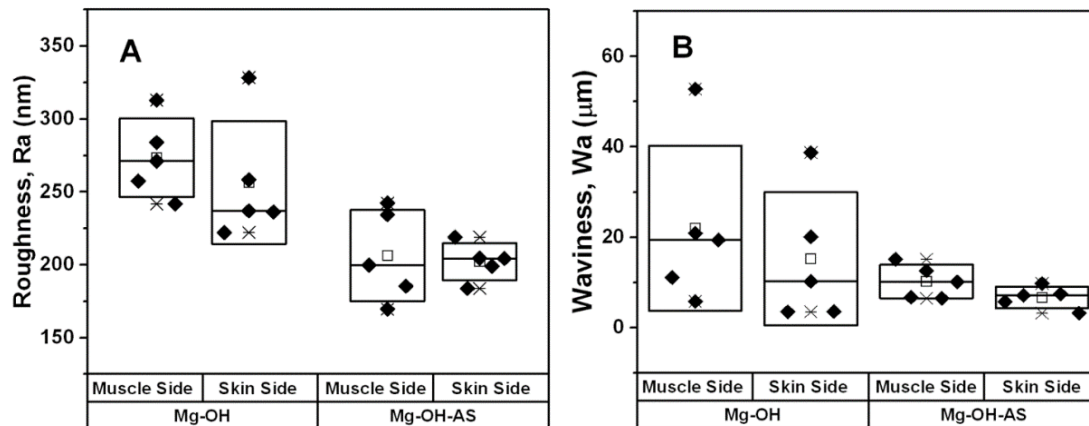


Figure 23. Box plots of (A) Roughness (Ra) and (B) Waviness (Wa) data of the samples implanted for 6 weeks after the implantation. The diamonds (◆) represent individual values from individual samples. The median values are represented by horizontal lines in the center of the box; the mean values are represented by the empty rectangle (□) on the box plot; the upper and lower box ranges represent standard deviation (SD).

6.5.5 Postmortem examination and histological analysis of the sites of implantation.

After euthanasia the cadavers were scanned in μ CT and the sites of implantation were visually examined (Figure 24 A-C). No significant signs of inflammation were observed visually in the tissues surrounding the Mg-OH and Mg-OH-AS discs (Figure 24 A). The histological analysis of the tissue samples collected 6 weeks post implantation from the area underneath the discs showed no differences in non-coated vs. AS coated samples. Normal muscle and connective tissue appearance, similar to intact tissue, were observed in both samples (Figure 24 D-F). No foreign body response was observed in tissue sampled collected around the non-coated and AS

coated Mg discs. These observations support the notion that the AS coatings are safe and do not cause adverse effects at the implantation sites.

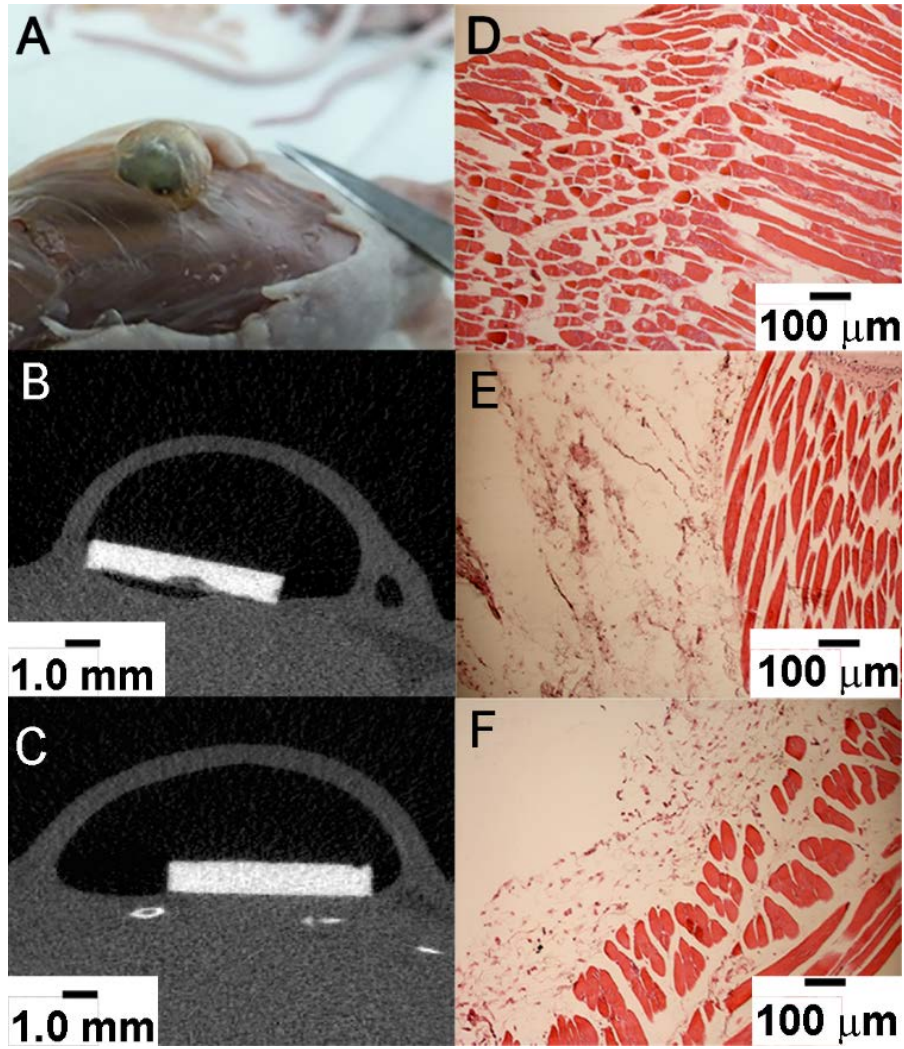


Figure 24. Photograph of a gas pocket on back of a mouse (A), X-ray images of Mg-OH (B) and Mg-OH-AS (C) disc in mice subcutaneous region, H & E stained images of muscle tissue collected around (D) no implanted disc (control mice) (E) Mg-OH disc (non-coated) and (F) Mg-OH-AS discs (coated).

6.6 DISCUSSION

Our results clearly showed that the AS coating effectively prevented the formation of gas pockets especially during initial 3 weeks post-implantation. These results demonstrate the feasibility of using the AS coatings for regulation of the gas pocket formation. The gas pockets around implantable devices were observed in human patients [33, 120] as well as animal models [193, 195, 204, 205]. In 1938 McBride observed significant gas pocket formation around the bone Mg fixation device [33, 120]. Berglund et al. observed gas pocket growth during a 3 weeks period after implantation in adult male Sprague–Dawley rats, however, these gas pockets disappeared at 6 weeks post implantation [195]. Fischerauer et al. observed substantial amount of gas formation between 1 week and 4 week in the intramedullary cavity and the soft tissues in the femoral mid-diaphyseal region in rat model. The volume of the gas pockets in this study also subsequently decreased in the 4 - 12 week period [206]. In contrast, the AS coating reduced the gas pocket formation especially during the first 3 weeks post-implantation. This reduction in gas pocket diameter was both highly significant and had a large effect size. Interestingly, in our study the size of the pockets did not decrease during the 4 week experiment in contrast to the studies cited above. This can be potentially explained by the differences in the experimental design, i.e. surgical sites, animal models used and the differences between surgical procedures.

The results of our weight loss studies show ~30% decrease in the mean % weight loss values in the AS coated group compared to the control. This difference however, was only marginally significant. The potential reason for this might lie in the greater variation of the corrosion rates in the uncoated samples, manifested by the SD values which are 3 times higher in the control than that in the AS coated group. Similar trend was also observed in the Wa results showing a 2 times difference in the mean values between the uncoated and AS coated groups,

while, in this case a 5 fold differences in the SD values were observed. The variability in the corrosion rates between Mg devices can pose significant problems for their clinical use, since this difference will affect the time these devices stay in the body. Therefore, the AS coatings can be potentially used to improve the reproducibility of the corrosion rates of the resorbable Mg devices.

The high resolution μ CT observations after the removal of the corrosion products revealed that the corroded surfaces of uncoated discs had clear signs of pitting corrosion, which is a typical mode of corrosion for Mg and its alloys [207, 208]. In contrast, AS coated Mg discs corroded more homogeneously with multiple shallow dimples distributed evenly throughout the disc surface, although the corrosion was more pronounced at the edges of the discs where the coating is more susceptible to the damage. Our observations of the muscle and skin sides of the same discs in the μ CT reconstructions suggested that the surfaces facing muscle side were rougher than the surfaces facing skin side in both groups, although the profilometry analysis did not show any significant differences in the Ra and Wa values between the muscle and skin (gas pocket) sides in both groups. This was unexpected, since we initially hypothesized that the mechanical forces at the interface between the discs and the muscle tissues in combination with the higher fluid access will lead to increased corrosion on the muscle side. At the same time, the analysis of the profilometry data revealed significant reduction in Ra values in the AS coated group. Surface roughness of implants plays important role in interaction of implants with its surrounding environment [209, 210]. It has been shown that increase in surface roughness enhances the degradation rate of Mg and its alloys [211-213]. Hence, it can be of importance for clinical applications that AS coatings reduces surface roughness and the amount of pitting corrosion. We can only surmise for the mechanisms underlying this decrease in the pitting

corrosion. One potential explanation will be that the coating masks the impurities and the grain boundaries which serve as nucleation sites for corrosion on the surface of the metal and therefore limiting the electrolyte access [214].

Mg and its alloys are highly biocompatible but rapid degradation of Mg and its alloys can initiate inflammatory response in surrounding tissue at the implantation site [204]. Several *in vivo* studies reported an inflammatory tissue response to rapidly degrading implants [215, 216]. Erdmann et al noticed fibrous tissue and inflammatory cells in the surrounding tissue of MgCa0.8 alloy screws implanted in tibiae of rabbits [215]. In similar study, Abidin et al observed foreign body reaction to products generated from degradation of pure Mg, WZ21 and AZ91 alloys when implanted in the lower back muscle of rats [216]. Reifenrath et al noticed inflammatory tissue response when implanted ZEK100 alloy screw in lateral tibial cortices of rabbit [204]. Miura et al also noticed little infiltration of inflammatory cells around the Mg-Al binary alloy implanted in the rat tissue [217]. Our H&E study provides an overview of the cells and tissues surrounding the implants. The degrading implants can cause myofiber degeneration that can be detected by H&E staining [218]. We did not notice any myofiber necrosis in the muscle tissue surrounding our samples, indicating that AS coating is nontoxic and does not cause a foreign body reaction. Structure of the myofibers was normal with well-defined nuclei at the implant interface as well as in the deeper layers of the muscle. In our previous *in vitro* study [115], we have shown that, AS coating is cytocompatible [115] and our current *in vivo* data are in a good agreement with these *in vitro* experiments. It is not surprising since the degradation products of AS coating are mainly hydrocarbon (fat) and polysiloxane chains that both are biocompatible [199]. The fats can be quickly processed by the body, whereas silanes are widely used in biomedical applications and are biocompatible [107, 199].

6.7 CONCLUSIONS

In conclusion, our results demonstrate that AS coatings can effectively control *in vivo* corrosion rate of Mg discs and prevent the initial burst of H₂ gas for 3 weeks. The surface morphology study revealed that AS coated Mg discs corroded homogenously and its surface roughness was less than the non-coated Mg discs. The histology study showed no tissue damage around the AS coated Mg discs 6 weeks after implantation, which suggests that the AS coating is nontoxic and biocompatible. Overall our study demonstrates a great potential of the AS coatings for the corrosion control of resorbable Mg implantable devices.

In this chapter, we addressed the aim 3A (AS coatings control the *in vivo* corrosion of Mg substrate), 3B (AS coatings control the surface roughness of *in vivo* corroding Mg substrate) and 3C (AS coatings is nontoxic to surrounding muscle tissue in a mouse subcutaneous model)

7.0 CONCLUSIONS

In this dissertation, we used a dip coating technique to self-assemble multilayer AS films on degradable Mg and its alloys to control their corrosion rate. We further functionalized the AS layer with (3-Aminopropyl) triethoxysilane (APTES) to modify physicochemical properties, i.e. wettability, or bioactivity of the device. Our results clearly demonstrate that AS coatings can effectively reduce the corrosion rate and prevent the initial burst of corrosion which *in situ* can lead to the formation of gas pockets around an implantable device.

We tested the cytocompatibility of the AS coated Mg samples *in vitro* under tissue culture conditions. In our *in vitro* tissue culture experiments cells survived and proliferated on the AS coated Mg discs for more than 2 weeks which indicates that the coatings are not cytotoxic and support cell attachment, spreading and proliferation. We further functionalized the AS layer with APTES to improve cell adhesion. Importantly, no calcium or phosphate was detected on the sample surface after 2 weeks under tissue culture conditions, suggesting that the coating can prevent calcium phosphate formation.

We studied the anticorrosive property of AS coated Mg discs in a mouse subcutaneous model over 6 weeks. Our results demonstrate that AS coatings can effectively control *in vivo* corrosion rate of Mg discs and prevent the initial burst of H₂ gas for 2 weeks. The surface morphology study revealed that AS coated Mg discs corroded homogeneously and had less surface roughness value compared to non-coated Mg discs. The histology study confirmed that

there is no toxic effect of AS coatings on muscles tissue surrounding the implantation site over 6 weeks, which indicates that the AS coating is nontoxic. Overall our study clearly demonstrates a great potential for the use of hybrid AS coatings for the corrosion control of resorbable Mg devices with no toxic effect.

8.0 FUTURE DIRECTIONS

This dissertation has demonstrated the potential of self-assembled multilayer AS coatings to control the corrosion rate of Mg and its alloys and further functionalization with APTES to enhance the cytocompatibility. Furthermore, AS coatings were shown to control the *in vivo* corrosion of Mg and its alloys and AS coatings is biocompatible. There are many opportunities that remain to be explored for extending the scope of this dissertation. In following sections, we will discuss some of the future work that can further strengthen the AS coating project.

8.1 FUTURE DIRECTIONS FOR AS COATINGS DEVELOPMENT

We have developed self-assembled multilayer AS coatings designed to control Mg corrosion. The AS coatings formed by copolymerization of n-Decyltriethoxysilane and Tetramethoxysilane followed by dip coating of Mg and its alloys discs and some of them were further functionalized with (3-Aminopropyl) triethoxysilane. Some of the following work will further strengthen the AS coatings project.

8.1.1 Heat treatment of AS coatings.

In current work, we did not use heat treatment to AS coatings. However, it has been shown that heat treatment further improves anti-corrosion properties of silane coating by removing alcohol, water and precursor molecules from the coating layer [219, 220]. Heat treatment also improves the inter-crosslinking of silane molecules improving structural organization of the coating layer [221]. We propose to use heat treatment for AS coated Mg devices at 100°C for 10 min. The effect of the heat treatment can be immediately measured by conducting H₂ evolution study and comparing it with non-heated AS coated Mg discs.

8.1.2 Mechanical properties of AS coatings layer.

Our goal is to use AS coatings on degradable orthopedic fixation devices such as plates and screws. It is important to have strong adhesion of AS coating to such implants to avoid delamination of AS coating during handling as well as due to the mechanical stresses at the implantation site. It is important to quantify the mechanical properties of AS coatings to better understand its performance. With nanoindentation technique, one can measure the mechanical properties of AS coatings layer such as hardness (H), Young's modulus (E) and fracture toughness (K_{1C}). The Mg substrate roughness can greatly affect the nanoindentation measurements. To avoid the substrate contribution one can use 100 nm layer of Mg deposited on a glass substrate. Four sets of nanoindentation (4×4=16 indents per set) at different loads within thin coating thickness (we can assume that thickness of the coating is 1 μm) will be performed. To eliminate the effect of substrate on H and E values to the mechanical properties have to be evaluated within 1/10 of coating thickness or under 100 nm depth.

Similarly, the scratch test can be conducted on AS coated Mg substrate with the constant load to evaluate the effect of low loads on the coefficient of friction and detect possible abrasive damage from the tip. Gradient loading allows determining critical load at which coating cracks and observing the type of cracking. Scratch tests can be done on four sets of 10 scratch tests per set (200 μm length, 50 μm apart) at constant loads 1, 2 and 3 mN and gradually increased load profile from 0 to 5 mN.

8.2 FUTURE DIRECTIONS FOR IN VITRO AND IN VIVO STUDIES

8.2.1 Study the effect of osteogenic functionalized AS coatings on hBMSC differentiation into osteogenic lineage

Most of the metals are considered inert. It is essential that orthopedic implant will integrate with surrounding bone tissues. One way to achieve this desired effect is to develop bio-inspired coatings which will have osteoinductive properties and can integrate with surrounding bone tissue. The BMP-2 derived peptide sequence KIPKASSVPTELSAISTLYL-amide will be attached to self-assembled multilayer AS coating via amide bonds with APTES. Such innovative coating will improve the osteointegration of Mg implant with surrounding bone tissue. Although the device selected for this project is an orthopedic fixation plate, the technology can extend to other areas of such as implantable resorbable devices for craniofacial applications. The technology developed in this project can also be used for a broader application such as peptide-based stent coating and development of biosensors.

8.2.2 The Antibacterial Activities of Tetracycline encapsulated AS coatings

In the Aim 1, we studied the release kinetics of TC from AS coatings. This study demonstrated an incremental increase in the concentration of TC in SBF media in which the AS coated Mg discs were incubated. The antibacterial activities of TC encapsulated AS coatings on Mg substrate can be further studied by bacterial inhibition assay using growth inhibition of *Escherichia coli* (E. coli).

8.2.3 Evaluating the AS-coated orthopedic fixation implant in higher animal model

We have demonstrated the anticorrosive properties of AS coated Mg discs in mice subcutaneous model. The histological study also confirmed that AS coatings are biocompatible. Large animals such as dogs, sheep and pigs are more appropriate to evaluate the response of bone tissue to AS coated degradable Mg implants because of their bone structure closely matching with humans. However, they pose ethical challenges as well as housing, handling and availability issues [222]. Rabbit bone structure is less similar to the human but does not have above challenges [222]. We can use rabbit ulna model to evaluate anticorrosive properties of AS coated Mg plates and screws [223]. We can study the effectiveness of AS coatings in preventing the initial H₂ burst and any effect of such control on fracture healing and new bone formation over a period of 6 weeks and 12 weeks. μ CT analysis can be used to study the device degradation over study time points. The histological analysis will be used to study the effect of degradation products on surrounding tissue for As coated and non-coated Mg fixation devices.

8.2.4 In vivo anticorrosive properties of laser patterned AS-coated Mg discs

We have shown that selective removal of AS coatings deposited on Mg substrate by laser patterning is effective to regulate in vitro corrosion rate of Mg substrate and hydrogen evolution. The laser patterning of AS coated Mg discs provides an opportunity to tune the corrosion rate of Mg substrate. The selective patterning technique gives the opportunity to construct/fabricate orthopedic fixation implants that require different corrosion rates according to their implantation site. It will be interesting to study the *in vivo* corrosion rate, tissue integration and osteoconduction of such patterned AS coated Mg discs in an animal model.

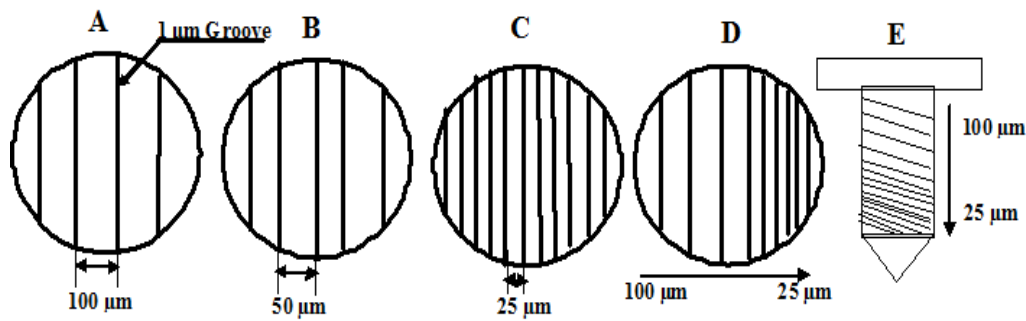


Figure 25. Schematic illustration of the laser-patterned AS coated Mg discs and screw.

The anticorrosive properties of laser patterned AS coated Mg discs can be evaluated subcutaneously in mice model. Varying degree of laser patterned AS coated Mg discs (Figure 25) can be compared to non-patterned AS coated Mg discs to study how patterning changes the *in vivo* corrosion rate.

APPENDIX A

SUPPLEMENTAL DATA

A.1 SUPPLEMENTAL TABLES

Supplementary Table 1. Mineral ion concentration in the SBF and blood plasma [144].

	Ion concentration (mM)							
	Na ⁺	K ⁺	Mg ²⁺	Ca ²⁺	Cl ⁻	HCO ₃ ⁻	HPO ₄ ²⁻	SO ₄ ²⁻
SBF	142.0	5.0	1.5	2.5	148.8	4.2	1.0	0.5
Blood plasma	142.0	5.0	1,5	2.5	103.0	2.7	1.0	0.5

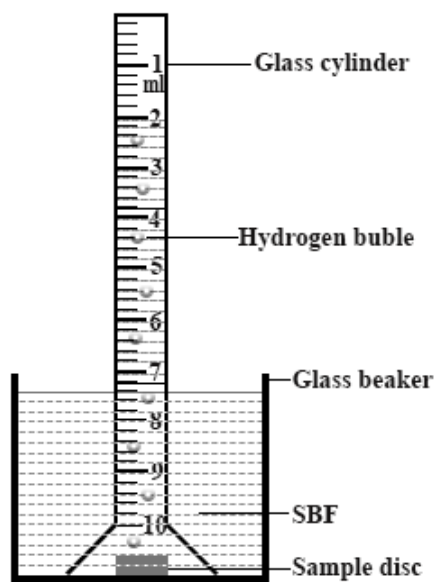
Supplementary Table 2. Cumulative H₂ evolution from Mg and AZ31 samples.

Sr. No	Time	Cumulative hydrogen evolution rate (ml/hr) (mean ± SD)			
		Mg	Mg-OH-AS	AZ31	AZ31-OH-AS
1)	Day 1 (24 h)	0.159±0.014	0.026±0.006	0.118±0.007	0.005±0.002
2)	Days 2-6 (144 h)	0.06±0.006	0.013±0.002	0.068±0.013	0.014±0.003

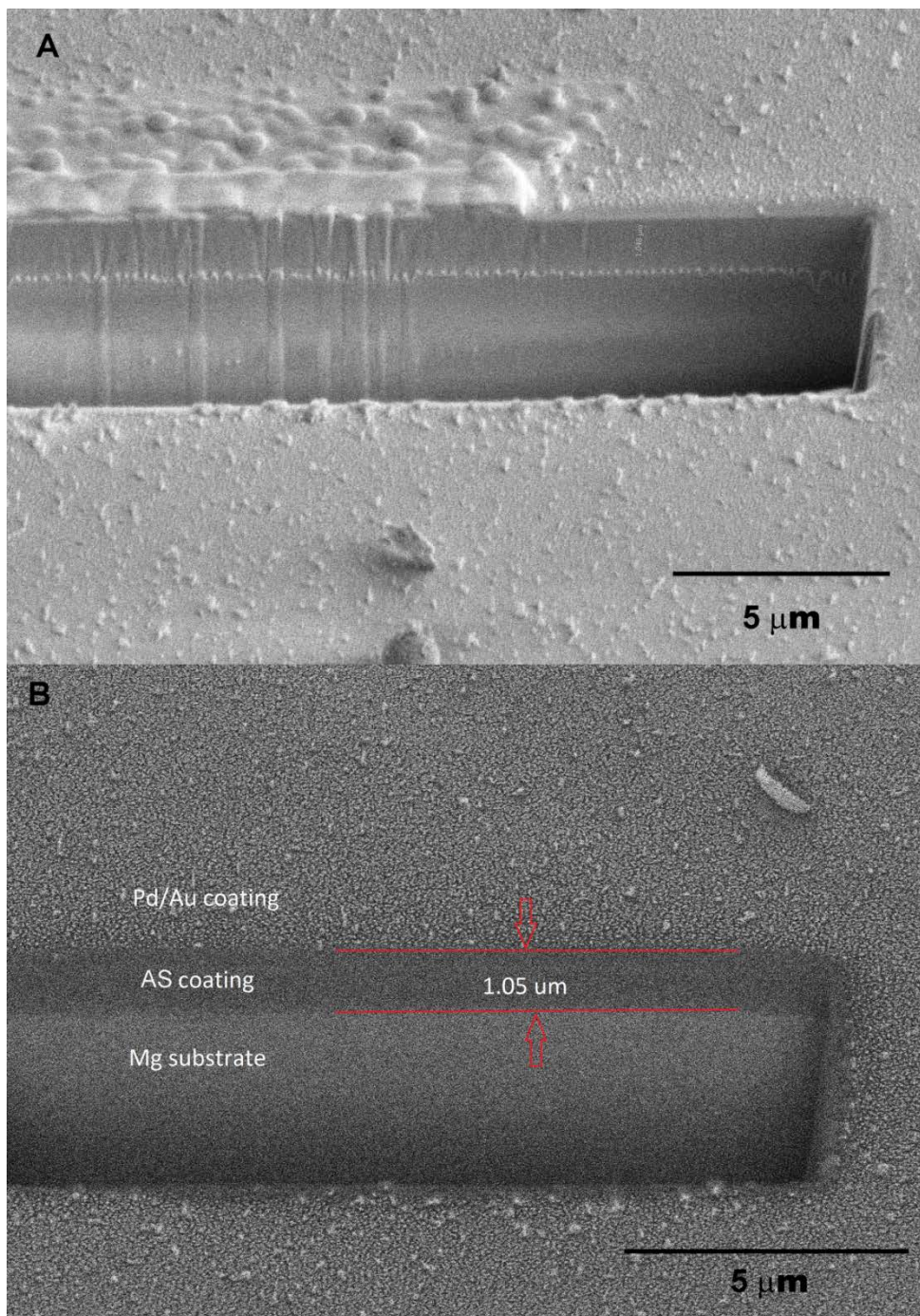
Supplementary Table 3. Elemental composition of non-coated Mg substrate and AS coated Mg substrate incubated in SBF for 7 days (From the coated and uncoated areas in Supplementary Figure 9A).

Sr. No	Element K edge	Corroded Side		Coated Side	
		Weight %	Atomic %	Weight %	Atomic %
1)	O	48.79	62.24	25.81	35.57
2)	Mg	29.69	24.93	50.88	46.14
3)	P	8.76	5.77	-	-
4)	Cl	8.57	4.93	-	-
5)	Ca	4.19	2.13	-	-
6)	Si	-	-	23.31	18.30

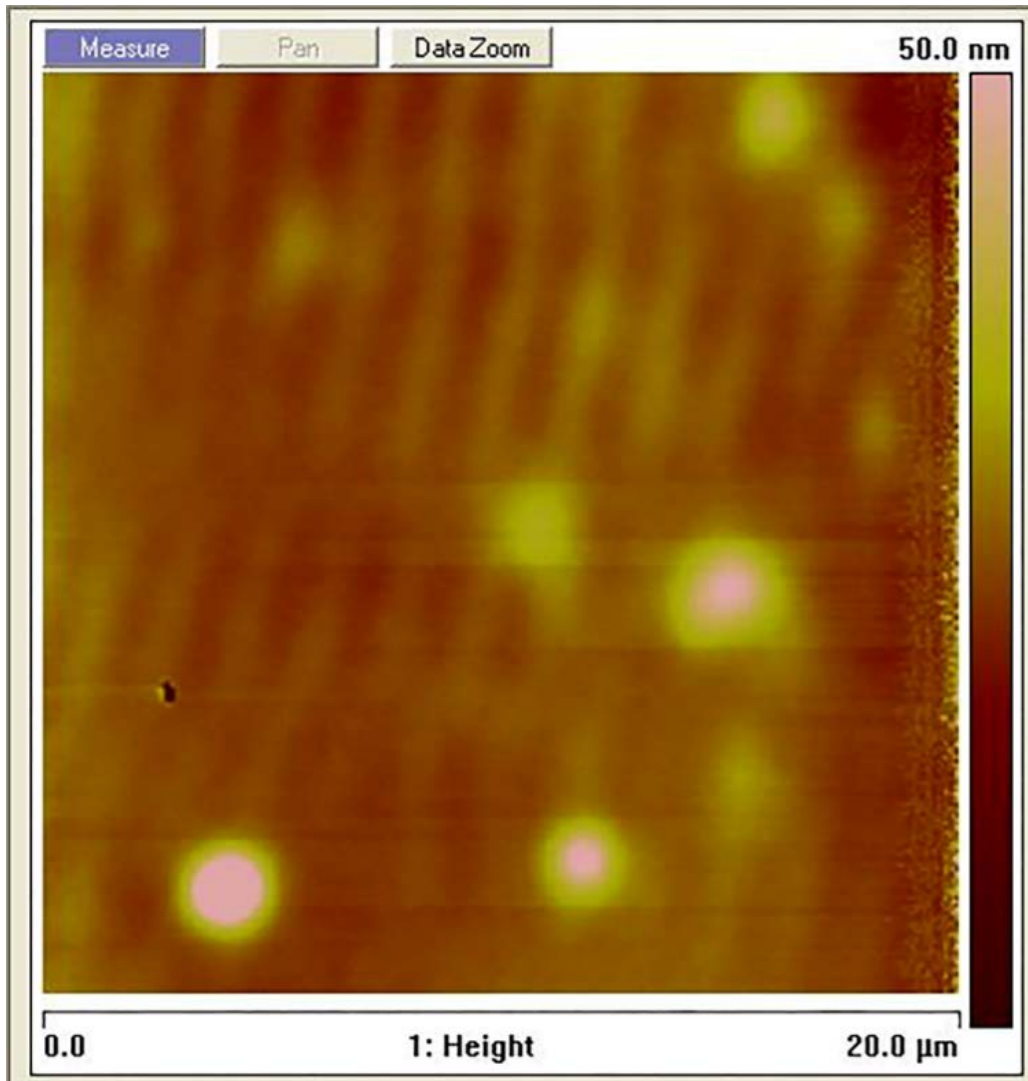
A.2 SUPPLEMENTAL FIGURES



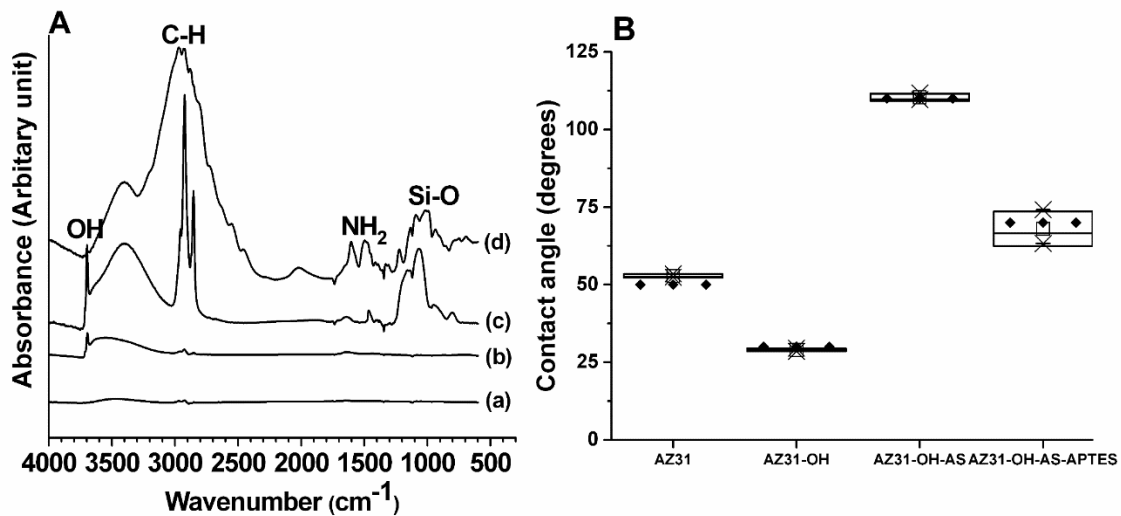
Supplementary Figure 1. Schematic illustration for the H₂ evolution experimental setup.



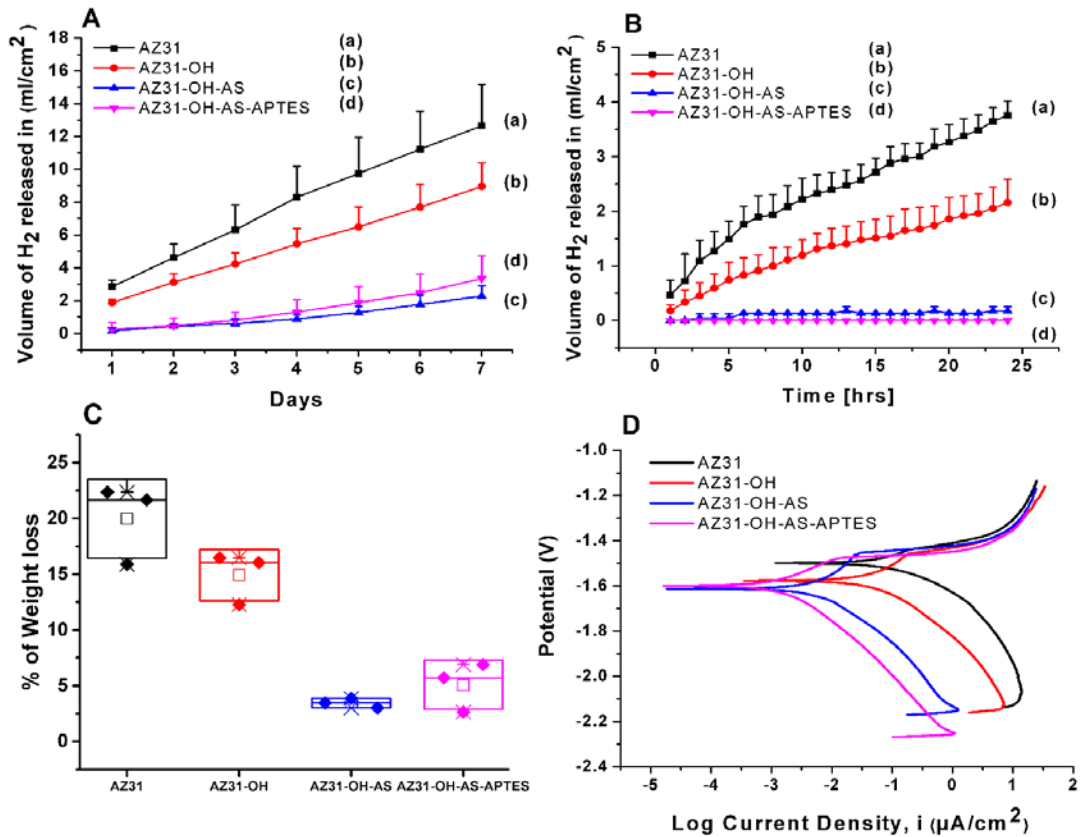
Supplementary Figure 2. SEM images of the FIBed Mg disc coated with AS self-assembled multilayer film in secondary (A) and backscattered (B) electron modes. Note that in the backscattered electron mode the coating appears darker due to its lesser density than Mg metal.



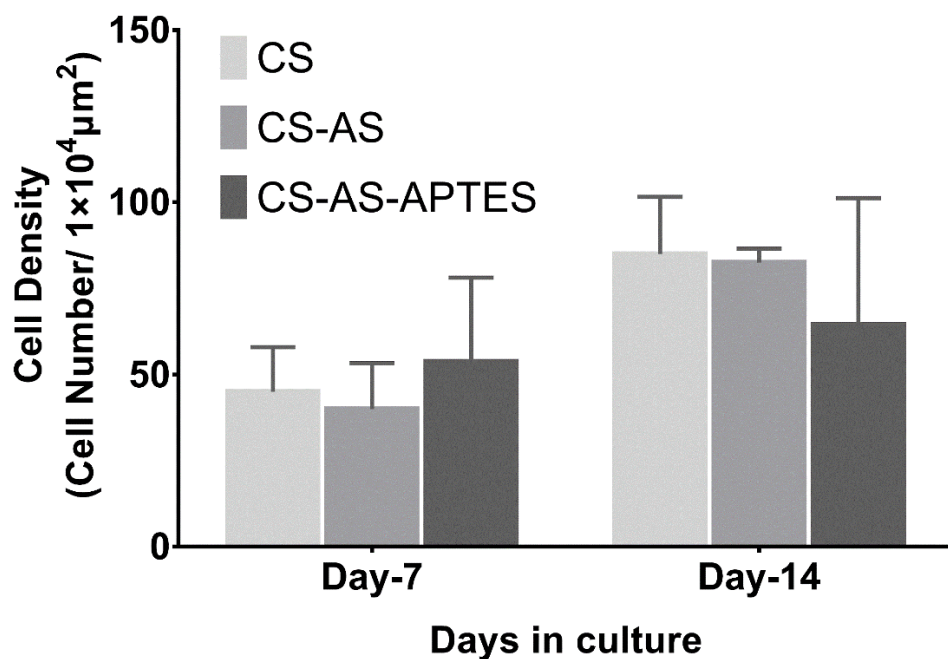
Supplementary Figure 3. AFM image of the surface of the AS coating on Mg. Note the step-like features representing the exposed edges of the individual lamellae. The bright spots are contaminants on the surface.



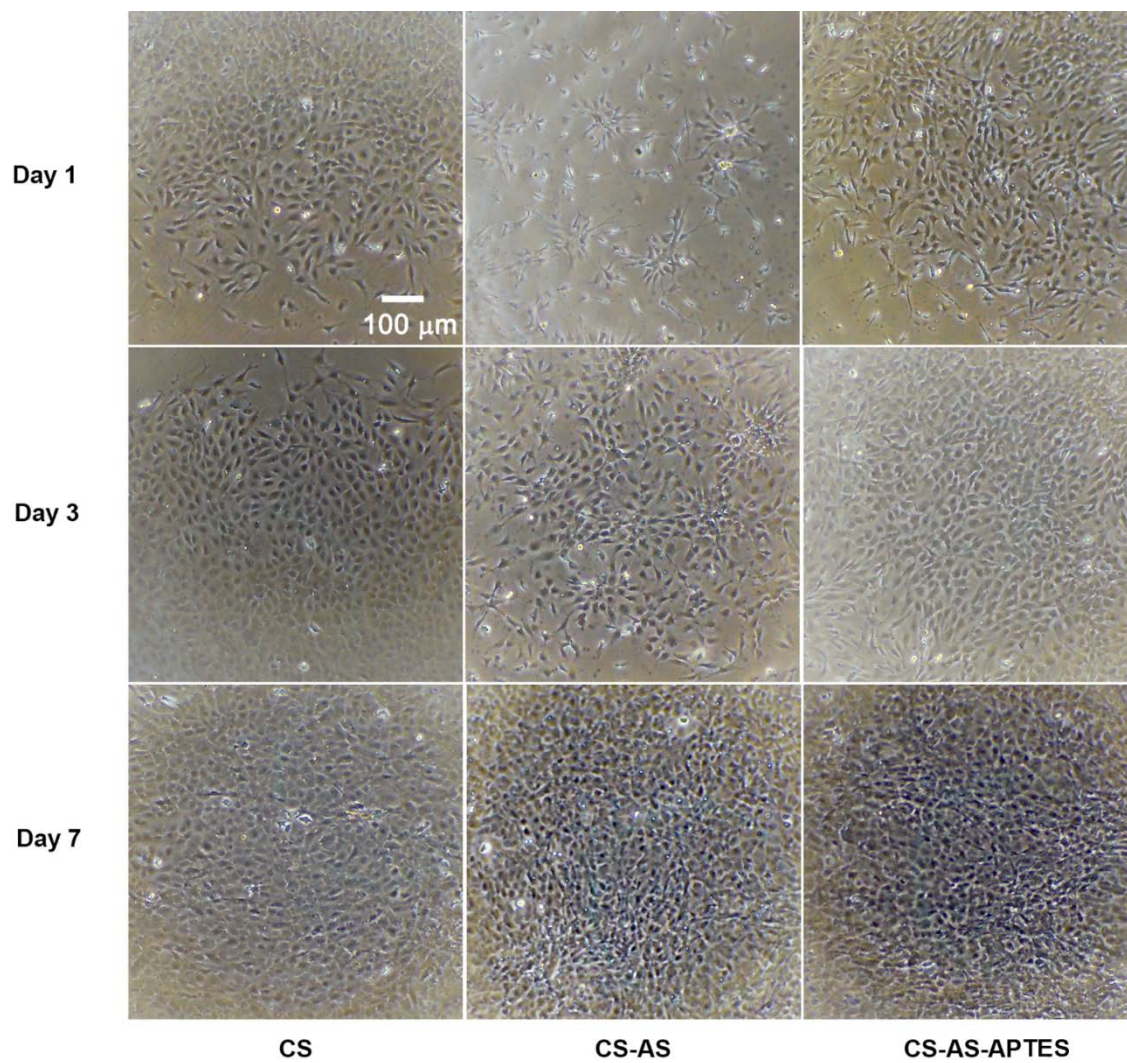
Supplementary Figure 4. ATR-FTIR spectra of AZ31 sample discs (Panel A), AZ31 (a), AZ31-OH (b), AZ31-OH-AS (c), AZ31-OH-AS-APTES (d) and box plot of static water contact angles measured on AZ31 sample discs (Panel B).



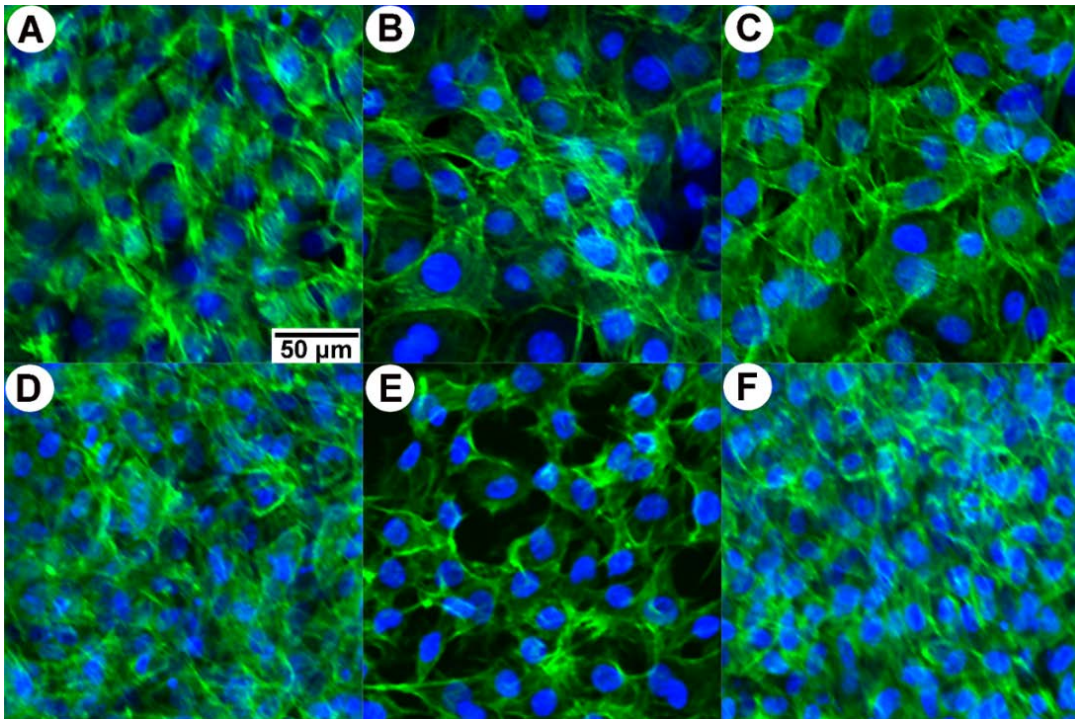
Supplementary Figure 5. Cumulative hydrogen release profiles from AZ31 discs over 7 days period (Panel A), 24 hours period (Panel B) following incubation in SBF, weight loss of AZ31 discs (Panel C) following 7 days incubation in SBF and Potentiodynamic polarization curve of Mg sample discs (Panel D) as a measure of corrosion rate.



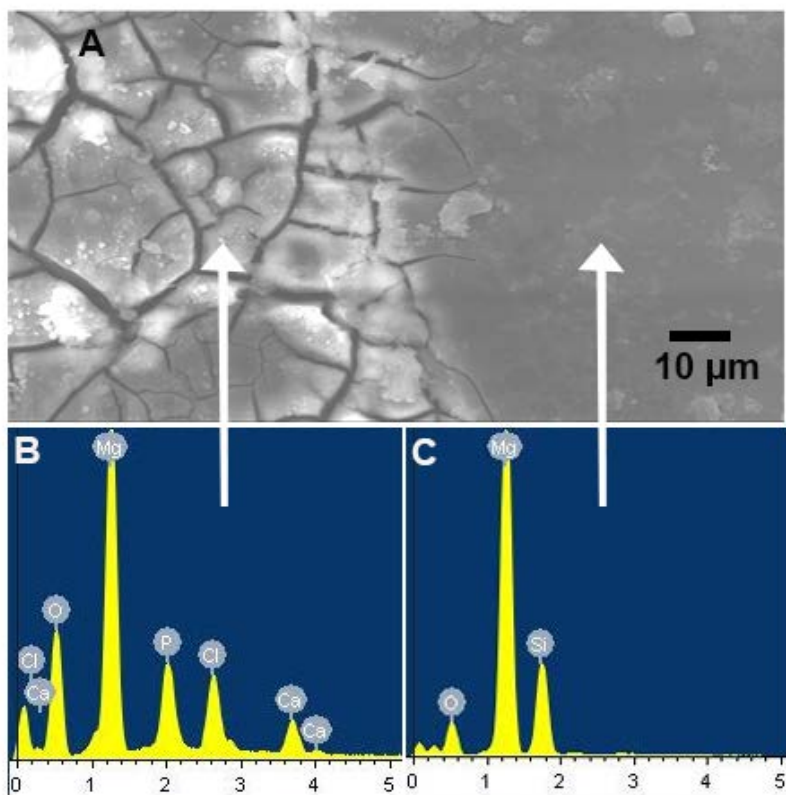
Supplementary Figure 6. Changes in cell density on glass coverslips (CS), glass coverslips coated with AS (CS-AS) films and glass coverslips coated with AS films and aminated with APTES (CS-AS-APTES) after 7 and 14 days in culture. The analysis was conducted using spectrophotometric analysis of DNA.



Supplementary Figure 7. Optical images of MC3T3 cells on non-coated and AS coated cover slips. All micrographs are taken at identical magnification.



Supplementary Figure 8. Confocal images of MC3T3 cells grown for 7 (A-C) and 14 (D-F) days on CS (A & D), CS-AS (B & E), CS-AS-APTES (C & F). The actin cytoskeleton is visualized using Alexa Fluor® 488 dye (green) and nuclear DNA is stained with Hoechst 33342 dye (blue).



Supplementary Figure 9. (Panel A) SEM image showing corrosion morphology of non-coated Mg and AS coated Mg surface after soaking in SBF for 7 days. (Panel B) EDS spectrum obtained from non-coated Mg substrate in A. C. EDS spectrum obtained from AS coated side in A. See the supplementary table 3 above for elemental composition.

BIBLIOGRAPHY

- [1] Hauret KG, Jones BH, Bullock SH, Canham-Chervak M, Canada S. Musculoskeletal injuries: Description of an under-recognized injury problem among military personnel. *American Journal of Preventive Medicine* 2010;38:S61-S70.
- [2] Wang H, Naghavi M, Allen C, Barber RM, Bhutta ZA, Carter A, et al. Global, regional, and national life expectancy, all-cause mortality, and cause-specific mortality for 249 causes of death, 1980–2015: a systematic analysis for the Global Burden of Disease Study 2015. *The Lancet* 2016;388:1459-544.
- [3] Woolf AD. Global burden of osteoarthritis and musculoskeletal diseases. *BMC Musculoskeletal Disorders* 2015;16:S3.
- [4] United States Bone and Joint Initiative: The Burden of Musculoskeletal Diseases in the United States (BMUS), Third Edition, 2014. Rosemont, IL. Available at <http://www.boneandjointburden.org>. Accessed on (2/29/2017).
- [5] Medtech Insight. U.S. Markets for fracture fixation products. 2011.
- [6] Chao Le Meng Bao, Erin Y. Teo, Mark S.K. Chong, Yuchun Liu, Mahesh Choolani, Chan JKY. *Advances in Bone Tissue Engineering*. In: Andrades PJA, editor. *Regenerative Medicine and Tissue Engineering: InTech*; 2013.
- [7] Marenzana M, Arnett TR. The Key Role of the Blood Supply to Bone. *Bone Research* 2013;1:203-15.
- [8] Wang T, Zhang X, Bikle DD. Osteogenic Differentiation of Periosteal Cells During Fracture Healing. *J Cell Physiol* 2017;232:913-21.
- [9] Hutmacher DW, Sittinger M. Periosteal cells in bone tissue engineering. *Tissue engineering* 2003;9:45-64.
- [10] Buck DWI, Dumanian GA. *Bone Biology and Physiology: Part I. The Fundamentals*. *Plastic and Reconstructive Surgery* 2012;129:1314-20.
- [11] Beniash E. *Biominerals—hierarchical nanocomposites: the example of bone*. *Wiley Interdisciplinary Reviews: Nanomedicine and Nanobiotechnology* 2011;3:47-69.

- [12] Raggatt LJ, Partridge NC. Cellular and Molecular Mechanisms of Bone Remodeling. *The Journal of Biological Chemistry* 2010;285:25103-8.
- [13] Proff P, Römer P. The molecular mechanism behind bone remodelling: a review. *Clinical Oral Investigations* 2009;13:355-62.
- [14] Whiting W, Zernicke R. *Biomechanics of Musculoskeletal Injury: Human Kinetics*; 2008.
- [15] Pivonka P, Dunstan CR. Role of mathematical modeling in bone fracture healing. *BoneKEY Rep* 2012;1.
- [16] Schatzker J, Tile M, Axelrod T, Hu R, Stephen D. *The rationale of operative fracture care: Third edition* 2005.
- [17] Colton C RP, Trafton P. *AO Surgery Reference*. Davos, Switzerland.
- [18] Rüedi T, Buckley R, Mora C. *AO Principles of Fracture Management*. Stuttgart: Thieme 2007.
- [19] Fraker AC, Ruff AW. Metallic surgical implants: state of the art. *JOM* 1977;29:22-8.
- [20] Chen Q, Thouas GA. Metallic implant biomaterials. *Materials Science and Engineering R: Reports* 2015;87:1-57.
- [21] Gyaneshwar T, Nitesh R, Sagar T, Pranav K, Rustagi N. Treatment of pediatric femoral shaft fractures by stainless steel and titanium elastic nail system: A randomized comparative trial. *Chinese Journal of Traumatology* 2016;19:213-6.
- [22] Metsemakers WJ, Moriarty TF, Nijs S, Pape HC, Richards RG. Influence of implant properties and local delivery systems on the outcome in operative fracture care. *Injury* 2016;47:595-604.
- [23] Hayes JS, Klöppel H, Wieling R, Sprecher CM, Richards RG. Influence of steel implant surface microtopography on soft and hard tissue integration. *Journal of Biomedical Materials Research - Part B Applied Biomaterials* 2017.
- [24] Hayes JS, Richards RG. The use of titanium and stainless steel in fracture fixation. *Expert Review of Medical Devices* 2010;7:843-53.
- [25] Krischak GD, Gebhard F, Mohr W, Krivan V, Ignatius A, Beck A, et al. Difference in metallic wear distribution released from commercially pure titanium compared with stainless steel plates. *Archives of Orthopaedic and Trauma Surgery* 2004;124:104-13.
- [26] Uthoff HK, Finnegan M. The effects of metal plates on post-traumatic remodelling and bone mass. *J Bone Joint Surg Br* 1983;65:66-71.
- [27] Jacobs JJ, Gilbert JL, Urban RM. Corrosion of metal orthopaedic implants. *J Bone Joint Surg Am* 1998;80:268-82.

- [28] Hallab N, Merritt K, Jacobs JJ. Metal sensitivity in patients with orthopaedic implants. *J Bone Joint Surg Am* 2001;83-A:428-36.
- [29] Bostman O, Pihlajamaki H. Routine implant removal after fracture surgery: a potentially reducible consumer of hospital resources in trauma units. *J Trauma* 1996;41:846-9.
- [30] Busam ML, Esther RJ, Obremskey WT. Hardware removal: Indications and expectations. *Journal of the American Academy of Orthopaedic Surgeons* 2006;14:113-20.
- [31] Reith G, Schmitz-Greven V, Hensel KO, Schneider MM, Tinschmann T, Bouillon B, et al. Metal implant removal: benefits and drawbacks - a patient survey. *BMC Surgery* 2015;15.
- [32] McBride E. Absorbable metal in bone surgery. *JAMA* 1938;111:2464-7.
- [33] McBride ED. Magnesium screw and nail transfixion in fractures. *Southern Medical Journal* 1938;31:508-15.
- [34] Rokkanen PU, Böstman O, Hirvensalo E, Mäkelä EA, Partio EK, Päätiälä H, et al. Bioabsorbable fixation in orthopaedic surgery and traumatology. *Biomaterials* 2000;21:2607-13.
- [35] Ciccone WJ, 2nd, Motz C, Bentley C, Tasto JP. Bioabsorbable implants in orthopaedics: new developments and clinical applications. *J Am Acad Orthop Surg* 2001;9:280-8.
- [36] Bostman OM, Pihlajamaki HK. Adverse tissue reactions to bioabsorbable fixation devices. *Clin Orthop Relat Res* 2000:216-27.
- [37] Hughes TB. Bioabsorbable implants in the treatment of hand fractures: an update. *Clin Orthop Relat Res* 2006;445:169-74.
- [38] Zheng YF, Gu XN, Witte F. Biodegradable metals. *Materials Science and Engineering: R: Reports* 2014;77:1-34.
- [39] Peuster M, Beerbaum P, Bach FW, Hauser H. Are resorbable implants about to become a reality? *Cardiol Young* 2006;16:107-16.
- [40] Witte F. The history of biodegradable magnesium implants: A review. *Acta Biomater* 2010;6:1680-92.
- [41] Zhao D, Witte F, Lu F, Wang J, Li J, Qin L. Current status on clinical applications of magnesium-based orthopaedic implants: A review from clinical translational perspective. *Biomaterials* 2017;112:287-302.
- [42] Witte F, Kaese V, Haferkamp H, Switzer E, Meyer-Lindenberg A, Wirth CJ, et al. In vivo corrosion of four magnesium alloys and the associated bone response. *Biomaterials* 2005;26:3557-63.

- [43] Witte F. The history of biodegradable magnesium implants: a review. *Acta Biomater* 2010;6:1680-92.
- [44] Kuhlmann J, Bartsch I, Willbold E, Schuchardt S, Holz O, Hort N, et al. Fast escape of hydrogen from gas cavities around corroding magnesium implants. *Acta Biomater* 2013;9:8714-21.
- [45] Staiger MP, Pietak AM, Huadmai J, Dias G. Magnesium and its alloys as orthopedic biomaterials: A review. *Biomaterials* 2006;27:1728-34.
- [46] Hornberger H, Virtanen S, Boccaccini AR. Biomedical coatings on magnesium alloys – A review. *Acta Biomater* 2012;8:2442-55.
- [47] Gray JE, Luan B. Protective coatings on magnesium and its alloys — a critical review. *Journal of Alloys and Compounds* 2002;336:88-113.
- [48] Uddin MS, Colin H, Peter M. Surface treatments for controlling corrosion rate of biodegradable Mg and Mg-based alloy implants. *Science and Technology of Advanced Materials* 2015;16:053501.
- [49] Shaw B. Corrosion resistance of magnesium alloys. In: Stephen D, editor. *ASM handbook volume 13a: corrosion: fundamentals, testing and protection*. UK: ASM Int; 2003:692-6.
- [50] Kirkland NT, Lespagnol J, Birbilis N, Staiger MP. A survey of bio-corrosion rates of magnesium alloys. *Corros Sci* 2010;52:287-91.
- [51] Witte F, Fischer J, Nellesen J, Crostack HA, Kaese V, Pisch A, et al. In vitro and in vivo corrosion measurements of magnesium alloys. *Biomaterials* 2006;27:1013-8.
- [52] Dziuba D, Meyer-Lindenberg A, Seitz JM, Waizy H, Angrisani N, Reifenrath J. Long-term in vivo degradation behaviour and biocompatibility of the magnesium alloy ZEK100 for use as a biodegradable bone implant. *Acta Biomater* 2013;9:8548-60.
- [53] Huehnerschulte TA, Angrisani N, Rittershaus D, Bormann D, Windhagen H, Meyer-Lindenberg A. In Vivo Corrosion of Two Novel Magnesium Alloys ZEK100 and AX30 and Their Mechanical Suitability as Biodegradable Implants. *Materials* 2011;4:1144-67.
- [54] Amerstorfer F, Fischerauer SF, Fischer L, Eichler J, Draxler J, Zitek A, et al. Long-term in vivo degradation behavior and near-implant distribution of resorbed elements for magnesium alloys WZ21 and ZX50. *Acta Biomater* 2016;42:440-50.
- [55] Kraus T, Fischerauer SF, Hanzi AC, Uggowitzer PJ, Loffler JF, Weinberg AM. Magnesium alloys for temporary implants in osteosynthesis: in vivo studies of their degradation and interaction with bone. *Acta Biomater* 2012;8:1230-8.
- [56] Krause A, von der Hoh N, Bormann D, Krause C, Bach FW, Windhagen H, et al. Degradation behaviour and mechanical properties of magnesium implants in rabbit tibiae. *J Mater Sci* 2010;45:624-32.

- [57] Witte F, Hort N, Vogt C, Cohen S, Kainer KU, Willumeit R, et al. Degradable biomaterials based on magnesium corrosion. *Curr Opin Solid St M* 2008;12:63-72.
- [58] Pagano G, Guida M, Tommasi F, Oral R. Health effects and toxicity mechanisms of rare earth elements-Knowledge gaps and research prospects. *Ecotoxicol Environ Saf* 2015;115:40-8.
- [59] Willbold E, Gu X, Albert D, Kalla K, Bobe K, Brauneis M, et al. Effect of the addition of low rare earth elements (lanthanum, neodymium, cerium) on the biodegradation and biocompatibility of magnesium. *Acta Biomater* 2015;11:554-62.
- [60] Feyerabend F, Fischer J, Holtz J, Witte F, Willumeit R, Drucker H, et al. Evaluation of short-term effects of rare earth and other elements used in magnesium alloys on primary cells and cell lines. *Acta Biomater* 2010;6:1834-42.
- [61] Hornberger H, Virtanen S, Boccaccini AR. Biomedical coatings on magnesium alloys - a review. *Acta Biomater* 2012;8:2442-55.
- [62] Cao FY, Song GL, Atrens A. Corrosion and passivation of magnesium alloys. *Corros Sci* 2016;111:835-45.
- [63] Song G-L. The Effect of Texture on the Corrosion Behavior of AZ31 Mg Alloy. *JOM* 2012;64:671-9.
- [64] Nordlien JH, Ono S, Masuko N, Nisancioglu K. A TEM investigation of naturally formed oxide films on pure magnesium. *Corros Sci* 1997;39:1397-414.
- [65] Chen C, Splinter SJ, Do T, McIntyre NS. Measurement of oxide film growth on Mg and Al surfaces over extended periods using XPS. *Surface Science* 1997;382:L652-L7.
- [66] Trinidad J, Arruebarrena G, Marco I, Hurtado I, Argandoña ESd. Effectivity of fluoride treatment on hydrogen and corrosion product generation in temporal implants for different magnesium alloys. *Proceedings of the Institution of Mechanical Engineers, Part H: Journal of Engineering in Medicine* 2013;227:1301-11.
- [67] Ye X-Y, Chen M-F, You C, Liu D-B. The influence of HF treatment on corrosion resistance and in vitro biocompatibility of Mg-Zn-Zr alloy. *Frontiers of Materials Science in China* 2010;4:132-8.
- [68] Witte F, Fischer J, Nellesen J, Vogt C, Vogt J, Donath T, et al. In vivo corrosion and corrosion protection of magnesium alloy LAE442. *Acta Biomater* 2010;6:1792-9.
- [69] Thomann M, Krause C, Angrisani N, Bormann D, Hassel T, Windhagen H, et al. Influence of a magnesium-fluoride coating of magnesium-based implants (MgCa0.8) on degradation in a rabbit model. *Journal of Biomedical Materials Research Part A* 2010;93A:1609-19.
- [70] Chen XB, Birbilis N, Abbott TB. Review of Corrosion-Resistant Conversion Coatings for Magnesium and Its Alloys. *CORROSION* 2011;67:035005-1--16.

- [71] Iglesias C, Bodelon OG, Montoya R, Clemente C, Garcia-Alonso MC, Rubio JC, et al. Fracture bone healing and biodegradation of AZ31 implant in rats. *Biomed Mater* 2015;10:11.
- [72] Deshpande PP, Jadhav NG, Gelling VJ, Sazou D. Conducting polymers for corrosion protection: a review. *Journal of Coatings Technology and Research* 2014;11:473-94.
- [73] Heise S, Virtanen S, Boccaccini AR. Tackling Mg alloy corrosion by natural polymer coatings—A review. *Journal of Biomedical Materials Research Part A* 2016;104:2628-41.
- [74] Zheludkevich ML, Salvado IM, Ferreira MGS. Sol-gel coatings for corrosion protection of metals. *J Mater Chem* 2005;15:5099-111.
- [75] Wang D, Bierwagen GP. Sol-gel coatings on metals for corrosion protection. *Progress in Organic Coatings* 2009;64:327-38.
- [76] Shadanbaz S, Dias GJ. Calcium phosphate coatings on magnesium alloys for biomedical applications: A review. *Acta Biomater* 2012;8:20-30.
- [77] Jagur-Grodzinski J. Polymers for tissue engineering, medical devices, and regenerative medicine. Concise general review of recent studies. *Polym Adv Technol* 2006;17:395-418.
- [78] Kannan MB. Biodegradable polymeric coatings for surface modification of magnesium-based biomaterials. *Surface Modification of Magnesium and Its Alloys for Biomedical Applications*: Elsevier Inc.; 2015. p. 355-76.
- [79] Heise S, Virtanen S, Boccaccini AR. Tackling Mg alloy corrosion by natural polymer coatings-A review. *J Biomed Mater Res Part A* 2016.
- [80] Park M, Lee JE, Park CG, Lee SH, Seok HK, Choy YB. Polycaprolactone coating with varying thicknesses for controlled corrosion of magnesium. *Journal of Coatings Technology and Research* 2013.
- [81] Johnson I, Wang SM, Silken C, Liu H. A systemic study on key parameters affecting nanocomposite coatings on magnesium substrates. *Acta Biomater* 2016;36:332-49.
- [82] León B, Jansen J. *Thin Calcium Phosphate Coatings for Medical Implants*: Springer publishing.
- [83] Dorozhkin SV. Calcium orthophosphate coatings, films and layers. *Progress in Biomaterials* 2012;1:1.
- [84] Lorenz C, Brunner JG, Kollmannsberger P, Jaafar L, Fabry B, Virtanen S. Effect of surface pre-treatments on biocompatibility of magnesium. *Acta Biomater* 2009;5:2783-9.
- [85] Dorozhkin SV. Calcium orthophosphate deposits: Preparation, properties and biomedical applications. *Materials Science and Engineering: C* 2015;55:272-326.

- [86] Dorozhkin SV. Calcium orthophosphate coatings on magnesium and its biodegradable alloys. *Acta Biomater* 2014;10:2919-34.
- [87] Plueddemann EP. Chemistry of Silane Coupling Agents. In: Plueddemann EP, editor. *Silane Coupling Agents*: Springer Publishing. p. 235.
- [88] Mittal KL. *Silanes and Other Coupling Agents*. Netherlands.: VSP BV 1992.
- [89] W. J. van Ooij TC. Protecting metals with silane coupling agents *Chemtech* 1998;28:12.
- [90] Chou TP, Chandrasekaran C, Limmer S, Nguyen C, Cao GZ. Organic-inorganic sol-gel coating for corrosion protection of stainless steel. *Journal of Materials Science Letters* 2002;21:251-5.
- [91] Gu XN, Guo HM, Wang F, Lu Y, Lin WT, Li J, et al. Degradation, hemolysis, and cytotoxicity of silane coatings on biodegradable magnesium alloy. *Mater Lett* 2017;193:266-9.
- [92] Swati G, Khanna AS, Singh Raman RK. Development of biodegradable coating for controlled dissolution of a magnesium alloy as an implant. In: Chikosha S, Chikwanda HK, editors. *7th International Light Metals Technology Conference, LMT 2015*: Trans Tech Publications Ltd; 2015. p. 321-6.
- [93] Gaur S, Raman RKS, Khanna AS. In vitro investigation of biodegradable polymeric coating for corrosion resistance of Mg-6Zn-Ca alloy in simulated body fluid. *Mat Sci Eng C-Mater* 2014;42:91-101.
- [94] Liu X, Yue Z, Romeo T, Weber J, Scheuermann T, Moulton S, et al. Biofunctionalized anti-corrosive silane coatings for magnesium alloys. *Acta Biomater* 2013;9:8671-7.
- [95] Peng S, Zeng Z, Han J, Chen J, Wu X. Progress of anticorrosion of silane based sol-gel coating. *Mat China* 2014;33:77-85.
- [96] Figueira RB, Silva CJR, Pereira EV. Organic-inorganic hybrid sol-gel coatings for metal corrosion protection: a review of recent progress. *Journal of Coatings Technology and Research* 2015;12:1-35.
- [97] Hermanson GT. *Silane Coupling Agents*. *Bioconjugate Techniques*: Academic Press Jul 25, 2013 p. 1200.
- [98] Shimojima A, Kuroda K. Structural Control of Multilayered Inorganic–Organic Hybrids Derived from Mixtures of Alkyltriethoxysilane and Tetraethoxysilane. *Langmuir* 2002;18:1144-9.
- [99] Shimojima A, Kuroda K. Designed synthesis of nanostructured siloxane–organic hybrids from amphiphilic silicon-based precursors. *The Chemical Record* 2006;6:53-63.

- [100] Urata C, Cheng DF, Masheder B, Hozumi A. Smooth, transparent and nonperfluorinated surfaces exhibiting unusual contact angle behavior toward organic liquids. *Rsc Advances* 2012;2:9805-8.
- [101] Urata C, Masheder B, Cheng DF, Hozumi A. A thermally stable, durable and temperature-dependent oleophobic surface of a polymethylsilsesquioxane film. *Chem Commun* 2013;49:3318-20.
- [102] Shimojima A, Kuroda K. Structural control of multilayered inorganic-organic hybrids derived from mixtures of alkyltriethoxysilane and tetraethoxysilane. *Langmuir* 2002;18:1144-9.
- [103] Garrido L, Pfliederer B, Papisov M, Ackerman JL. In vivo degradation of silicones. *Magnetic Resonance in Medicine* 1993;29:839-43.
- [104] Xu L, Shi Y, Wang T, Dong Z, Su W, Cai Y. Methyl Siloxanes in Environmental Matrices around a Siloxane Production Facility, and Their Distribution and Elimination in Plasma of Exposed Population. *Environmental Science & Technology* 2012;46:11718-26.
- [105] Andersen ME, Sarangapani R, Reitz RH, Gallavan RH, Dobrev ID, Plotzke KP. Physiological Modeling Reveals Novel Pharmacokinetic Behavior for Inhaled Octamethylcyclotetrasiloxane in Rats. *Toxicological Sciences* 2001;60:214-31.
- [106] Rucker C, Kummerer K. Environmental Chemistry of Organosiloxanes. *Chemical Reviews* 2015;115:466-524.
- [107] Kros A, Jansen JA, Holder SJ, Nolte RJM, Sommerdijk NAJM. Silane-based hybrids for biomedical applications. *J Adhes Sci Technol* 2002;16:143-55.
- [108] Avnir D, Lev O, Livage J. Recent bio-applications of sol-gel materials. *J Mater Chem* 2006;16:1013-30.
- [109] Figueira RB, Silva CJR, Pereira EV. Organic-inorganic hybrid sol-gel coatings for metal corrosion protection: a review of recent progress. *Journal of Coatings Technology and Research* 2015;12:1-35.
- [110] Mojsiewicz-Pieńkowska K, Jamrógiewicz M, Szymkowska K, Krenczkowska D. Direct Human Contact with Siloxanes (Silicones) – Safety or Risk Part 1. Characteristics of Siloxanes (Silicones). *Frontiers in Pharmacology* 2016;7.
- [111] Ahmad Agha N, Willumeit-Römer R, Laipple D, Luthringer B, Feyerabend F. The Degradation Interface of Magnesium Based Alloys in Direct Contact with Human Primary Osteoblast Cells. *PLoS ONE* 2016;11:e0157874.
- [112] Mostofi S, Bonyadi Rad E, Wiltsche H, Fasching U, Szakacs G, Ramskogler C, et al. Effects of Corroded and Non-Corroded Biodegradable Mg and Mg Alloys on Viability, Morphology and Differentiation of MC3T3-E1 Cells Elicited by Direct Cell/Material Interaction. *PLoS ONE* 2016;11:e0159879.

- [113] Cecchinato F, Agha NA, Martinez-Sanchez AH, Luthringer BJC, Feyerabend F, Jimbo R, et al. Influence of magnesium alloy degradation on undifferentiated human cells. *PLoS ONE* 2015;10.
- [114] Mochizuki A, Yahata C, Takai H. Cytocompatibility of magnesium and AZ31 alloy with three types of cell lines using a direct in vitro method. *Journal of Materials Science: Materials in Medicine* 2016;27:145.
- [115] Patil AJ, Jackson O, Fulton LB, Hong D, Desai PA, Kelleher SA, et al. Anticorrosive Self-Assembled Hybrid Alkylsilane Coatings for Resorbable Magnesium Metal Devices. *ACS Biomaterials Science & Engineering* 2017;3:518-29.
- [116] Witte F, Hort N, Vogt C, Cohen S, Kainer KU, Willumeit R, et al. Degradable biomaterials based on magnesium corrosion. *Curr Opin Solid State Mater Sci* 2008;12:63-72.
- [117] Zhang Y, Xu J, Ruan YC, Yu MK, O'Laughlin M, Wise H, et al. Implant-derived magnesium induces local neuronal production of CGRP to improve bone-fracture healing in rats. *Nat Med* 2016;advance online publication.
- [118] Chaya A, Yoshizawa S, Verdelis K, Myers N, Costello BJ, Chou DT, et al. In vivo study of magnesium plate and screw degradation and bone fracture healing. *Acta Biomater* 2015;18:262-9.
- [119] Yoshizawa S, Brown A, Barchowsky A, Sfeir C. Magnesium ion stimulation of bone marrow stromal cells enhances osteogenic activity, simulating the effect of magnesium alloy degradation. *Acta Biomater* 2014;10:2834-42.
- [120] McBride E. Absorbable metal in bone surgery: A further report on the use of magnesium alloys. *Journal of the American Medical Association* 1938;111:2464-7.
- [121] Hort N, Huang Y, Fechner D, Stormer M, Blawert C, Witte F, et al. Magnesium alloys as implant materials - Principles of property design for Mg-RE alloys. *Acta Biomater* 2010;6:1714-25.
- [122] Cha PR, Han HS, Yang GF, Kim YC, Hong KH, Lee SC, et al. Biodegradability engineering of biodegradable Mg alloys: Tailoring the electrochemical properties and microstructure of constituent phases. *Scientific Reports* 2013;3.
- [123] Macdonald ML, Samuel RE, Shah NJ, Padera RF, Beben YM, Hammond PT. Tissue integration of growth factor-eluting layer-by-layer polyelectrolyte multilayer coated implants. *Biomaterials* 2011;32:1446-53.
- [124] Schmidmaier G, Wildemann B, Stemberger A, Haas NP, Raschke M. Biodegradable poly(D,L-lactide) coating of implants for continuous release of growth factors. *Journal of Biomedical Materials Research* 2001;58:449-55.
- [125] Reyes CD, Petrie TA, Burns KL, Schwartz Z, Garcia AJ. Biomolecular surface coating to enhance orthopaedic tissue healing and integration. *Biomaterials* 2007;28:3228-35.

- [126] Nanci A, Wuest JD, Peru L, Brunet P, Sharma V, Zalzal S, et al. Chemical modification of titanium surfaces for covalent attachment of biological molecules. *Journal of Biomedical Materials Research* 1998;40:324-35.
- [127] Johnson I, Wang SM, Silken C, Liu HN. A systemic study on key parameters affecting nanocomposite coatings on magnesium substrates. *Acta Biomater* 2016;36:332-49.
- [128] Ostrowski N, Lee B, Enick N, Carlson B, Kunjukunju S, Roy A, et al. Corrosion protection and improved cytocompatibility of biodegradable polymeric layer-by-layer coatings on AZ31 magnesium alloys. *Acta Biomater* 2013;9:8704-13.
- [129] Doepke A, Xue D, Yun Y, Vanooij WJ, Brian Halsall H, Heineman WR. Corrosion of organosilane coated Mg4Y alloy in sodium chloride solution evaluated by impedance spectroscopy and pH changes. *Electrochimica Acta* 2012;70:165-70.
- [130] Cui W, Beniash E, Gawalt E, Xu Z, Sfeir C. Biomimetic coating of magnesium alloy for enhanced corrosion resistance and calcium phosphate deposition. *Acta Biomater* 2013;9:8650-9.
- [131] Ehlert N, Mueller PP, Stieve M, Behrens P. Immobilization of alkaline phosphatase on modified silica coatings. *Microporous and Mesoporous Materials* 2010;131:51-7.
- [132] Liu X, Yue Z, Romeo T, Weber J, Scheuermann T, Moulton S, et al. Biofunctionalized anti-corrosive silane coatings for magnesium alloys. *Acta Biomater* 2013;9:8671-7.
- [133] Shimojima A, Sugahara Y, Kuroda K. Synthesis of Oriented Inorganic–Organic Nanocomposite Films from Alkyltrialkoxysilane–Tetraalkoxysilane Mixtures. *Journal of the American Chemical Society* 1998;120:4528-9.
- [134] Chemtob A, Ni LL, Croutxe-Barghorn C, Boury B. Ordered Hybrids from Template-Free Organosilane Self-Assembly. *Chem-Eur J* 2014;20:1790-806.
- [135] de Araujo AD, Palomo JM, Cramer J, Kohn M, Schroder H, Wacker R, et al. Diels-Alder ligation and surface immobilization of proteins. *Angewandte Chemie-International Edition* 2006;45:296-301.
- [136] Adessi C, Matton G, Ayala G, Turcatti G, Mermod JJ, Mayer P, et al. Solid phase DNA amplification: characterisation of primer attachment and amplification mechanisms. *Nucleic Acids Res* 2000;28.
- [137] Finnie KS, Waller DJ, Perret FL, Krause-Heuer AM, Lin HQ, Hanna JV, et al. Biodegradability of sol–gel silica microparticles for drug delivery. *Journal of Sol-Gel Science and Technology* 2009;49:12-8.
- [138] Irimia-Vladu M. "Green" electronics: biodegradable and biocompatible materials and devices for sustainable future. *Chemical Society Reviews* 2014;43:588-610.

- [139] Sanchez C, Julian B, Belleville P, Popall M. Applications of hybrid organic-inorganic nanocomposites. *J Mater Chem* 2005;15:3559-92.
- [140] Sanchez C, Belleville P, Popall M, Nicole L. Applications of advanced hybrid organic-inorganic nanomaterials: from laboratory to market. *Chemical Society Reviews* 2011;40:696-753.
- [141] Willbold E, Gu X, Albert D, Kalla K, Bobe K, Brauneis M, et al. Effect of the addition of low rare earth elements (lanthanum, neodymium, cerium) on the biodegradation and biocompatibility of magnesium. *Acta Biomater* 2015;11:554-62.
- [142] Banerjee PC, Raman RKS. Electrochemical impedance spectroscopic investigation of the role of alkaline pre-treatment in corrosion resistance of a silane coating on magnesium alloy, ZE41. *Electrochimica Acta* 2011;56:3790-8.
- [143] Witucki GL. A silane primer - chemistry and applications of alkoxy silanes. *Journal of Coatings Technology* 1993;65:57-60.
- [144] Kokubo T, Takadama H. How useful is SBF in predicting in vivo bone bioactivity? *Biomaterials* 2006;27:2907-15.
- [145] Song G, Atrens A, Stjohn D, Nairn J, Li Y. The electrochemical corrosion of pure magnesium in 1 N NaCl. *Corros Sci* 1997;39:855-75.
- [146] Xin Y, Hu T, Chu PK. In vitro studies of biomedical magnesium alloys in a simulated physiological environment: A review. *Acta Biomater* 2011;7:1452-9.
- [147] Lorking KF. Inhibition of corrosion of magnesium in chromic acid. *Nature* 1964;201:75.
- [148] Bobe K, Willbold E, Morgenthal I, Andersen O, Studnitzky T, Nellesen J, et al. In vitro and in vivo evaluation of biodegradable, open-porous scaffolds made of sintered magnesium W4 short fibres. *Acta Biomater* 2013;9:8611-23.
- [149] McCafferty E. Validation of corrosion rates measured by the Tafel extrapolation method. *Corros Sci* 2005;47:3202-15.
- [150] Shi ZM, Liu M, Atrens A. Measurement of the corrosion rate of magnesium alloys using Tafel extrapolation. *Corros Sci* 2010;52:579-88.
- [151] Kim BS, Putnam AJ, Kulik TJ, Mooney DJ. Optimizing seeding and culture methods to engineer smooth muscle tissue on biodegradable polymer matrices. *Biotechnology and Bioengineering* 1998;57:46-54.
- [152] Rampersad SN. Multiple Applications of Alamar Blue as an Indicator of Metabolic Function and Cellular Health in Cell Viability Bioassays. *Sensors* 2012;12:12347-60.
- [153] Bowen PK, Drelich J, Goldman J. Magnesium in the murine artery: Probing the products of corrosion. *Acta Biomater* 2014;10:1475-83.

- [154] Bowen PK, McNamara CT, Mills OP, Drelich J, Goldman J. FIB-TEM Study of Magnesium Corrosion Products after 14 Days in the Murine Artery. *ACS Biomaterials Science & Engineering* 2015;1:919-26.
- [155] Bowen PK, Shearier ER, Zhao S, Guillory RJ, Zhao F, Goldman J, et al. Biodegradable Metals for Cardiovascular Stents: from Clinical Concerns to Recent Zn-Alloys. *Adv Healthc Mater* 2016;5:1121-40.
- [156] Munemasa J, Kumakiri T. Effect of the surface-roughness of substrates on the corrosion properties of films coated by physical vapor-deposition. *Surface & Coatings Technology* 1991;49:496-9.
- [157] Grundmeier G, Schmidt W, Stratmann M. Corrosion protection by organic coatings: electrochemical mechanism and novel methods of investigation. *Electrochimica Acta* 2000;45:2515-33.
- [158] Stratmann M, Feser R, Leng A. Corrosion protection by organic films. *Electrochimica Acta* 1994;39:1207-14.
- [159] Ng WF, Chiu KY, Cheng FT. Effect of pH on the in vitro corrosion rate of magnesium degradable implant material. *Mat Sci Eng C-Mater* 2010;30:898-903.
- [160] Song G, Atrens A, StJohn D. An Hydrogen Evolution Method for the Estimation of the Corrosion Rate of Magnesium Alloys. *Magnesium Technology 2001: John Wiley & Sons, Inc.*; 2001. p. 254-62.
- [161] Witte F, Fischer J, Nellesen J, Crostack H-A, Kaese V, Pisch A, et al. In vitro and in vivo corrosion measurements of magnesium alloys. *Biomaterials* 2006;27:1013-8.
- [162] Song GL, Atrens A. Understanding magnesium corrosion - A framework for improved alloy performance. *Advanced Engineering Materials* 2003;5:837-58.
- [163] Duan HP, Du KQ, Yan CW, Wang FH. Electrochemical corrosion behavior of composite coatings of sealed MAO film on magnesium alloy AZ91D. *Electrochimica Acta* 2006;51:2898-908.
- [164] Stern M, Geary AL. Electrochemical Polarization: I. A Theoretical Analysis of the Shape of Polarization Curves. *Journal of The Electrochemical Society* 1957;104:56-63.
- [165] Xin YC, Huo KF, Tao H, Tang GY, Chu PK. Influence of aggressive ions on the degradation behavior of biomedical magnesium alloy in physiological environment. *Acta Biomater* 2008;4:2008-15.
- [166] Kramer M, Schilling M, Eifler R, Hering B, Reifenrath J, Besdo S, et al. Corrosion behavior, biocompatibility and biomechanical stability of a prototype magnesium-based biodegradable intramedullary nailing system. *Mat Sci Eng C-Mater* 2016;59:129-35.

- [167] Yang L, Zhang EL. Biocorrosion behavior of magnesium alloy in different simulated fluids for biomedical application. *Materials Science & Engineering C-Biomimetic and Supramolecular Systems* 2009;29:1691-6.
- [168] Cui F-z, Yang J-x, Jiao Y-p, Yin Q-s, Zhang Y, Lee I-S. Calcium phosphate coating on magnesium alloy for modification of degradation behavior. *Frontiers of Materials Science in China* 2008;2:143-8.
- [169] Gray-Munro JE, Seguin C, Strong M. Influence of surface modification on the in vitro corrosion rate of magnesium alloy AZ31. *Journal of Biomedical Materials Research Part A* 2009;91a:221-30.
- [170] Kunjukunju S, Roy A, Ramanathan M, Lee B, Candiello JE, Kumta PN. A layer-by-layer approach to natural polymer-derived bioactive coatings on magnesium alloys. *Acta Biomater* 2013;9:8690-703.
- [171] Park M, Lee JE, Park CG, Lee SH, Seok HK, Choy YB. Polycaprolactone coating with varying thicknesses for controlled corrosion of magnesium. *Journal of Coatings Technology and Research* 2013;10:695-706.
- [172] Gupta RK, Mensah-Darkwa K, Kumar D. Corrosion Protective Conversion Coatings on Magnesium Disks Using a Hydrothermal Technique. *Journal of Materials Science & Technology* 2014;30:47-53.
- [173] Zhu YY, Wu GM, Zhang YH, Zhao Q. Growth and characterization of Mg(OH)(2) film on magnesium alloy AZ31. *Applied Surface Science* 2011;257:6129-37.
- [174] Huo HW, Li Y, Wang FH. Corrosion of AZ91D magnesium alloy with a chemical conversion coating and electroless nickel layer. *Corros Sci* 2004;46:1467-77.
- [175] Ye S-H, Jang Y-S, Yun Y-H, Shankaraman V, Woolley JR, Hong Y, et al. Surface Modification of a Biodegradable Magnesium Alloy with Phosphorylcholine (PC) and Sulfobetaine (SB) Functional Macromolecules for Reduced Thrombogenicity and Acute Corrosion Resistance. *Langmuir* 2013;29:8320-7.
- [176] Lee JH, Khang G, Lee JW, Lee HB. Interaction of Different Types of Cells on Polymer Surfaces with Wettability Gradient. *Journal of Colloid and Interface Science* 1998;205:323-30.
- [177] Ayala R, Zhang C, Yang D, Hwang Y, Aung A, Shroff SS, et al. Engineering the cell-material interface for controlling stem cell adhesion, migration, and differentiation. *Biomaterials* 2011;32:3700-11.
- [178] Xu LP, Pan F, Yu GN, Yang L, Zhang EL, Yang K. In vitro and in vivo evaluation of the surface bioactivity of a calcium phosphate coated magnesium alloy. *Biomaterials* 2009;30:1512-23.

- [179] Johnson I, Liu H. In vitro Evaluation of Magnesium-based Metallic Biomaterials and the Need for Standardization Biomaterials Forum 2012;34:9-14.
- [180] Curran JM, Chen R, Hunt JA. Controlling the phenotype and function of mesenchymal stem cells in vitro by adhesion to silane-modified clean glass surfaces. *Biomaterials* 2005;26:7057-67.
- [181] Sauberlich S, Klee D, Richter EJ, Hocker H, Spiekermann H. Cell culture tests for assessing the tolerance of soft tissue to variously modified titanium surfaces. *Clinical Oral Implants Research* 1999;10:379-93.
- [182] Tsaras G, Osmon DR, Mabry T, Lahr B, Sauveur JS, Yawn B, et al. Incidence, Secular Trends, and Outcomes of Prosthetic Joint Infection: A Population-Based Study, Olmsted County, Minnesota, 1969–2007. *Infection Control & Hospital Epidemiology* 2015;33:1207-12.
- [183] Getzlaf MA, Lewallen EA, Kremers HM, Jones DL, Bonin CA, Dudakovic A, et al. Multi-Disciplinary Antimicrobial Strategies for Improving Orthopaedic Implants to Prevent Prosthetic Joint Infections in Hip and Knee. *Journal of orthopaedic research : official publication of the Orthopaedic Research Society* 2016;34:177-86.
- [184] Alt V, Franke J, Schnettler R. Local delivery of antibiotics in the surgical treatment of bone infections. *Tech Orthop* 2015;30:230-5.
- [185] Luo D, Gould DJ, Sukhorukov GB. Local and Sustained Activity of Doxycycline Delivered with Layer-by-Layer Microcapsules. *Biomacromolecules* 2016;17:1466-76.
- [186] King D, McGinty S. Assessing the potential of mathematical modelling in designing drug-releasing orthopaedic implants. *Journal of Controlled Release* 2016;239:49-61.
- [187] Radin S, Ducheyne P. Controlled release of vancomycin from thin sol-gel films on titanium alloy fracture plate material. *Biomaterials* 2007;28:1721-9.
- [188] Waizy H, Seitz J-M, Reifenrath J, Weizbauer A, Bach F-W, Meyer-Lindenberg A, et al. Biodegradable magnesium implants for orthopedic applications. *J Mater Sci* 2013;48:39-50.
- [189] Reifenrath J, Bormann D, Meyer-Lindenberg A. Magnesium Alloys as Promising Degradable Implant Materials in Orthopaedic Research. In: Czerwinski F, editor. *Magnesium Alloys - Corrosion and Surface Treatments: InTech* 2011.
- [190] Yoshizawa S, Brown A, Barchowsky A, Sfeir C. Role of magnesium ions on osteogenic response in bone marrow stromal cells. *Connect Tissue Res* 2014;55:155-9.
- [191] Rettig R, Virtanen S. Composition of corrosion layers on a magnesium rare-earth alloy in simulated body fluids. *Journal of Biomedical Materials Research Part A* 2009;88:359-69.

- [192] Witte F, Hort N, Vogt C, Cohen S, Kainer KU, Willumeit R, et al. Degradable biomaterials based on magnesium corrosion. *Curr Opin Solid State Mater Sci* 2008;12:63-72.
- [193] Thormann U, Alt V, Heimann L, Gasquere C, Heiss C, Szalay G, et al. The biocompatibility of degradable magnesium interference screws: An experimental study with sheep. *BioMed Research International* 2015;2015.
- [194] Angrisani N, Reifenrath J, Zimmermann F, Eifler R, Meyer-Lindenberg A, Vano-Herrera K, et al. Biocompatibility and degradation of LAE442-based magnesium alloys after implantation of up to 3.5 years in a rabbit model. *Acta Biomater* 2016;44:355-65.
- [195] Berglund IS, Jacobs BY, Allen KD, Kim SE, Pozzi A, Allen JB, et al. Peri-implant tissue response and biodegradation performance of a Mg-1.0Ca-0.5Sr alloy in rat tibia. *Materials Science and Engineering C* 2016;62:79-85.
- [196] Wong HM, Yeung KWK, Lam KO, Tam V, Chu PK, Luk KDK, et al. A biodegradable polymer-based coating to control the performance of magnesium alloy orthopaedic implants. *Biomaterials* 2010;31:2084-96.
- [197] Wong HM, Zhao Y, Leung FKL, Xi T, Zhang Z, Zheng Y, et al. Functionalized Polymeric Membrane with Enhanced Mechanical and Biological Properties to Control the Degradation of Magnesium Alloy. *Adv Healthc Mater* 2017;6:1601269-n/a.
- [198] Liu X, Yue Z, Romeo T, Weber J, Scheuermann T, Moulton S, et al. Biofunctionalized anti-corrosive silane coatings for magnesium alloys. *Acta Biomater* 2013;9:8671-7.
- [199] Mojsiewicz-Pienkowska K, Jamrógiewicz M, Szymkowska K, Krenczkowska D. Direct human contact with siloxanes (silicones) - safety or risk part 1. Characteristics of siloxanes (silicones). *Frontiers in Pharmacology* 2016;7.
- [200] Chemtob A, Ni L, Croutxé-Barghorn C, Boury B. Ordered Hybrids from Template-Free Organosilane Self-Assembly. *Chemistry – A European Journal* 2014;20:1790-806.
- [201] Bhushan B. Surface Roughness Analysis and Measurement Techniques. In: Bhushan B, editor. *Modern Tribology Handbook, Two Volume Set*. Boca Raton, Florida, 33431, USA: CRC press LLC; 2000. p. 1760.
- [202] Farayibi PK, Abioye TE, Murray JW, Kinnell PK, Clare AT. Surface improvement of laser clad Ti-6Al-4V using plain waterjet and pulsed electron beam irradiation. *Journal of Materials Processing Technology* 2015;218:1-11.
- [203] Frade M, Enguita JM, Álvarez I. In-Situ Waviness Characterization of Metal Plates by a Lateral Shearing Interferometric Profilometer. *Sensors (Basel, Switzerland)* 2013;13:4906-21.
- [204] Reifenrath J, Angrisani N, Erdmann N, Lucas A, Waizy H, Seitz JM, et al. Degrading magnesium screws ZEK100: Biomechanical testing, degradation analysis and soft-tissue biocompatibility in a rabbit model. *Biomedical Materials (Bristol)* 2013;8.

- [205] Rössig C, Angrisani N, Helmecke P, Besdo S, Seitz JM, Welke B, et al. In vivo evaluation of a magnesium-based degradable intramedullary nailing system in a sheep model. *Acta Biomater* 2015;25:369-83.
- [206] Fischerauer SF, Kraus T, Wu X, Tangl S, Sorantin E, Hänzi AC, et al. In vivo degradation performance of micro-Arc-oxidized magnesium implants: A micro-CT study in rats. *Acta Biomater* 2013;9:5411-20.
- [207] Ghali E, Dietzel W, Kainer K-U. General and localized corrosion of magnesium alloys: a critical review. *Journal of Materials Engineering and Performance* 2004;13:7-23.
- [208] Xin Y, Huo K, Tao H, Tang G, Chu PK. Influence of aggressive ions on the degradation behavior of biomedical magnesium alloy in physiological environment. *Acta Biomater* 2008;4.
- [209] Hacking SA, Boyraz P, Powers BM, Sen-Gupta E, Kucharski W, Brown CA, et al. Surface roughness enhances the osseointegration of titanium headposts in non-human primates. *Journal of Neuroscience Methods* 2012;211:237-44.
- [210] Novaes Jr AB, Souza SLSd, Barros RRMd, Pereira KKY, Iezzi G, Piattelli A. Influence of implant surfaces on osseointegration. *Brazilian Dental Journal* 2010;21:471-81.
- [211] Walter R, Kannan MB. Influence of surface roughness on the corrosion behaviour of magnesium alloy. *Materials & Design* 2011;32:2350-4.
- [212] Alvarez RB, Martin HJ, Horstemeyer MF, Chandler MQ, Williams N, Wang PT, et al. Corrosion relationships as a function of time and surface roughness on a structural AE44 magnesium alloy. *Corros Sci* 2010;52:1635-48.
- [213] Nguyen TL, Blanquet A, Staiger MP, Dias GJ, Woodfield TBF. On the role of surface roughness in the corrosion of pure magnesium in vitro. *Journal of Biomedical Materials Research Part B: Applied Biomaterials* 2012;100B:1310-8.
- [214] Tian P, Liu X. Surface modification of biodegradable magnesium and its alloys for biomedical applications. *Regenerative Biomaterials* 2015;2:135-51.
- [215] Erdmann N, Angrisani N, Reifenrath J, Lucas A, Thorey F, Bormann D, et al. Biomechanical testing and degradation analysis of MgCa0.8 alloy screws: A comparative in vivo study in rabbits. *Acta Biomater* 2011;7:1421-8.
- [216] Zainal Abidin NI, Rolfe B, Owen H, Malisano J, Martin D, Hofstetter J, et al. The in vivo and in vitro corrosion of high-purity magnesium and magnesium alloys WZ21 and AZ91. *Corros Sci* 2013;75:354-66.
- [217] Miura C, Shimizu Y, Imai Y, Mukai T, Yamamoto A, Sano Y, et al. In vivo corrosion behaviour of magnesium alloy in association with surrounding tissue response in rats. *Biomedical Materials (Bristol)* 2016;11.

- [218] Xiao J, Huang C, Shi D, Zhu R, Gu R, Wang H, et al. Inflammatory and immuno-reactivity in mice induced by intramuscular implants of HSNGLPL peptide grafted-polyurethane. *Journal of Materials Chemistry B* 2016;4:1898-907.
- [219] Carvalho RFd, Martins MEMN, Queiroz J, eacute, Renato Cavalcanti d, Leite F, et al. Influence of silane heat treatment on bond strength of resin cement to a feldspathic ceramic. *Dental Materials Journal* 2011;30:392-7.
- [220] Yavuz T, Eraslan O. The effect of silane applied to glass ceramics on surface structure and bonding strength at different temperatures. *The Journal of Advanced Prosthodontics* 2016;8:75-84.
- [221] Metwalli E, Haines D, Becker O, Conzone S, Pantano CG. Surface characterizations of mono-, di-, and tri-aminosilane treated glass substrates. *Journal of Colloid and Interface Science* 2006;298:825-31.
- [222] Pearce AI, Richards RG, Milz S, Schneider E, Pearce SG. Animal models for implant biomaterial research in bone: a review. *European cells & materials* 2007;13:1-10.
- [223] Chaya A, Yoshizawa S, Verdelis K, Noorani S, Costello BJ, Sfeir C. Fracture Healing Using Degradable Magnesium Fixation Plates and Screws. *Journal of Oral and Maxillofacial Surgery* 2015;73:295-305.